Network properties of the mammalian circadian clock

Rohling, J.H.T.

Network properties of the mammalian circadian clock

Network properties of the mammalian circadian clock

Proefschrift
ter verkrijging van
de graad van Doctor aan de Universiteit Leiden,
op gezag van de Rector Magnificus Prof.mr. P.F. van der Heijden,
volgens besluit van het College voor Promoties
te verdedigen op dinsdag 15 december 2009
klokke 11:15 uur
door

Johannes Hermanus Theodoor Rohling

geboren te Schoonebeek
in 1970

PROMOTIECOMMISSIE

Promotoren	Prof. dr. H.A.G. Wijshoff
	Prof. dr. J.H. Meijer
Co-promotor	Dr. A.A. Wolters
Leden	Prof. dr. G.D. Block (University of California, Los Angeles)
	Prof. dr. D.G.M. Beersma (Rijksuniversiteit Groningen)
	Prof. dr. S.M. Verduyn Lunel
	Prof. dr. J.N. Kok
	Prof. dr. F.J. Peters

ISBN/EAN: 978-90-9024776-2

This work was supported by Netherlands Organization for Scientific Research (NWO), program grant nr 805.47.212 'From Molecule to Cell'.

Netherlands Organisation for Scientific Research

This work was carried out in the ASCI graduate school.
ASCI dissertation series number 186.

Advanced School for Computing and Imaging

Printed by Universal Press, Veenendaal

Table of contents

Chapter 1

Introduction

Combining sciences is a challenge. Scientists from different fields often do not speak the same language and certainly do not always agree on methodology and proof finding. However, when taking the risk, the combined efforts can also lead to new and surprising results for both sciences: the results can be more than the sum of parts.

In this thesis, computer science and life sciences join hands. More specifically, computational models are created to investigate the biological clock, which is present in all living organisms. The biological clock is a large network containing thousands of neurons that may challenge the computational techniques. These techniques were used, and elaborated where needed, to investigate research goals that were previously difficult to target in the biological clock field.

1.1 The biological clock

The rotation of the earth around its axis subjects every organism to a daily 24 h cycle. Apart from this daily rhythm, every organism is under the influence of seasons, due to the rotation of the earth around the sun. The daily and seasonal fluctuations cause cycles in illumination, temperature and humidity (Hofman, 2004). Evolutionary advantages can be obtained if the organism can anticipate to these daily and seasonal changes.

The ability to anticipate the daily light-dark cycle can be a life-saving property. Certain one-cellular algae, the *Gonyaulax polyedra*, need to photosynthesize during the day and rise to the surface shortly before sunrise. Before sunset they migrate to great depths to take advantage of high nutrient concentrations and a short wavelength light spectrum present at deeper sea levels (Roenneberg and Mittag, 1996). Small nocturnal rodents save their lives when they anticipate sunrise. These rodents are active during the night and need to return to their burrows before the day starts and the predators become active.

Anticipation to seasonal changes can also be of vital importance. Most animals get their offspring in periods of the year that are most advantageous for survival (Lincoln et al., 2003;Dawson et al., 2001). For mammals, the most advantageous time for survival is when the temperatures are optimal for a prolonged period of time and when there is an abundance of food, enabling the offspring to be strong enough for the colder seasons when less food is available. Other annual rhythms in mammals exist in pelage moult, food intake, body weight and hibernation (Lincoln et al., 2003). Seasonal rhythms are also apparent in other organisms. For instance, in plants, flowering, stem and leaf elongation and other mechanisms are well known for their seasonality (Carre, 2001).

It is well conceived that the daily and seasonal rotations of the earth are deeply rooted and essential for living organisms. Despite the fact that humans can escape these rhythms, also in humans many seasonal and daily rhythms can be observed if carefully studied. The influence of seasonality becomes apparent in seasonal affective disorder, or winter depression. Daily rhythms in humans can be observed in blood pressure levels, several hormonal levels, body temperature, arousal level and REM sleep propensity (Wehr, 2001;Meijer, 2008). The anticipation of humans to daily rhythms can be observed in the rising of blood pressure and body temperature at the end of the night, during sleep and *before* awakening (Meijer, 2008).

In many organisms, the so-called biological clock takes care of both daily and seasonal rhythms. The location of this clock differs between organisms. In plants for example, this clock is believed to be located somewhere in the leafs (Carre, 2001), in snails it is located in the eyes (Jacklet, 1969; Block

and Wallace, 1982), and in mammals it is located in specialized hypothalamic nuclei residing just above the optic chiasm on either side of the third ventricle (Moore and Eichler, 1972;Stephan and Zucker, 1972).

This central pacemaker plays a critical role in controlling rhythmic functions. It serves as a master clock that is able to synchronize to the environmental cycle (Daan, 1981; Morin and Allen, 2006) and synchronizes or even imposes its rhythm to downstream peripheral oscillators in the body of the organism (Vansteensel et al., 2008). For mammals, examples of peripheral oscillators working under the influence of the master clock are the lung and liver (Yamazaki et al., 2000).

Rhythmic environmental cues that influence the pacemaker are called Zeitgebers (German for "time providers"). Examples of Zeitgebers are the cycle of light and dark, temperature and social cues (Lowrey and Takahashi, 2004). The light-dark cycle is the most predictable Zeitgeber, because the light-dark cycle is a precise indicator of the daily cycle and it accurately reflects the seasons. The length of a day, also called *photoperiod*, is a robust indicator of time of year (Johnston, 2005). It is much more robust than other Zeitgebers, such as temperature, that can have large fluctuations between days. For this reason, the light-dark cycle became the functional Zeitgeber in evolution and Zeitgeber Time (ZT) is thus defined relative to the light-dark cycle. ZT 12 is defined as lights off, which means that ZT 0 coincides with lights on when entrained to a light-dark cycle with 12 hours of light and 12 hours of darkness (LD 12:12) (Lowrey and Takahashi, 2004).

In the absence of environmental Zeitgebers the clock maintains a *circadian* rhythm of *about* 24 h (circa dies = about one day). In an experimental setting, organisms can be isolated from any environmental cues and be maintained in constant conditions, such as constant darkness (DD) or constant light (LL) conditions. In these constant conditions, the endogenous rhythm, or "free-running period" of the circadian clock can be measured (Lowrey and Takahashi, 2004).

The endogenous rhythm is generated within individual neurons of the clock on the basis of a molecular feedback loop. The genetic machinery of the master clock is surprisingly similar in different organisms (Devlin and Kay, 2001). The basic principle of the molecular mechanisms of the

biological clock in humans largely resembles the one found in algae, fruit flies and in mice and rats, and most of the genes involved are in fact conserved.

The endogenous rhythm produced by neurons of the clock is *about* 24 h, but not exactly 24 h (Herzog et al., 2004). As the endogenous rhythm often differs from the 24 h light-dark cycle, another timescale is used to specify the 'subjective' time of the organism. The endogenous rhythm is given in circadian time (CT) and is divided into 24 circadian hours. CT 12 is taken as the start of the subjective night, so the onset of behavioural activity for nocturnal (night-active) organisms and the start of the sleeping period for diurnal (day-active) organisms (Lowrey and Takahashi, 2004). The circadian hours differ slightly from the external hours. The circadian time represents the state of the organism in its endogenous cycle. This state is also called its *phase*.

In order to anticipate to the 24 h rhythm, the clock mechanism needs to adjust its rhythm to exactly 24 h on a daily basis. In other words, the endogenous rhythm needs to be entrained, or synchronized, to the daily environmental light-dark cycle. Organisms that have an endogenous cycle that is less than 24 h must delay their phase to keep synchronized to the daily light-dark cycle, while organisms having an endogenous cycle of more than 24 h must phase advance (Lowrey and Takahashi, 2004). By applying light pulses to organisms that are kept in constant darkness, the phase responsiveness of the clock can be investigated as a function of the time of the light application. For example by fitting a straight line through the activity onsets of a behavioural recording of an animal, the behaviour of the animal can be analyzed and its phase can be determined. The phases of the animal before and after a light pulse are compared. If an animal starts its activity earlier than the day before, its phase has advanced. A delay has occurred if the animal's activity starts later. Light pulses given at the beginning of the subjective night produce phase delays, while light pulses during the end of the subjective night produce phase advances. The corresponding function which summarizes phase responses to light pulses given at different circadian times is known as the phase response curve (PRC) of the organism (DeCoursey, 1960;Daan and Pittendrigh, 1976).

The endogenous circadian rhythm is generated within individual cells. An intracellular genetic feedback loop is responsible for this endogenous rhythm. In order to generate a consistent output for the clock as a whole, these cellular clocks need to be synchronized (Herzog et al., 2004). This synchronization is established by different intercellular communication mechanisms that exist between neurons. The communication can be humoral, via synaptic connections, or electrical (for an overview, see Michel and Colwell, 2001). Through these different means of communication the neurons are connected creating a network. Certain properties of the clock are encoded at this network level, and not on the cellular level (Vansteensel et al., 2008). While the endogenous rhythms are clearly a property of the intracellular feedback loops of single cells, properties such as entrainment, resetting, or day length encoding are encoded on the network level. This implicates that different levels of organization are responsible for different properties of the circadian pacemaker.

The topic of this thesis is the organization of the intercellular communication networks of the circadian clock. A lot of scientific research focuses on uncovering the cellular mechanisms of clock cells. However, less research is aimed to understand the functionality that is emerging from the network level, even though these network properties have many implications for people's health. Shift work and jet lag are becoming important topics in today's society, and seasonal diseases are better understood. All these topics should be explained at the network level. In this thesis I aim to contribute to understanding the network properties of the biological clockwork.

For these studies, computer science methods and techniques have been used and applied to simulate the network properties of the circadian clock. Before describing the aims of this thesis and which studies have been conducted to achieve these aims, the reason for the use of simulation models will be explained.

1.2 Modelling and simulation

Empirical experiments are often cumbersome and take a lot of time. One experiment is never enough; dozens are needed for statistical purposes. Every experiment takes time, time for preparation, time to perform

measurements, time to analyze and so on. Before enough data from experiments is available for validation, a lot of time has passed. Apart from being time consuming, some experiments are very difficult to perform, or even impossible under controlled conditions (Guala, 2002).

Simulations can help overcome some of the problems that arise with experiments. They are mostly much faster than the empirical experiments and they can be designed to gain insight in mechanisms that are difficult to measure (Guala, 2002). For example, in animal research of the biological clock, animals first need to be entrained to a certain light-dark regime, which may take weeks. In a computer simulation, the model can be trained to any light-dark regime instantly. Furthermore, experiments are vulnerable to uncontrollable external factors that can disturb the recordings and make the results worthless. External factors can also disturb computer simulations, like power failure, but simulations can be restarted in a certain state if it was stored, and the simulation does not need start again from the beginning. However, simulations alone can never validate results, because the simulations are derived from a model. Empirical experiments must be performed to validate the model predictions (Orynski and Pawlowski, 2004). But simulations can be very useful to decide which experiments are worthwhile and which do not look promising, and simulations can help design smaller (sub-) experiments for experiments that are impossible to do all in one go (Guala, 2002). Consider the animals that die too early, the data coming from the simulations can direct the research in such a way that sub-experiments can be designed where the animals do not die and empirical experiments can be performed. In this way, treatments for diseases or illnesses can be found.

1.2.1 Mental models

Nowadays, new research topics are often found in the laboratory. In the early days, discoveries came in a more romantic fashion. Sir Isaac Newton was sitting in the garden when an apple fell from a tree. He wondered why the apple always descended perpendicularly to the ground, and following this idea he came up with the idea of gravity. From this idea, he developed experiments and found the theory of gravity (Westfall, 1993).

Science is not that romantic anymore, but the process for theory-building is comparable. In the laboratory, some peculiar findings are done, oftentimes in experiments dealing with completely different topics. Some scientists start wondering about a peculiar result, and try to find an explanation for it. In doing so, they build a hypothesis, or model, inside their head. Based on this model they design new experiments to find out more about the new phenomenon they observed. The results from the experiments are either positive, which strengthens the model, or negative, which will lead to a modification of the model. This process of constantly updating the model continues.

The models that gradually evolve in one's head are called mental or conceptual models (Sterman, 1991;Beersma, 2005). These models globally describe the possible mechanisms that might drive the new observation. Conceptual models are very flexible. They can easily be adapted when new information becomes available, and they are not restricted to data that can be expressed in (reproducible) quantities (Sterman, 1991). This is also the first drawback of a mental model: it is difficult to reproduce, because the assumptions on which they are based are not explicitly stated and the results have not been quantified. The implicit assumptions can easily be misinterpreted, often causing mental models to be badly understood by others. Furthermore, ambiguities and contradictions can easily slip into these models (Sterman, 1991). To resolve the disadvantages, mental, models are formalized by transforming them into formal mathematical models (Beersma, 2005).

1.2.2 Formal models

Formal mathematical models, explicitly describe the conceptual model using mathematical equations. No misinterpretation of the model can occur because there is only one way to interpret a mathematical equation. In other words, mathematical models show the logical consequences of the assumptions that underlie the model (Sterman, 1991).

A disadvantage of the mathematical models is that they can not interpret relationships and factors that are difficult to quantify (Sterman, 1991). Another pitfall of mathematical models is that they can become very

complex if more information becomes available. Each time more knowledge is discovered about the observed phenomenon, the model is updated and sometimes extended. This may result in a model that is almost as complex as the real system, and results from the model can become as puzzling as results from the real system. Due to the complexity, the models can become *black boxes*, they are difficult to interpret and hard to understand (Sterman, 1991). People may loose trust in such a model, if they can not understand how the model arrives at its results, and the results can not be verified.

If mathematical models become complex, and exact solutions can not be derived anymore, they are often simulated using computational techniques. Numerical analysis is used to estimate the answer within acceptable error bounds. These models will be referred to as 'computational models' in this thesis.

1.2.3 Models

To gain a better understanding of the advantages and disadvantages of models, I will now describe what I mean when I talk about a model. In models abstract notions derived from empirical data are formalized into a theory that is more generally applicable. This general notion represents the real system. This representation does not intend to be the real system, it is a simplification of reality (Beersma, 2005). As such, modelling does not give one correct answer, and for complex problems, many models can provide correct, although not necessarily similar, solutions (Shiflet and Shiflet, 2006).

Models can either be static or dynamic. A static model, or optimization model, can only represent a system at rest. They are prescriptive. They prescribe the best possible solution that the model can offer (Sterman, 1991). Dynamic models are simulation models. The latin verb *simulare* means to imitate or mimic. A simulation model thus mimics the real system in order to study its behaviour under different circumstances (Sterman, 1991). In a simulation model the time-evolution of the real system is considered by being in a different state at different times (Guala, 2002;Shiflet and Shiflet, 2006). Each state corresponds to a specific combination of values for the different variables in the model (Guala, 2002). This makes a simulation

model descriptive. It does not calculate the best possible solution, but it clarifies what would happen in a certain situation. They are 'what if' tools, and can predict how the real system might behave under certain circumstances and promote understanding of underlying mechanisms (Sterman, 1991).

Simulation models often use numerical methods, because the models under consideration are mostly complex systems. The numerical simulation models can be used to reconstruct and understand empirical data and to predict how the processes in the real system might behave that are difficult to investigate in other ways or that are very time consuming. The computational model makes it possible to make specific and sometimes nonintuitive predictions (Beersma, 2005).

1.2.4 Usability of models and simulations

Models are simplified versions of the real system and do not completely represent reality. The usefulness of a model does not depend on its ability to correctly describe reality. It depends on the extent to which it promotes understanding mechanisms in the real system and how well it is able to predict the outcome of new empirical experiments (Beersma, 2005).

In order to achieve this, a model should not be too comprehensive. A model needs to focus on a particular problem or question to solve (Sterman, 1991). It must focus on specific functional issues of the real system in order to deal with the question. There is not one recipe of how to do this (Beersma, 2005). Models must be as simple as possible in order to promote understanding in the best possible way. However, if too little detail is included in the model, the model might be useless because relevant pieces of information are left out of the model. Too much detail makes the model overly complicated and may cause the model to become just as difficult to understand as the real system. Thus, a modeller must find a trade-off in the level of detail to include in the model. One does not want the model to be as complicated as the real system, because what would be the point of the model? But one also does not want to miss relevant mechanisms of the real system. The model should be as simple as possible provided that is it sufficient for the question posed.

One of the real benefits of modelling and numerical simulation is its ability to accomplish a time and space compression between the interrelationships within a system. This brings into view the results of interactions that would normally escape us because they are not closely related in time and space. Modelling and simulation can provide a way of understanding dynamic complexity. Numerical simulation models are used in all kinds of areas. Weather prediction, aircraft aerodynamics, and airport scheduling are just a few examples where numerical simulation models are indispensable. With computing power still increasing every year, the computer can perform its calculation on numerical models ever faster and more efficiently.

1.3 More than the sum of parts

Numerical simulations are mostly used in combination with empirical research. And empirical sciences can take great advantage from computational simulations. The data from the empirical experiments together with the computational simulations proved to bring advantages over using only one of those methods separately.

The simulation studies described in this thesis provided better insight into the possible working mechanisms of the intercellular communication of the clock. The studies were performed in close association with empirically derived experimental data obtained from the mammalian clock of rats and mice. This section introduces the research and results that have been acquired.

First, seasonal changes in day length were examined. A summer day has a longer light period than a winter day. The length of a day is perceived by the biological clock. In chapter 3, computer simulations, which are supported by empirical data, are described. The phase relations between neurons, which are influenced by interneuronal communication, are compared to a change in the activity duration of single cells. The phase relation between neurons, resulting from neuronal interactions, appears to be more effective to reflect changes in day length than adjustments at the single cell level.

Jet lag was investigated in chapter 4. Jet lag is caused after sudden changes of the light-dark cycle, for example due to transatlantic flight. The

rhythms of several organs of the body are not immediately adjusted to the new light-dark regime. It appears that a sudden shift of the light-dark schedule leads to a desynchronization of neurons within the central clock.

In different times of the year, the phase shifting responses to light pulses, that are also responsible for jet lag, are found to differ. In long days, the phase shifts induced by light pulses are small while in short days, light pulses of the same intensity and duration induce much larger shifts. Empirical research has been conducted in concert with simulation studies to understand the mechanisms underlying these differences that occur due to a change of the day length. In chapter 5 we provide evidence that the difference in the phase relations between neurons in long and short days is responsible for the differences in the capacity to phase shift.

In chapter 6 a mathematical model is presented that gives one explanation of how the phase shifting mechanism of the biological clock might work. The model is fitted to empirical data and tested for different experimental protocols using numerical simulations of the ordinary differential equations. Chapter 7 concludes this thesis with a summary and interpretation of the obtained results.

This thesis starts with a review of the master mammalian clock, in chapter 2. The molecular mechanisms responsible for generating an endogenous circadian rhythm at the cellular level are described, as well as the means of communication between clock neurons. The regional and functional organization of the clock in mammals will also be discussed. Different means to measure the rhythm of the mammalian master clock are presented, followed by a description of a number of properties of the clock, including seasonality, jet lag, and arrhythmicity. In the final section of chapter 2, an overview will be presented of different models that have been constructed for the biological clock.

Chapter 2

Mechanisms of the mammalian clock

The master circadian clock in mammals is located in the suprachiasmatic nuclei (SCN) of the anterior hypothalamus. The SCN consist of two bilaterally paired nuclei situated on opposite sides of the third ventricle, just above the optic chiasm (figure 2.1) (Klein et al., 1991).

The SCN were initially identified as the mammalian circadian clock in lesion studies. When the SCN was lesioned from the brain, a loss of rhythmicity in behaviour was observed (Moore and Eichler, 1972;Stephan and Zucker, 1972). Transplantation studies strengthened this hypothesis. When SCN tissue was transplanted in animals without an SCN circadian rhythms returned, also when the transplanted tissue was from a completely different animal strain (Ralph et al., 1990). In addition, electrical activity studies showed that the SCN has circadian rhythms, also when kept in constant darkness (Groos and Hendriks, 1982). When techniques became more refined, circadian rhythmicity profiles in electrical activity of single SCN neurons could also be obtained (Welsh et al., 1995;Liu et al., 1997;Herzog et al., 1998;Honma et al., 1998). This indicated that SCN neurons have an endogenous circadian rhythm.

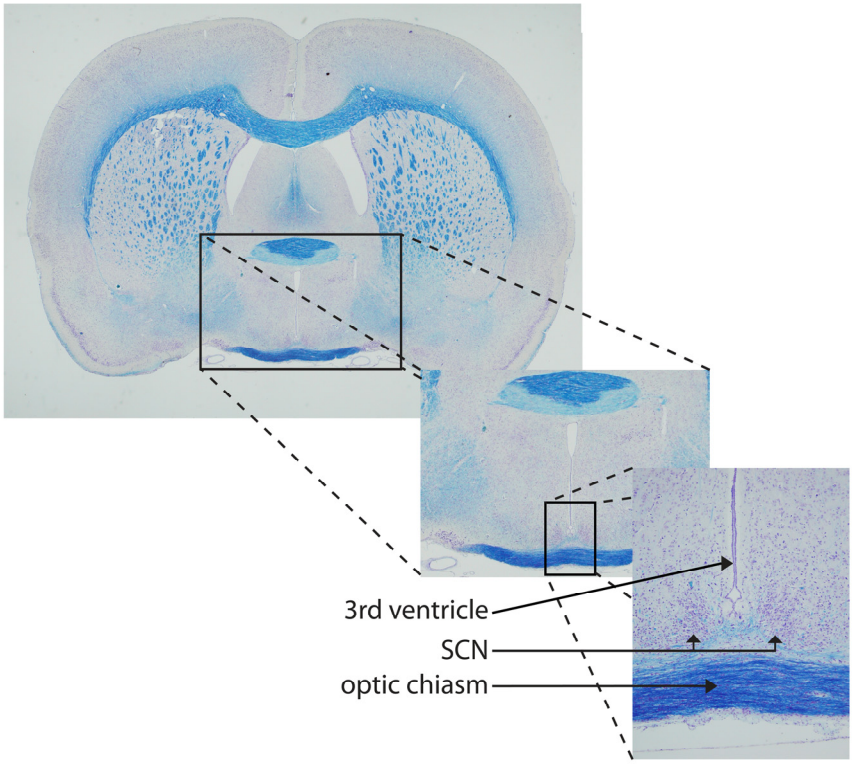

Figure 2.1 Brain of a rat containing both suprachiasmatic nuclei on opposite sides of the third ventricle, just above the optic chiasm.

2.1 Intracellular feedback loops

Underlying the endogenous rhythms of the SCN neurons are transcriptional translational feedback loops. The main genes that are involved in these regulatory loops are Clock, Bmal1, the three period genes (Per1, Per2, and Per3) and the two cryptochrome genes (Cry1 and Cry2) (see figure 2.2).

A rhythmic expression of Bmal1 enables the formation of CLOCK and BMAL1 protein complex. This complex, while in the cell nucleus, activates the transcription of the period and cryptochrome genes into mRNA. Liposomes then translate the mRNA into the PER and CRY proteins. These proteins form heterodimers (complexes with each other), enabling localization into the cell nucleus, where complexes containing CRY1 and CRY2 protein then inhibit the activity of the CLOCK- BMAL1 complex,

and with it their own expression. This is a negative feedback loop (Reppert and Weaver, 2002;Lowrey and Takahashi, 2004).

The CLOCK-BMAL1 complex also activates transcription of Rev-Erbα. The resulting REV-ERBα protein then represses the transcription of Bmal1. When the complexes containing PER2 have entered the nucleus, PER2 may be involved in the activation of Bmal1 expression. This is a positive feedback loop. Note that both loops are interlocked, because of the CLOCK-BMAL1 protein complex (Reppert and Weaver, 2002;Lowrey and Takahashi, 2004).

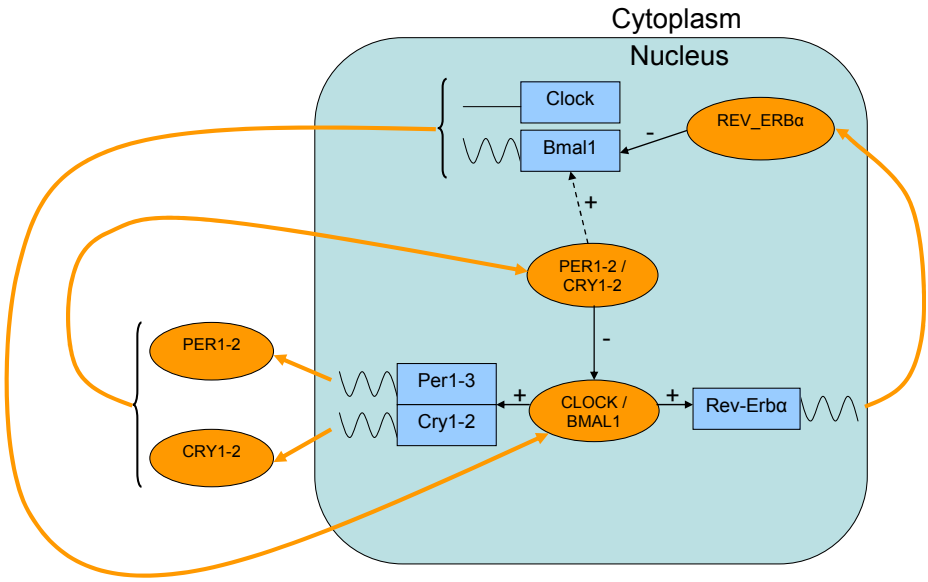

Figure 2.2 Simplified model for the molecular transcriptional / translational feedback loop underlying endogenous rhythms in SCN clock cells. Important clock genes are Bmal1, Clock, Per1-3, Cry1-2 and Rev-Erbα, where Clock is the only gene that is not rhythmically expressed. The genes are depicted in the figure as blue squares. These clock genes are expressed in the nucleus and transformed to proteins in the cytoplasm (BMAL1, CLOCK, PER1-3, CRY1-2 and REV-ERBα). There they form complexes that can re-enter the nucleus to perform its excitatory or inhibitory task (BMAL1/CLOCK, PER/CRY, the complex for REV_ERBα is unknown at this time). The protein and protein complexes are orange circles. BMAL1/CLOCK stimulates expression of Per, Cry and Rev-Erbα, complexes containing CRY inhibit the activity of the BMAL1/CLOCK complex, and the complex containing REV-ERBα represses the expression of Bmal1 (all denoted by black arrows where a + sign means stimulating and a – sign inhibitory influence). Complexes containing PER2 may be involved in activation of Bmal1 expression (black dashed arrow).

While the Clock transcription remains constant, the Bmal1 expression is rhythmic. The transcription of Bmal1 peaks in the middle of the circadian night. Per1 expression is at its peak at the beginning of the subjective day, while Per2 expression peaks at the end of the subjective day, just like Cry1 and Cry2. Per1 and Per2 are believed to be the most important genes involved in phase adjustment to entrain to the light dark cycle (Lowrey and Takahashi, 2004).

2.2 How to measure the rhythm of the clock

The rhythms of the SCN can be measured in behaviour, in multiunit output, in single unit output or in gene expression profiles, using a wide range of approaches. Each method has its own advantages and disadvantages. For example, some methods are better suited for long-term measurements, some methods are especially suited for measurements at a very small timescale, and other methods are suited to do very precise measurements (Aton and Herzog, 2005).

Behavioural rhythms can be measured using running wheels or by measuring drinking activity. The rhythm of the clock can be determined by measuring clock controlled hormone levels in blood samples. Technological advances have allowed also to measure directly from the SCN. This last method is a powerful method because of the direct way of measuring the SCN activity.

Electrical activity in the SCN can be measured, both *in vivo*, where an electrode is implanted in the central nervous system of an animal, as well as *in vitro*, in brain slices, where the SCN is recorded in relative isolation. Electrodes are used to record the spikes. A computer program counts the number of action potentials that exceed a noise-threshold, either for one neuron using patch clamp techniques, or for neuronal populations using extracellular recordings which do not damage the neurons that are measured.

Numerous bioluminescence and fluorescence markers are nowadays available to measure in one neuron the expression of genes, protein products, or intracellular messengers, such as calcium concentrations. Animal models have been created that have a mutation to react to a specific marker, and when concentrations of a particular gene or substance is high, the marker is

also abundantly present in the SCN and this concentration can be visualized with the aid of a camera. Sometimes, the mRNA levels are measured using these methods and in other occasions protein levels are used.

One can also measure the rhythms of cultured SCN neurons. In this case, neuronal populations of SCN cells are transferred to dishes. In these cell cultures it is easier to measure electrical activity and gene expression in the single cells as the individual cells can be better visualized. Cultures are also the preparation of choice when electrophysiological recordings are performed with microelectrode arrays. Note that these cells are not in a 'physiological' environment, which means that the natural network of cells has been disturbed.

2.3 Networks of oscillating neurons

The electrical activity patterns and gene expression profiles of single SCN neurons that are connected in a network have been compared to those measured in isolated or dispersed SCN neurons. The average period length was similar between the neurons with and without a network. However, the variance of the periods was much wider in the isolated neurons, compared to the connected neurons in a network (Herzog et al., 2004). It has become apparent that the interaction between SCN neurons improves the precision of the circadian rhythm. In order for the complete SCN to produce a consistent rhythmic output, the rhythms of the individual neurons must be synchronized, and some communication between the neurons is necessary to realize synchronization (Herzog et al., 1998;Honma et al., 1998;Herzog et al., 2004;Aton and Herzog, 2005).

To examine the synchronization between neurons it is important to realize that the SCN is not one homogeneous population of neurons, and that not all neurons are identical (figure 2.3). The SCN consist of two nuclei, one to the left of the third ventricle and the other to the right of the third ventricle. Each nucleus contains about 8,000 – 10,000 neurons. The neurons in both nuclei are organized in different functional subregions and serve different functions in the regulation of the circadian clock (Antle and Silver, 2005;Aton and Herzog, 2005). This means that there is a heterogeneous population of neurons present in the SCN.

A common distinction that is made for functional subregions of the SCN is between the dorsal SCN (also called *shell*) and the ventral SCN (or historically named *core*). In the rat, a clear distinction between these regions exists anatomically (van den Pol, 1991), whereas in the mouse SCN this anatomical distinction is less clear. However, in the mouse, the functionality of ventral and dorsal neurons still exists (Vansteensel et al., 2008).

The ventral SCN receives most of the light input fibers and mainly contains neurons that produce vasoactive intestinal polypeptide (VIP) or gastrin-releasing peptide (GRP). The dorsal SCN receives input from non-visual cortical and subcortical regions and light information via the ventral SCN. The dorsal SCN mainly consists of neurons producing arginine vasopressin (AVP) (Moore et al., 2002). Other studies also show that there must be a connection from dorsal to the ventral SCN (Albus et al, 2005). Figure 2.4 shows the location of the AVP, VIP and GRP in the dorsal and ventral SCN.

2.4 Properties of the clock: seasonality

A number of attributes of the circadian clock are thought to be produced at the network level, and do not originate at the molecular level. Seasonality is one example of a network driven property of the clock. Seasonal changes have a considerable influence in the lives of many organisms. Reproduction in different organisms is driven by seasonality (plants: Carre, 2001; birds: Dawson et al., 2001; fungi: Roenneberg and Merrow, 2001; mollusks: Wayne, 2001; mammals: Messager et al., 2000). Other mechanisms that are also under influence of the seasons are stem and leaf elongation in plants (Carre, 2001), molt and song behaviour in birds (Dawson et al., 2001), and pelage, appetite and body weight in mammals (Messager et al., 2000).

The most predictable indicator for the different seasons is the change in day length. In summer, the days are longer and the nights shorter, while in winter, vice versa, the days are shorter and the nights longer. In mammals, an impressive amount of research has been carried out on photoperiodism. Changes in photoperiod are observed in locomotor behaviour, melatonin levels in the pineal gland, gene expression profiles and electrical activity rhythms in the SCN (Goldman, 2001;Johnston, 2005;Meijer et al., 2007).

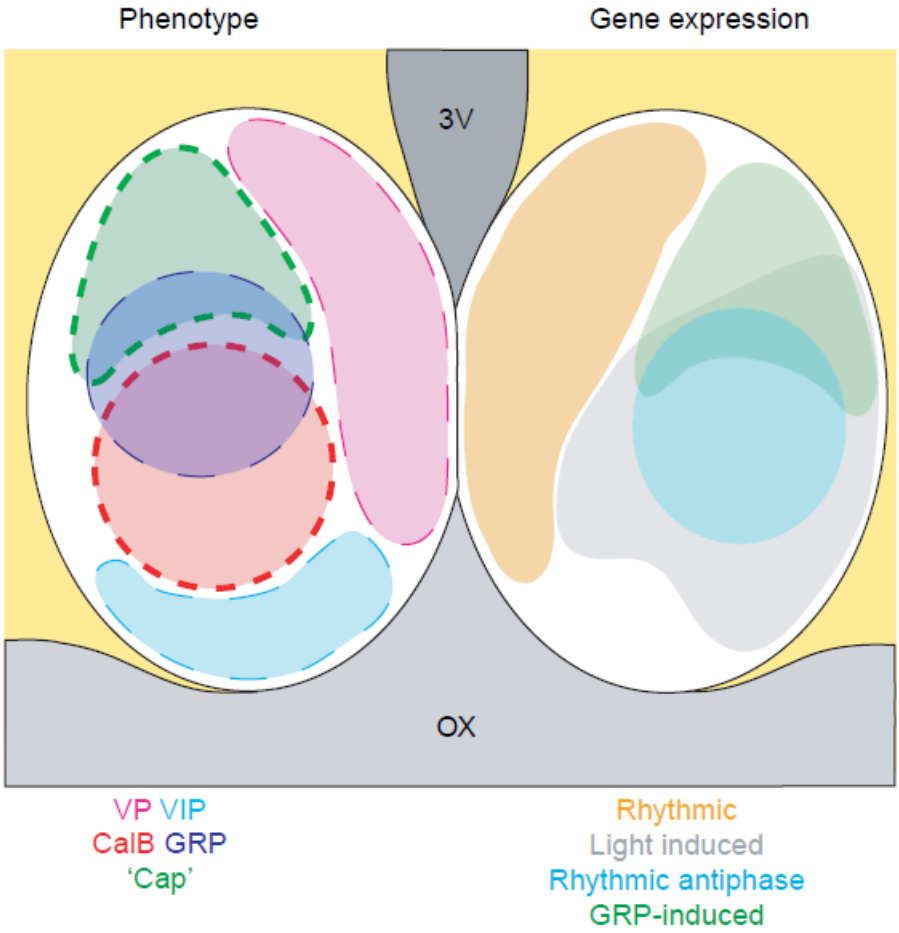

Figure 2.3 Heterogeneous SCN in hamster. The left depicts the different phenotypic subregions in the hamster SCN. In the dorsomedial part of the SCN, vasopressin (VP)-expressing cells (pink) can be found. In the ventral part of the SCN, vasoactive intestinal polypeptide (VIP)-containing cells (light blue) are present. Immediately dorsal to the VIP cells lie calbindin (CalB)-expressing cells (red). The phenotype of the 'cap' cells (green) has not yet been identified, but lie dorsal to the CalB cells, while the gastrin-releasing peptide (GRP)-expressing cells (dark blue) overlap with the CalB and the 'cap' regions. In the right SCN regions are shown that depend on the expression of the Period genes. Per gene expression can either be rhythmic (pale orange region), light-induced (gray region) or follow GRP administration (green region). The blue region contains cells expressing Per in antiphase to the rhythmic Per gene expression. However, these cells are only found in mice and rats, not in hamsters. (Reprinted from TRENDS in Neuroscience, Vol. 28 No. 3, Antle and Silver, Orchestrating time: arrangements of the brain clock, 145-151, Copyright 2005, with permisson from Elsevier.)

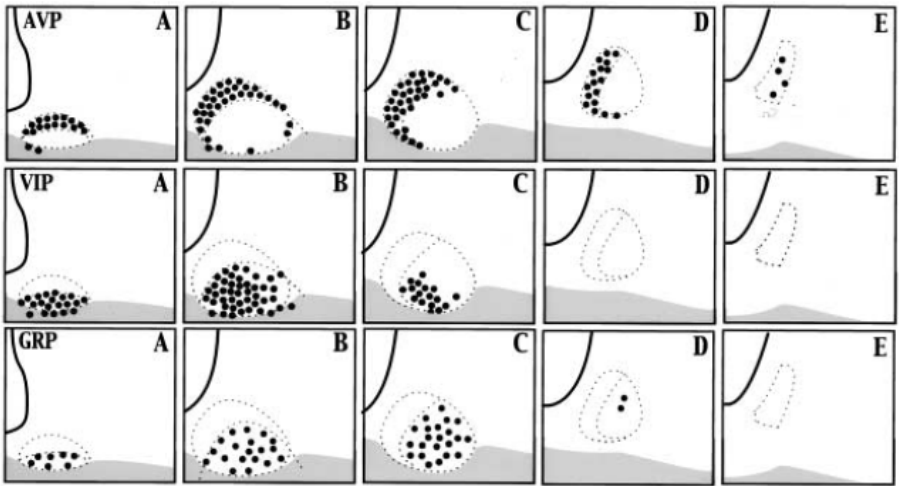

Figure 2.4 Drawings of successive rostral to caudal levels (A-E) depicting the distribution of peptide phenotype of SCN neurons. Arganine vasopressin (AVP) is mainly produced in the dorsal part of the SCN, while ventral neurons mainly produce vasoactive intestinal polypeptide (VIP) and gastrin-releasing peptide (GRP) (With kind permission from Springer Science+Business Media: Cell and Tissue Research, Suprachiasmatic nucleus organization, Vol. 309, 2002, 89-98, Moore, R.Y., Speh, J.C., Leak, R.K., part of figure 2).

The behaviour of rats and mice and hamsters can be observed by recording running wheel activity. Rats, mice and hamsters are active during the night, and their behavioural periods are in the night. It has been shown that short photoperiods leads to longer activity profiles while long day lengths lead to compressed periods of activity (Refinetti, 2002;Weinert et al., 2005). Also in Syrian and Siberian hamsters, the wheel running activity period increased in short day lengths (Elliott and Tamarkin, 1994;Nuesslein-Hildesheim et al., 2000). The total amount of behavioural activity does not increase in short photoperiods but the activity is spread out over a longer time interval (Refinetti, 2002).

The rhythms of pineal *N*-acetyltransferase activity, which is responsible for the nighttime synthesis of melatonin in the pineal gland, are also affected by day length. The melatonin level is high during the night en low during the day. Therefore, in mice (Weinert et al., 2005) and in Syrian hamsters (Elliott and Tamarkin, 1994) the phase and duration of the pineal melatonin peak is strongly correlated to the phase and duration of locomotor activity. Locomotor activity as well as the rhythms of pineal *N*-acetyltransferase

activity are both controlled by the SCN (Klein and Moore, 1979). This indicates that the SCN is directly under the influence of photoperiod (Sumova et al., 2000).

The output of the SCN, measured as locomotor activity or melatonin levels, thus shows a clear distinction between long and short day lengths. The genes that are thought to be involved in the transcriptional-translational feedback loops that compose the molecular clockwork are also affected by photoperiod. Per1 mRNA level rise occurs in the morning. In long photoperiods, the duration of the high level of Per1 mRNA is extended, while the amplitude is lower than under short photoperiods (Messager et al., 1999;Messager et al., 2000;Steinlechner et al., 2002;Sumova et al., 2003;Tournier et al., 2003). The amplitude of the expression of Per2 is higher on short days than on long days, similar to Per1 expression, but the duration of the peaks under both photoperiods does not substantially differ (Steinlechner et al., 2002;Tournier et al., 2003). Similar results were found for the level of PER1 and PER2 protein (Nuesslein-Hildesheim et al., 2000). Per3 mRNA levels do not differ in amplitude but in duration between short and long photoperiods. In short photoperiods the peak duration is not as long as in long photoperiods (Tournier et al., 2003). Cry1 mRNA rises at dawn. In a long photoperiod its phase was advanced compared to a short photoperiod. However, the duration of the Cry1 mRNA level did not change. Thus, the phase of the Cry1 mRNA rhythm only advanced in a long photoperiod without influencing the duration of the waveform. The amplitude in a short photoperiod did appear to be larger, similar to Per1 and Per2 mRNA (Sumova et al., 2003;Tournier et al., 2003). The duration and amplitude of the nightly peak of Cry2 expression decreases during short photoperiods (Tournier et al., 2003). The Bmal1 mRNA level is high during the dark period. In short photoperiods, the decrease in the morning shifts phase, the duration expands, and the amplitude decreases. This is opposite to what is observed in the daytime-active mPer1 rhythm (Sumova et al., 2003;Tournier et al., 2003). The expression of Clock is constantly high in long photoperiods, while in short photoperiods, a rhythmic pattern emerges (Sumova et al., 2003;Tournier et al., 2003). It is apparent that the clock genes all respond differently to changes in day length.

At the network level photoperiodic differences can be observed in the electrical activity pattern. The electrical activity level is high during the day and low during the night. In vitro and in vivo electrophysiological recordings show long activity during long photoperiods and short activity peaks in short photoperiods. In Syrian hamsters, the electrical activity peak, measured in vitro, is twice as broad as in short photoperiods. However, the duration of the electrical activity in 'normal' photoperiod (12:12) is not longer than in short days. It appears that the critical photoperiod of hamsters (which is 12.5 h) brings about a sudden transition towards longer electrical activity peaks (Mrugala et al., 2000). In vivo and in vitro recordings in mice show short electrical activity patterns in short photoperiod and long patterns in long photoperiod (VanderLeest et al., 2007). In rats the electrical activity pattern measured in vitro increases in width in long photoperiods. Furthermore, the amplitude of the peak decreases and is phase advanced. In short photoperiods the electrical activity pattern was narrower, with increased amplitude and delayed phase with regard to a 12 h photoperiod (Schaap et al., 2003). In rats and mice, as opposed to hamsters, no sign of a sudden transition towards a longer electrical activity peak could be identified.

In subpopulation and single cell analysis of electrical recordings it was shown that the distribution of small subpopulations of neurons in long photoperiods were more dispersed over the 24 h cycle than in short photoperiods (VanderLeest et al., 2007). This serves as an indication for a tighter coupling in the network in short day lengths and a looser coupling between the neurons of the SCN in long photoperiods.

In summary, photoperiod has a profound effect on the duration, the amplitude and the phase of many parts of the circannual and circadian system. To account for photoperiod, different models have been proposed. In the model proposed by Aschoff (1960) the parametric effects of light were emphasized. This means that the duration and intensity of light was taken to be important and resulted in a phase response curve (Aschoff, 1960;Wever, 1972). Nowadays this model is often referred to as the external coincidence model (Tauber and Kyriacou, 2001;Dawson et al., 2001). An alternative model was suggested by Pittendrigh and Daan (Pittendrigh and Daan, 1976b). In this model non-parametric effects of light were assumed to

determine photoperiodic encoding. The transitions from dark to light during dawn and from light to dark during dusk were considered to be the most important clues. This model is also referred to as the E-M model (evening-morning model) or the internal coincidence model (Pittendrigh and Daan, 1976b;Daan and Berde, 1978;Tauber and Kyriacou, 2001;Dawson et al., 2001;Elliott and Tamarkin, 1994;Sumova et al., 1995;Vuillez et al., 1996;Schwartz et al., 2001;Steinlechner et al., 2002;Weinert et al., 2005). Daan et al. (2001) tried to relate this model to available and new molecular findings. It was proposed that the Per1 mRNA levels reflected the timing of the M oscillator, while the Per2 mRNA levels determined the E oscillator (Daan et al., 2001). However, with the findings of photoperiodic effects on different clock genes, this model is no longer accepted (Sumova et al., 2003;Tournier et al., 2003).

2.5 Properties of the clock: jet lag

Another example of an alleged network driven property of the SCN is the phenomenon of jet lag, which is associated with sudden shifts in the phase of the light period. The circadian clock in mammals has an endogenous rhythm of approximately 24 hours. For humans this is somewhat longer, while for rats and mice this rhythm is a bit shorter. In normal circumstances, the daily light-dark cycle adjusts the clock every day to its 24 hour cycle by the induction of small phase shifts. Mammals experience no problems when such small corrections happen at a daily basis. However, when sudden larger shifts in phase take place, for instance as a consequence of a transatlantic flight, jet lag problems like fragmented sleep, premature awakening, excessive sleepiness and a decrement in performance can occur (Waterhouse et al., 2007;Reddy et al., 2002). Jet lag phenomena take place because the different circadian rhythms in the body are not (yet) synchronized to the new time zone (Waterhouse et al., 2007;Takahashi et al., 2002). The same phenomena can also occur with rotational shift work or sleep disturbance (Reddy et al., 2002).

The severity of jet lag increases with the number of time zones crossed and flights to the east cause more problems than westward flights (Waterhouse et al., 2007). Eastward travelers experience a shorter total sleep

time, are more active in their sleep and this sleeping phase is shifted towards earlier hours. Westward travelers experience a sleep phase shift towards later hours, but experience less sleeping problems (Takahashi et al., 2002).

The SCN is directly influenced by the daily light dark cycle, and is therefore directly affected by a sudden change in this regime. The SCN is supposed to re-entrain all peripheral oscillators to the new time regime (Yamazaki et al., 2000). Peripheral oscillators are for example rhythms in body temperature, pineal melatonin levels, plasma hormone concentrations, and organs, like skeletal muscle, liver and lung (Waterhouse et al., 2007;Yamazaki et al., 2000). These rhythms should not immediately be perturbed by external factors so that the system is able to retain a stable phase in a noisy environment. However, this protection against unrequired phase shifts also causes the problems associated with jet lag (Waterhouse et al., 2007).

In a laboratory, jet lag situations can be simulated by advancing the light phase (mimicking eastward flights) or delaying the light phase (simulating westward flights). Using these schemes, effects of phase delays and advances on different mechanisms, such as gene expression and electrical activity, in the SCN have been assessed.

After a phase delay of 6 hours, which is comparable to a flight from Amsterdam to New York, behavioral rhythms entrain very rapidly to the new regime. The transition takes less than two days. After a phase advance however, comparable to the return flight mentioned, the behavioral rhythm takes at least six days before it is completely shifted to the new phase, which emphasizes the difference between westward and eastward flight (Yamazaki et al., 2000;Reddy et al., 2002). When using a different protocol, similar differences were found between a delay and an advance of the light-dark cycle (Albus et al., 2005;Vansteensel et al., 2003;van Oosterhout et al., 2008). What becomes clear is that a behavioral phase shift due to an advance of the light-dark cycle is more difficult than due to a delay of the light-dark cycle.

Different genes have been assessed after a phase advance or delay of the light cycle. The expression of Per1 showed a rapid phase shift immediately after a delay or an advance (Reddy et al., 2002;Nagano et al.,

2003;Yamazaki et al., 2000;Vansteensel et al., 2003). In different regions of the SCN, the response appeared to be different. In the ventral part of the SCN the shifts were rapid, while in the dorsal part the shift took much longer, and an advance was more difficult than a delay (Nagano et al., 2003). Per2 expression showed the same characteristics as Per1 (Reddy et al., 2002;Nagano et al., 2003). For delays, Cry1 gene expression also showed the same characteristics, but for phase advances it took longer before Cry1 was fully re-entrained (Reddy et al., 2002).

At the network level, in vitro electrical activity measurements showed two concurrent peaks following a delay of the light-dark cycle of 6 hours. The electrical activity in the ventral SCN appeared to be shifted immediately to the new phase, while in the dorsal SCN, the shift was completed only after 6 days (Albus et al., 2005). In vitro electrical activity measurements after 6 hour advances of the light-dark cycle showed an immediate shift of about 3 hours. When the slice was prepared 6 days after the shift, the phase of the SCN was back at the old light-dark regime (so no phase shift did take place in the end). In vivo electrical activity showed no phase shift at all, indicating that the dorsal SCN does not shift and prevents the ventral SCN from shifting (Vansteensel et al., 2003). For mice, similar results are observed after phase advances of the light-dark cycle. The in vitro recordings show immediate phase shifts on the first day, while the shift obtained in in vivo recordings is only very small (van Oosterhout et al., 2008).

In conclusion, it is clear that regional differences in functionality of the SCN lead to a desynchronization of (groups of) neurons after a sudden large shift of the light-dark cycle, leading to jet lag.

2.6 Properties of the clock: arrhythmicity

Jet lag phenomena are caused by different oscillatory mechanisms of the body that run out of phase with each other. We have seen which profound problems this can cause and that only after the SCN and the peripheral oscillators are resynchronized with each other, these jet lag problems disappear.

Another well known example that disrupts behavioral and physiological rhythmicity is the exposure to constant light (LL). Hamsters show peculiar

behavior when put into a regime where the light is constantly on and no dark period is given to these night-active animals. A number of animals in such a constant light (LL) regime begin to show a so-called 'split' rhythm, which is a rhythm of 6 hours of activity and 6 hours of inactivity. So two 12-hour rhythms in one circadian day (Pittendrigh and Daan, 1976b;Zlomanczuk et al., 1991;Mason, 1991;de la Iglesia et al., 2000;de la Iglesia et al., 2003;Ohta et al., 2005). Animals may also become arrhythmic in their behavior, meaning that the animal is active and inactive irregularly throughout the 24 h day and no circadian rhythm can be observed (Pittendrigh and Daan, 1976b;Mason, 1991;Ohta et al., 2005).

Pittendrigh and Daan (1976b) developed a model for splitting that comprises two mutually coupled oscillators, an evening (E) and a morning (M) oscillator. If splitting occurs, both oscillators become 180 degrees out of phase with each other (Daan and Berde, 1978). When research progressed, splitting was shown to result from the two suprachiasmatic nuclei getting 180 degrees out of phase (de la Iglesia et al., 2000;Herzog and Schwartz, 2002;Ohta et al., 2005). However, the left and right SCN were found not to be the evening and morning component which were envisioned by Pittendrigh and Daan (Herzog and Schwartz, 2002).

A split rhythm was also found when rats were put in an extremely short light-dark regime of 22 hours (de la Iglesia et al., 2004). This is called forced desynchronization. The gene expression in the ventral part of the SCN corresponded to the 22 hour light-dark schedule, while the gene expression in the dorsal SCN was free-running with a rhythm longer than 24 hours (de la Iglesia et al., 2004). Also in this example, two parts of the SCN are desynchronized in phase.

When animals are exposed to high intensity light, they will become arrhythmic in their behavior as well as in their electrical activity (Zlomanczuk et al., 1991). Arrhythmicity in the SCN was found not to be present at the cell-level. The Per1 expression in the neurons was still rhythmic, but the electrical activity patterns of the single neurons were desynchronized and scattered over the 24 h day (Ohta et al., 2005). Total asynchrony between the SCN neurons do not necessarily stop rhythmicity in

peripheral oscillators, but can lead to decoupling of the peripheral oscillators with the SCN (Granados-Fuentes et al., 2004).

Aschoff (1960) found that the endogenous rhythms of mammals in constant light conditions varied under different light intensities. In LL, with increasing light intensity, light-active animals increase their spontaneous frequency, which means that the endogenous rhythm becomes shorter, while dark-active animals decrease their endogenous frequency. Aschoff explained this 'rule' by introducing a parametric model of light intensity. As the light intensity becomes higher, the clock runs faster (for day-active animals).

It appears that this is partly true for cells. The light responsive cells in the SCN have a threshold value to respond to light, below which they do not, or only negligibly, respond to the light input. Above this threshold value, the reaction of the cell increases or decreases monotonically with light intensity (Meijer et al., 1986). The threshold values are reached during dusk and dawn transitions (Meijer et al., 1986). However, the beginning of a light exposure period contributes more to an overall change in discharge activity than later portions of the light period (Meijer et al., 1992). This indicates that light pulses have a more profound effect on phase changes in the SCN than light intensity.

2.7 Intercellular communication: coupling between neurons

In the previous discussion on photoperiod it was shown that differences in the encoding for day length in the SCN may be explained by a change in the phase distribution between the neuronal activity patterns. For long days, the neurons are more widely dispersed in their timing of activation than in short days.

Jet lag and constant light both lead to desynchrony between populations of neurons in the SCN. Constant light conditions can lead to asynchrony or to a desynchronization between the left and right SCN. Jet lag causes a temporal desynchronization between the dorsal and ventral SCN, but the dorsal and ventral SCN resynchronize after a few days. The question arises which mechanisms in the SCN may explain these phenomena.

For proper functioning of the SCN, synchronization and phase differences between neurons and subpopulations of neurons are important mechanisms. Without synchronization stable rhythms will not occur, and phase differences provide plasticity to the biological clock. Synchronization can only occur when neurons or neuronal subpopulations can interact. Neurons and subpopulations of neurons must be able to communicate to each other about their phases. There is little known about how the phase distribution information contributes to a functioning circadian clock. Also the underlying mechanisms of synchronization are unresolved. How do the neurons transmit phase information to each other? Are the same mechanisms involved in day length encoding, in constant light, and in jet lag?

It is known that the main Zeitgeber for the SCN is the daily light-dark cycle. The photic information is a direct input to the SCN from the retinal hypothalamic tract (RHT). The retinal ganglion cells of the RHT appear to utilize the neuropeptide pituitary adenylyl cyclase-activating peptide (PACAP) and glutamate to communicate with the SCN (Hofman, 2004). The ventral SCN holds most of the neurons that receive retinal input from these cells. These SCN neurons express γ-amino butyric acid (GABA) and, often, vasoactive intestinal polypeptide (VIP) and the peptide histidine isoleucine (PHI) (Colwell et al., 2003;Harmar et al., 2002). GABA and VIP are the most likely candidates that can synchronize neurons or neuronal subpopulations.

2.7.1 GABA

GABA is produced by most of the neurons present in the SCN (Moore, et al, 2002). Jet lag studies show that GABA plays an important role in the synchronization between ventral and dorsal SCN (Albus et al., 2005). Albus et al. show that, in the rat, after a phase delay, $GABA_A$ is used to synchronize the dorsal and ventral SCN. In control slices, bimodal peaks in electrical activity are observed in both the ventral and the dorsal part of the SCN, which appear to be caused by one endogenous peak and one peak that was imposed by the other part of the SCN. Using the $GABA_A$ receptor blocker bicuculline the imposed peak in both regions disappears, leaving only the endogenous peak. This indicates that $GABA_A$ communicates the

phase of the endogenous ventral peak to the dorsal SCN, and vice versa, the endogenous dorsal peak to the ventral SCN.

Furthermore Albus et al. (2005) show that $GABA_A$ works differently in the dorsal and ventral SCN. In the ventral SCN endogenous GABA has inhibitory effects, while in the dorsal SCN it elicits excitatory responses (Albus et al., 2005). This dual role of GABA was reported before in earlier studies (Wagner et al., 1997;Wagner et al., 2001;De Jeu and Pennartz, 2002) but also contested in other studies (Gribkoff et al., 1999;Gribkoff et al., 2003). In all these studies however, it was not clear where in the SCN the measurements were performed. The finding that GABA acts differently in dorsal en ventral SCN might be a solution to this debate.

For single cell recordings, Liu and Reppert (Liu and Reppert, 2000) reported an inhibition of neuronal firing when GABA was added to the culture media. The inhibition occurred at all phases of the circadian period. However, the GABA application also elicited phase shifts (Liu and Reppert, 2000). The direction and magnitude of these phase shifts was depending on the circadian phase of treatment. Liu and Reppert (Liu and Reppert, 2000) found that only GABA acting through A-type receptors can induce phase shifts. The inhibition was mediated both through the $GABA_A$ and $GABA_B$ receptor. Liu and Reppert (2000) also succeeded to synchronize two clock cells in the same culture with opposite phase angles by applying daily GABA pulses.

Recently, Choi et al. (2008) found that GABA-expressing neurons can switch from GABA-mediated inhibition to GABA-mediated excitation, due to the expression of Na^+-K^+-$2Cl^-$ Cotransporter isoform1 (NKCC1). NKCC1 is expressing itself more in the dorsal SCN, and predominantly during the night. This indicates that GABA-mediated excitation will mainly be present during the night in the dorsal SCN.

In conclusion, there is strong evidence that GABA plays an important role in the synchronization between the dorsal and ventral SCN. GABA thus might play a role in the interregional communication of phase information between populations of neurons.

2.7.2 VIP

There are many clues that VIP may play a role in intercellular synchronization, rather than in interregional synchronization. VIP plays two roles in the SCN. Firstly, it sustains circadian rhythms of single cells. Secondly, it synchronizes single cells to one another (Welsh, 2007).

VIP signals through VPAC2 receptors, as does PACAP (Harmar et al., 2002). It has been shown that both VPAC2 receptor deficient mice (vipr2-/-) (Harmar et al., 2002) as well as VIP deficient mice (vip-/-) (Colwell et al., 2003) show weakened locomotor activity rhythms.

Harmar et al. (2002) showed that VPAC2 receptor deficient mice show only weak locomotor activity rhythms and that these mice do not actually entrain to a light-dark regime; they only show masking. This became apparent by the immediate shift of the locomotor activity rhythm in vipr2-/- mice after a phase advance or delay, whereas wild-type mice needed several days to adjust to the new regime. Also dark pulses during the day caused an increment of activity in the VPAC2 receptor deficient mice, while wild-type mice barely reacted to these pulses (Harmar et al., 2002). Finally, Harmar et al also showed that expression of clock genes (mPer1, mPer2, mCry1, mBmal1) was dramatically reduced in VPAC2 deficient mice as compared to wild-types.

It is concluded that the VPAC2 receptor is essential for the expression of robust circadian rhythms of behaviour and that the predominant factor determining the pattern of wheel-running activity in vipr2-/- mice is masking by light. The behavioural phenotype of vipr2-/- mice is associated with a lack of coordinated clock gene expression in the SCN (Harmar et al., 2002). This suggests that the VPAC2 receptor is critical for the generation and/or maintenance of rhythmic activity in the SCN (Harmar et al., 2002).

Colwell et al. (2003) developed VIP/PHI deficient mice. These mice show similar characteristics as the VPAC2 deficient mice from Harmar et al. (2002): weak rhythmicity, masking effects to a light-dark cycle and no entrainment to the light-dark regime. The vip-/- mice also show an expanded duration of their activity period (Colwell et al., 2003). Furthermore, when treated with a skeleton photoperiod with two 1-hour light pulses per 24-hour

cycle, the vip-/- mice exhibited a split rhythm of two activity periods instead of one (Colwell et al., 2003).

It appears that loss of the VPAC2 receptor is slightly more severe than loss of VIP/PHI. This indicates that many of the symptoms caused by a deficient VPAC2 receptor are due to a loss of VIP/PHI. However, other ligands, such as PACAP, also act on the VPAC2 receptor. In VIP/PHI deficient mice, PACAP can still work on the VPAC2 receptor, which may cause the less severe deficiencies in VIP/PHI deficient mice (Welsh, 2007;Colwell et al., 2003).

VIP/PHI deficient mice show masking effects to a light-dark regime, and when released in constant darkness the actual period to which they are entrained appears to have an extremely positive phase angle, as they start being active ~8 hours before lights off in the prior light-dark schedule (Colwell et al., 2003). This phenomenon is also found in the VPAC2 deficient mice and is a strong indication that VIP is required to synchronize the SCN to the external light-dark schedule (Colwell et al., 2003). Colwell et al. (2003) conclude that the function of VIP and the VPAC2 receptor can be explained in two, possibly complementary ways. First, VIP and the VPAC2 receptor may be required for the basic molecular oscillation in certain cells. Another possible explanation is that VIP and the VPAC2 receptor are directly involved in the communication between cell populations in the SCN (Colwell et al., 2003).

Aton et al. (2005) examined just these two possible functions of VIP by examining behavioral recordings and firing rates of individual neurons from vip-/-, vipr2-/- and wild-type mice. Harmar et al. (2002) and Colwell et al. (2003) used different breeds of mice for their knock-outs. Aton et al. (2005) therefore repeated their experiments in mice with the same genetic background. Compared to wild-type mice, the free-running rhythms of both vip-/- and the vipr2-/- mice were equally low and about the same percentage of mice expressed multiple periods. This confirmed that the rhythms in vip-/- and vipr2-/- mice both expressed weak circadian rhythms which are less synchronized than wild-type mice, but no differences were found between both knock-out mice (Aton et al., 2005).

Furthermore, in wild-type mice, about 70 % of the SCN neurons show circadian rhythmicity, while for both mutant types this was reduced to only 30 %. It appeared that a large proportion of neurons lost rhythmicity in the mutant mice (Aton et al., 2005). The single cell rhythms observed in the VIP and VPAC2 deficient mice are decreased in amplitude. This also indicates that intercellular signalling in the SCN, which regulates cycle-to-cycle stability of the circadian period, is decreased. Aton et al. (2005) measured that in high-density dispersals the period distribution between the SCN neurons is higher than in wild-type mice, which indicates a loss of synchrony. When a VPAC2-specific agonist was applied on a daily basis to vip-/- mice, the number of rhythmic neurons was restored to the level of wild-type mice (Aton et al., 2005), which further indicates that the VPAC2 receptor suffices for maintaining rhythmicity and synchrony between SCN neurons. Thus, Aton et al. (2005) conclude that VIP signalling through the VPAC2 receptor is promoting circadian rhythmicity in a subset of SCN neurons and it maintains synchrony between intrinsically rhythmic neurons.

In cell cultures, neurons can not synchronize their rhythms as well as in brain slice preparations in which the SCN network is preserved (Brown et al., 2007;Welsh, 2007). Maywood et al. (2006) show strong evidence for a role of VPAC2 receptors in SCN synchrony (Welsh, 2007). Maywood et al. (2006) used bioluminescence profiles to assess Per1 gene expression in the SCN and found that, compared to wild-type mice, the circadian rhythm in vipr2-/- slices was low in amplitude and also unstable, for it damped rapidly. These weak rhythms in gene expression may provide an explanation for the weak behavioural rhythms of these mutant mice (Maywood et al., 2006).

In wild-type brain slices, most Per1-expressing cells were circadian and their activity patterns were synchronized to a 4-5 hour interval. In vipr2-/- slices fewer rhythmic cells could be detected and the ones that were rhythmic were desynchronized (Maywood et al., 2006). Thus, vipr2-/- mice have a weakened rhythm in Per1 expression and the cells were desynchronized in their activity. These results confirm the results found by Harmar et al. (2002).

By depolarizing with K^+ or treatment with GRP, vipr2-/- mice can temporally get higher luminescence levels indicating that more cells become

rhythmic in Per1 gene expression and also synchronize more closely. When the treatment is stopped, the effect diminishes, because of the absence of VIPergic signals (Maywood et al., 2006). Thus, VIP appears to be essential for maintaining intrinsic synchrony of molecular rhythms in the intact SCN.

Brown et al. (2007) measured extracellular multiunit electrical activity patterns from SCN slices. The vip-/- mice showed a very weak electrical activity rhythm with variable periodicity and many peaks that were mutually out of phase. In accordance to other studies, the single cell electrical activity recordings showed that less cells in the vip-/- mice were rhythmic compared to wild-type (Brown et al., 2007). Furthermore, the vip-/- neurons showed decreased amplitude, the period was more irregular and the neurons were not clustered in phase for their peak times (Brown et al., 2007). This means that neurons in vip-/- mice are less capable of synchronizing their activity patterns to environmental light-dark schedules and to each other.

For adult mice, Brown et al. (2007) showed that the vipr2-/- mice show more severe disruptions in circadian rhythmicity than the vip-/- mice. This provides additional evidence that the VPAC2 receptor potentially carries out actions that do not involve VIP, as stated before by Colwell et al. (2003). PACAP may be a possible candidate to act on the VPAC2 receptor. Although SCN neurons do not produce PACAP, in adult brain slices RHT terminals that can produce PACAP are present in the SCN. These can be a source to activate VPAC2 receptors (Brown et al., 2007). Aton et al. (2005) used young mice in which the RHT terminals are not yet present in the SCN. This might explain why they did not find differences between vip-/- and vipr2-/- mice.

To conclude, VIP is important in coordinating the rhythmicity in the SCN, both by synchronizing intrinsically rhythmic neurons, as well as promoting circadian rhythmicity in other neurons.

2.7.3 Gap junctions

Besides chemical coupling mechanisms, electrical coupling mechanisms, or gap junctions, are often observed as mechanisms of communication between neurons in other parts of the brain. Long et al. (2005) showed that in the SCN about 26 % of the neurons are electrically coupled. They stimulated

one of a pair of neurons and measured electrical activity in both neurons. Compared to other brain areas, the percentage of electrically coupled neurons in the SCN is relatively low. Long et al. (2005) propose that electrical coupling in the SCN only occurs between neurons in specific subpopulations, in order to strengthen the output of these subpopulations. If this is the case, then electrical synapses in the SCN may form distinct networks of coupled neurons.

Long et al. (2005) show that gap junction protein connexin 36 (Cx36) seems to be the primary (if not exclusive) constituent of the electrical synapses in the SCN, because all electrical coupling was absent in Cx36-knockout mice but not in wild-type. The locomotor activity patterns of Cx36-knockout mice showed deficits in circadian behavior, especially in constant dark conditions, as well as a delayed onset of activity in the first DD cycle and a sustained reduction in circadian amplitude, indicating that light is entraining and amplifying the relatively weak circadian rhythms (Long et al., 2005). Therefore, electrical synapses, in the form of gap junctions, may play a role in the SCN for intercellular communication in order to maintain circadian rhythmicity.

Unlike chemical coupling, electrical coupling is bidirectional and symmetrical. It was observed in both dorsal and ventral SCN and the coupling strength appeared to be higher during the light phase of the light-dark cycle (Long et al., 2005). This means that the electrical coupling itself may be changing throughout the daily light-dark cycle (Colwell, 2005). This may indicate that gap-junctions actively regulate the communication between neurons depending on the time of the day (Colwell, 2005).

2.7.4 Coupling in the SCN

Summarizing the discussion, GABA seems to have an important share in the interregional communication of phases between the dorsal and ventral SCN. VIP and gap junctions might be working between neurons in a region, each in their own way. VIP might synchronize single cells within the dorsal and ventral region. GABA might synchronize populations of neurons to each other, such as the dorsal and ventral SCN. Gap junctions may strengthen certain groups of neurons in their coordinated output, which may vary in

strength throughout the daily cycle. Because of the low percentage of gap junctions in the SCN, the gap junctions may work for very specific groups of neurons.

2.8 Computer models and computer simulations of the clock

Over the years, computer models were constructed for the biological clock and computer simulations were performed to gain more information about the clock. The following section provides an overview of the circadian clock models that have emerged over time.

Around 1960, the Cold Spring Harbor Symposium on Quantitative Biology on Biological Clocks was held. At that time, not much was known about the circadian system. The location of the clock in mammals was not identified. Therefore one could only study behavioural data and temperature data. The studies revealed that there had to be an endogenous oscillatory mechanism in organisms, and that this mechanism could be perturbed by the influence of a light-dark schedule.

During the aforementioned symposium, there was general agreement on the endogenous nature of circadian rhythms (all except for the Brown lab agreed on this at that time). This endogenous clock was often represented as a single oscillator (Klotter, 1960a;Klotter, 1960b;Kalmus and Wigglesworth, 1960). These single oscillator models were fit to the behavioural experimental data available at that time. Limit cycle oscillators were used by Kalmus and Wiggelsworth to describe the pacemaker (its 'phase portrait'), where the system was in a 'phase' (referred to as θ) specified by two variables *x* and *y*, which vary over time. The dynamic system of the clock is since then often described by limit cycle oscillators. An introduction into these limit cycle oscillators seems therefore appropriate.

2.8.1 Interlude: Limit cycle oscillators

A system is called dynamic if it transfers from one state to another over time. Each state of the system can be described in terms of *N* variables, the so-called *state variables*. The number of variables involved in defining a state is the number of *dimensions* of the dynamic system (Pikovsky et al., 2001). If

the values of the state variables repeat themselves periodically, the system shows oscillatory behavior.

In order to gain a better understanding of the mathematical principles involved in oscillatory systems, a two-dimensional model system for the relation between the populations of a prey and a predator will be discussed. The two state variables in this system are the populations of both species. In an idealized situation, if the population of the prey is growing, then the population of the predator will follow. At a certain time, the numbers of predators become so high that the population of prey starts to decline. This, in its turn, causes the predator population to decrease. An example is presented in the figure 2.5 A. If we plot both populations in one graph on the two axes, we get a picture that resembles the one in figure 2.5 B.

Note that in figure 2.5 B the two state variables involved in the system are used for the axes. The curves in this state-variable-plot are closed, meaning that the system returns to a previous state every time after a period *T*. The closed curve is called a trajectory. This closed trajectory is called a *limit cycle* (Pavlidis, 1978b).

The equations belonging to the predator-prey system are (see Goel et al., 1971)

$$\frac{dx}{dt} = x(\alpha - \beta y) \tag{1}$$

$$\frac{dy}{dt} = -y(\gamma - \delta x), \tag{2}$$

where

- y is the number of some predator (for example, wolves);
- x is the number of its prey (for example, rabbits);
- t represents the time;
- dy/dt and dx/dt represents the growth of the two populations against time;
- β and δ are parameters representing the interaction of the two species; and
- α and γ are parameters representing the separate evolution of the two species.

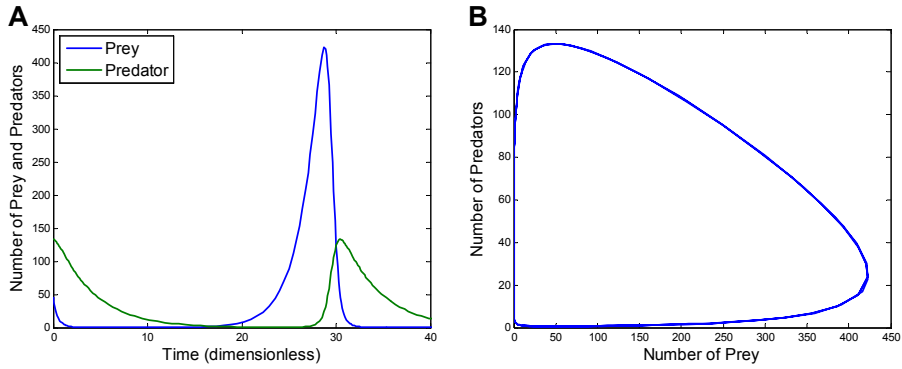

Figure 2.5 Predator – prey models. The left figure shows the population size over time. In the right figure the population sizes are plotted against each other.

Or written in a more general way

$$\frac{dx}{dt} = f(x, y)x \tag{3}$$

$$\frac{dy}{dt} = g(x, y)y. \tag{4}$$

The state of the system at a certain moment is defined by the values of the different state variables. In a limit cycle oscillator, the states of the system will return after its period *T*. It will always return to that state. We can also define the state of such a system to its *phase*, which is the angle on the cycle with respect to some initial phase (which is defined as 0). If the phase is at timepoint *T*, or 360°, the system is back at its original phase. Thus, at some timepoint t_0, the system is in a certain phase of the cycle, and after one period *T*, so at timepoint t_0+T it returns to the same phase (Winfree, 2000).

The different state variables are coordinates in the phase space (see figure 2.6 B), and its plot is called a phase portrait and the point on the limit cycle constructed by the values of the state variables is called a phase point (Pikovsky et al., 2001).

The phase as described in limit cycle models of the biological clock can be understood as subjective circadian time (CT) of the clock (Pavlidis, 1978b). Note that this phase is not one of the state variables involved in the limit cycle characteristics of the clock. What the state variables are that

describe the limit cycle behavior of the clock is not known (Kawato et al., 1982).

A special property of the limit cycle is that the original rhythm is restored when it is perturbed, just like the endogenous rhythm of the clock. Small deviations from the limit cycle trajectory tend to return to the curve after some time (Pikovsky et al., 2001).

One example of a limit cycle oscillator is the Van der Pol oscillator. Van der Pol equations describe an oscillator that has nonlinear damping, and can be used to describe the oscillations of the biological clock in a mathematical manner (Wever, 1972;Kronauer et al., 1982;Kronauer, 1990). Within certain parameter boundaries, the oscillator will become attracted to, or entrained to, the limit cycle, which ensures stable oscillations (Kalmus and Wigglesworth, 1960).

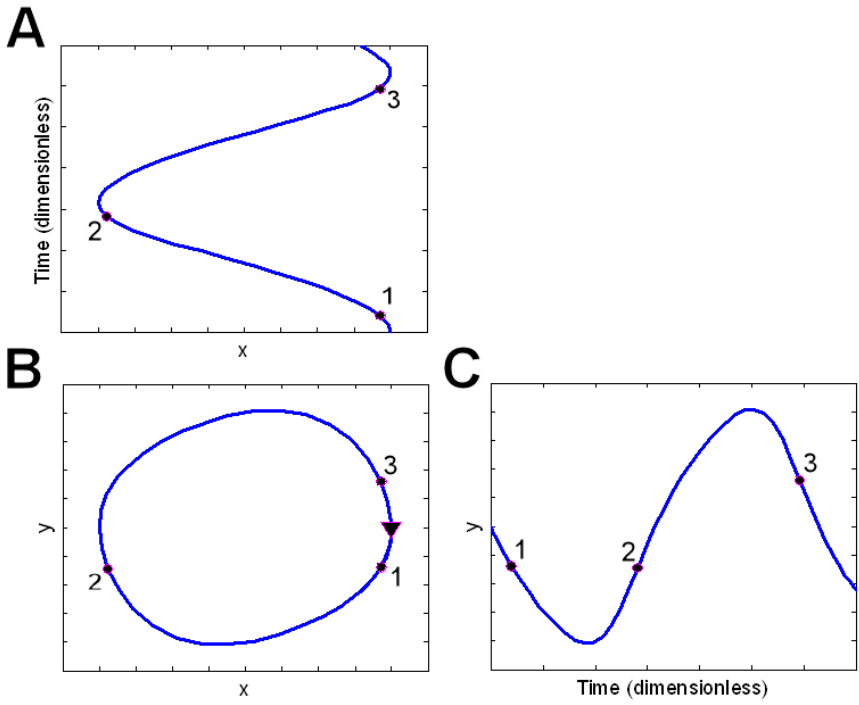

Figure 2.6 Limit cycle oscillators and their phase portrait. The two oscillating state variables *x* and *y* are oscillating in time (A and C). When the variables are plotted against each other in the phase space, the phase portrait of these two states is shown in B, where *x* is plotted on the x-axes, and *y* on the y-axes. This is a periodic function. When starting one period at the arrow, first point 1 is encountered, then point 2, and finally point 3.

2.8.2 Two-oscillator models

Before and during the Cold Spring Harbor Symposium, the endogenous circadian clock was represented as one single oscillator. However, certain behavioural results could not fully be explained by one oscillator.

In 1958 a two-oscillator model was proposed that could explain transient behaviour in phase resetting of the *Drosophila*. The so-called A oscillator is a pacemaking, self-sustaining, temperature-compensated system, which is the ultimate clock and is sensitive to light. This oscillator is supposed to shift immediately after light input. The second oscillator (called B) is coupled to and driven by the first oscillator (A) and is supposed to be light-insensitive but temperature-sensitive. Oscillator B drives the behavioural pattern. Resetting light input directly drives the A oscillator. The B oscillator takes several cycles to be re-entrained by the A oscillator, explaining the transients in behaviour (Pittendrigh et al., 1958;Pittendrigh and Bruce, 1959;Pittendrigh, 1960).

In 1976, in their famous series of articles, Pittendrigh and Daan (1976b) suggested another two-oscillator model in order to explain the phenomenon of splitting. Splitting involves a 24-h behavioural rhythm which consists of two periods of rest and of activity. The phenomenon of splitting was mainly found in hamsters. In this model the clock consists of a morning (M) and evening (E) oscillator. Daan and Berde (1978) described a mathematical system based on the E and M oscillator. They used two limit cycle oscillators, one for the morning component and one for the evening component. Each oscillator had its own endogenous period, but both oscillators were able to influence the other by resetting each others phase by a small amount on the basis of a phase resetting curve.

According to Kawato and Suzuki continuous resetting between oscillators is more plausible than resetting according to a phase resetting curve (Kawato and Suzuki, 1980). For this reason they used two identical limit cycle oscillators that are coupled continuously. If one oscillator is in rest, it does not affect the other oscillator and the coupling is symmetrical (Kawato and Suzuki, 1980). Splitting can be explained by the two steady states in which the oscillators can be synchronized: either they are *in-phase*, having a phase angle of 0°, or they are in *opposite* phase, which means that their phase is

180° separated (Kawato and Suzuki, 1980). This two-oscillator model could also describe transient phase resetting (Kawato, 1981).

Next to the two-oscillator models of Pittendrigh, Aschoff and Wever also studied two-oscillator systems that represented the clock. From the first extensive bunker experiments with human subjects (Aschoff and Wever, 1962;Aschoff, 1965a), Aschoff and Wever found that the rhythms in core body temperature and the sleep-wake cycles could diverge completely, a state they named 'internal desynchrony' (Aschoff, 1965a;Wever, 1985;Wever, 1989).

Wever modeled the 'clock' as a series of differential equations based on the Van der Pol equations (Wever, 1972). For all general clock properties, including entrainment in different light conditions according to Aschoff's rule, this model is sufficient (Aschoff, 1960;Wever, 1962;Wever, 1972). However, for special properties, like internal desynchrony, a second oscillator that is controlled by the first oscillator needs to be added to the model (Wever, 1989;Wever, 1962).

Kronauer designed a model in 1982 that was based on sleep research on humans (Kronauer et al., 1982). Humans also seemed to have two oscillatory processes: the sleep-wake process and a temperature oscillator. Kronauer modeled these by two Van der Pol oscillators. Also in this system of differential equations the coupling is continuous, as in the model of Kawato and Suzuki (Kawato and Suzuki, 1980) and unlike the model of Wever. In Wever's model, the second oscillator was controlled by the first oscillator but did not feed back to the first oscillator (Wever, 1962;Wever, 1989). By decomposing the sleep-wake process oscillator into two oscillators, one for a wake cycle, which determines the onset of sleep, and one oscillator for the sleep cycle, determining the onset of awakening, Kawato et al (1982) created a three oscillator model to describe the problem of internal desynchrony.

Note that a two-oscillator model can be described by one limit cycle oscillator. However, the dimensionality of the oscillator would then increase and the mathematics would become difficult to understand, and would not contribute to the understanding of the circadian clock mechanism (Kawato, 1981). Using two oscillators provides a better understanding of the mechanisms that may govern the clock.

The two-oscillator models could thus explain splitting, transient behaviour, after-effects and Aschoff's rule. In the 1980s the sleep homeostasis 2-process model was introduced. By that time there was general consensus that the suprachiasmatic nuclei contained the mammalian circadian clock. When the electrical activity of the SCN could be measured (Groos and Hendriks, 1982) the research focused on the activity rhythms of the SCN itself, instead of the driven rhythms such as the behavioural or temperature rhythms.

With the process S model for the sleep-wake cycle in place and the available data of the SCN, Kronauer updated his earlier model in 1990. He created a model based on two Van der Pol oscillators and added the forcing effects of light to this model (Kronauer, 1990). This was fit to experimentally obtained temperature data from human subjects.

The model was as follows

$$\frac{24}{2\pi}\frac{dx}{dt} = y + \varepsilon(x - \frac{4}{3}x^3) + B \tag{5}$$

$$\frac{24}{2\pi}\frac{dy}{dt} = -(\frac{24}{\tau})^2 x + By \tag{6}$$

$$B = (1 - mx)CI^{\frac{1}{3}}, \tag{7}$$

where

- x and y are the state variables of the oscillator,
- τ denotes the endogenous period of the oscillator,
- ε is the stiffness of the oscillator,
- B is the brightness; which is the influence of light on the oscillator,
- I is the light intensity in lux,
- m the modulation index weighting the magnitude of the feedback of the oscillator,
- C a constant.

This model was able to predict experimentally obtained data (Klerman et al., 1996), however it did not adhere to experimental data obtained in bright or dim light conditions and after brief light stimuli. Therefore the Kronauer model was refined (see figure 2.7). The light input was updated to contain a

new pre-process, called L, which processes the light intensity *I* and produces a drive $\hat{B}$ that serves as the light input into the circadian system, which is called process P. Process P contains a stimulus modulator (*S.M.*) and the circadian oscillator (~). The stimulus modulator (*S.M*) does not receive direct light input, but receives the drive $\hat{B}$. Depending on the phase of the oscillator, the stimulus modulator (*S.M.*) produces a modulated drive *B*, which can adjust the phase and amplitude of the oscillator (~). The process that modulates the light input in the previous model was only depending on the state variable *x*. In the new model this process is replaced by the stimulus modulator (*S.M.*) and this process is now dependent on both state variables *x* and *y* (Kronauer et al., 1999;Jewett et al., 1999).

Interesting new viewpoints were provided by Achermann and Kunz (Achermann and Kunz, 1999;Kunz and Achermann, 2003). Where Kronauer and his team used the Van der Pol oscillator in their model as a single oscillatory unit describing the SCN as a whole, Achermann and Kunz use this same oscillator model to describe only one oscillatory neuron in the SCN. They used the model of Kronauer (Kronauer, 1990) and added a coupling term to each oscillatory unit, so that the oscillators can 'communicate' about their phase and amplitude with other oscillators in their neighborhood, through the use of local coupling with either 4, 8 or 20 surrounding cells. They placed 10,000 of these oscillators in a regular grid of 100 by 100 units. The global output of the SCN as a whole is given as the arithmetic average of the values of all oscillators (Achermann and Kunz, 1999). This was an attempt to create a model on the basis of a network of oscillators. However, the coupling mechanisms between the units were not very realistic, because they were based on the mathematical notion of neighborhood coupling.

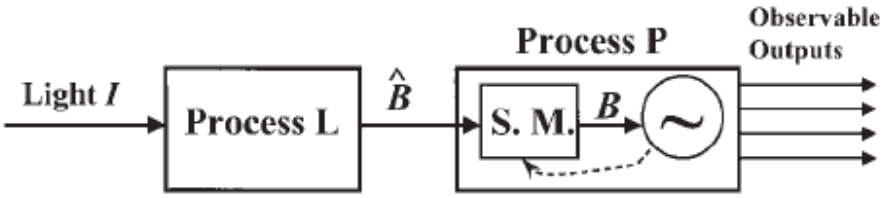

Figure 2.7 Updated model for circadian rhythms and light influence. The light input enters the clock through a pre-process, called L, which processes the light intensity *I* and produces a drive $\hat{B}$ that serves as the light input into the circadian system, which is called process P. Process P contains a stimulus modulator (*S.M.*) and the circadian oscillator (~). The stimulus modulator (*S.M*) does not receive direct light input, but receives the drive $\hat{B}$. Depending on the phase of the oscillator, the stimulus modulator (*S.M.*) produces a modulated drive *B*, which can adjust the phase and amplitude of the oscillator (~). (Reprinted from Journal of Biological Rhythms 14, Jewett et al, 1999).

2.8.3 Molecular models

It has become clear that the circadian system is a heterogeneous system containing endogenously oscillating pacemaker cells. This insight affected the construction of the models. Some models were developed to describe primarily the interaction between the neurons to describe the SCN network output. The second line of research focused on modeling the endogenous pacemaker cell, and the generation of circadian rhythms itself.

The Goldbeter group developed an impressive number of molecular models for circadian pacemaker cells of different species (Goldbeter, 1995;Leloup and Goldbeter, 1998;Leloup et al., 1999;Leloup and Goldbeter, 2000;Leloup and Goldbeter, 2001;Leloup and Goldbeter, 2003;Leloup and Goldbeter, 2004). The models described the circadian expression of genes and their protein products. These models were based on the model first proposed by Goodwin, where a protein that represses the transcription of its own gene is able to produce sustained oscillations in the levels of protein and mRNA (Goodwin, 1965;Griffith, 1968). Drescher was the first to use this model in the field of circadian rhythms to determine PRCs with respect to transient perturbations (Drescher et al., 1982).

The first model from the Goldbeter group described the rhythmic expression of Per in the Drosophila clock (Goldbeter, 1995). The period of

the rhythm arises because of the cascade of phosphorylation states the protein goes through, in which each step introduces a time delay.

The following kinetic equations describe this model (see figure 2.8)

$$\frac{dM}{dt} = v_s \frac{K_I^n}{K_I^n + P_N^n} - v_m \frac{M}{K_m + M} \tag{8}$$

$$\frac{dP_0}{dt} = k_s M - V_1 \frac{P_0}{K_1 + P_0} + V_2 \frac{P_1}{K_2 + P_1} \tag{9}$$

$$\frac{dP_1}{dt} = V_1 \frac{P_0}{K_1 + P_0} - V_2 \frac{P_1}{K_2 + P_1} - V_3 \frac{P_1}{K_3 + P_1} - V_4 \frac{P_2}{K_4 + P_2} \tag{10}$$

$$\frac{dP_2}{dt} = V_3 \frac{P_1}{K_3 + P_1} - V_4 \frac{P_2}{K_4 + P_2} - k_1 P_2 + k_2 P_N - v_d \frac{P_2}{K_d + P_2} \tag{11}$$

$$\frac{dP_N}{dt} = k_1 P_2 - k_2 P_N \tag{12}$$

The total quantity of PER protein is given by

$$P_t = P_0 + P_1 + P_2 + P_N , \tag{13}$$

where

- M is the concentration of *per* mRNA
- P_0 is the concentration of unphosphorilated PER protein
- P_1 is the concentration of monophosphorilated PER protein
- P_2 is the concentration of biphosphorilated (or fully phosphorilated) PER protein
- P_N is the concentration of PER protein in the nucleus
- P_t is the total quantity of PER protein
- v_s is the maximum rate of accumulation of Per mRNA in the cytosol
- v_m is the maximum rate of cytosolic Per mRNA degradation
- v_d is the maximum rate of degradation of biphosphorylated PER protein
- $V_{1\text{-}4}$ denote the maximum rate of kinase and phosphotase in the reversible phosphorylation of P_0 into P_1 and P_1 into P_2.

- k_s is the first-order rate constant for the synthesis of the PER protein (P_0) from Per mRNA.
- k_1 is the first-order rate constant for the transport of fully phosphorylated PER protein (P_2) into the nucleus (P_N)
- k_2 is the first-order rate constant for the transport of nuclear PER protein (P_N) into the cytosol (P_2)
- K_m, K_d, and K_{1-4} are Michaelis constants
- K_I is the threshold constant for repression of *per* transcription by nuclear PER protein concentrations (P_N)

This model shows a rhythm in total PER protein (P_t) and in Per mRNA level (M). These two levels are treated as state variables for the limit cycle oscillator.

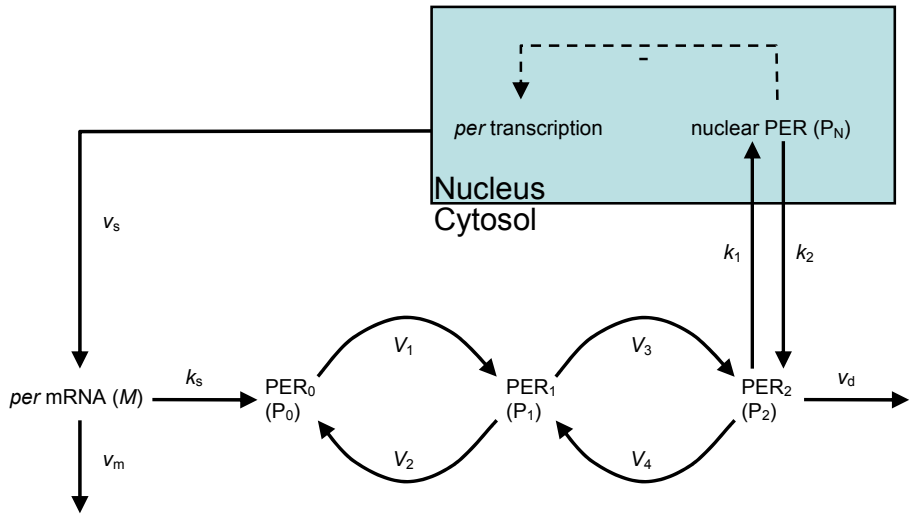

Figure 2.8 Molecular model for Per expression in the Drosophila clock. *per* mRNA (M) is synthsized in the nucleus and transfers to the cytosol, where it accumulates at a maximum rate v_s. In the cytosol, the *per* mRNA is degraded with maximum rate v_m and synthesized into PER protein with a maximum rate k_s. PER protein can be present in different phosphorylation states, P_0, P_1, and the fully phosphorylated form P_2. The maximum rate of phosphorylation and dephosphorylation between the phosphorylation states is characterized by the parameters V_i. P_2 is degraded at a maximum rate v_d and transported into the nucleus according to rate constant k_1. The transport of the nuclear, fully phosphorilated form of PER (P_N) into the cytosol is characterised by constant k_2. The nuclear PER (P_N) negatively feeds back on *per* transcription. (Reprinted from Figure 1 in Goldbeter, A., 1995. A model for circadian oscillations in the Drosophila period protein (PER). Proc. R. Soc. Lond. B 261, page 320, with kind permission of Royal Society Publishing)

In 1998, the Tim gene cycle was added to the model (Leloup and Goldbeter, 1998). Two interlocked loops can account for more complex behaviour as is observed from the circadian system, such as rhythm splitting and arrhythmicity. The equations that are used to describe this model are similar to the ones that describe the simpler version of this model, with only Per. The model is depicted in figure 2.9.

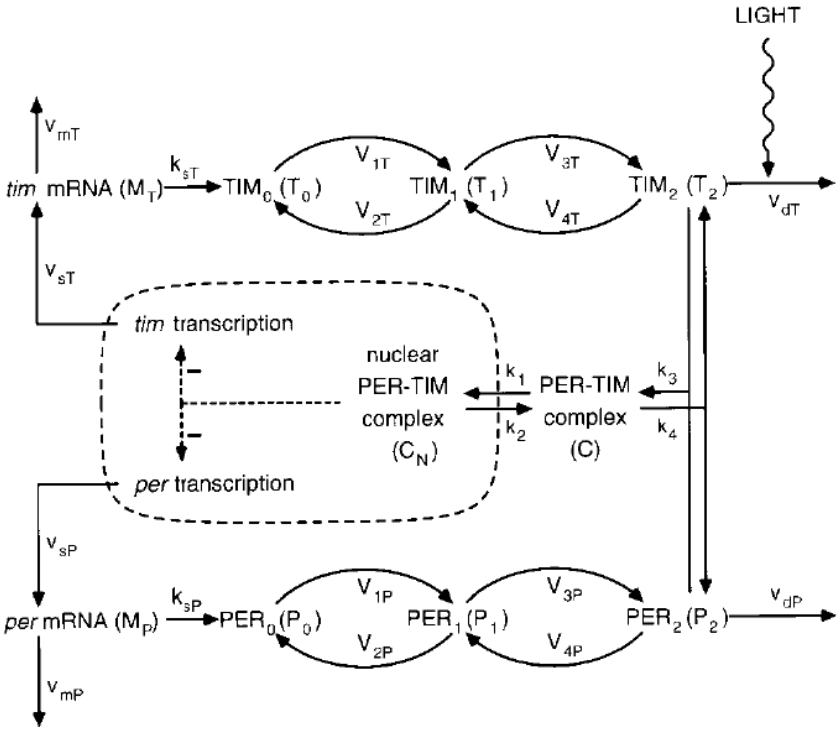

Figure 2.9 Addition of the Tim gene cycle describing the clock of *Drosophila* to the model described in figure 2.8 (Reprinted from Journal of Biological Rhythms 13, Leloup and Goldbeter, 1998).

Different modifications of the model were made, and the model was also designed for the Neurospora circadian clock (Leloup et al., 1999;Leloup and Goldbeter, 2000;Leloup and Goldbeter, 2001). When the clock genes for the mammalian clock were identified, the model was transferred to a mammalian circadian clock model, involving the Per, Cry, Bmal1, Clock, and Rev-Erbα genes (Leloup and Goldbeter, 2003;Leloup and Goldbeter, 2004). A similar molecular model for the mammalian clock was created by Forger and Peskin. In their model more effort was made to precisely mimic

the molecular components that play a role in the clock cell (Forger and Peskin, 2003;Forger and Peskin, 2004;Gallego et al., 2006).

2.8.4 Network models

In 1967, Winfree speculated on the clock being a network of coupled oscillators (Winfree, 1967). Interestingly, Daan and Berde also speculate on the nature of both oscillators, and suggested that each may consist of a multitude of tightly coupled oscillators (Daan and Berde, 1978).

Winfree was probably the first who proposed that certain clock properties were network properties instead of the properties of a single oscillator (Winfree, 1967). In order to investigate the rhythmical interaction of populations of periodic processes, he introduced the "generalized relaxation oscillator". This is a limit cycle oscillator which has weak coupling. The phase (φ) is always close to the phase of an entraining periodic stimulus (θ). The maximal difference from θ is ψ. Besides the influence of the Zeitgeber (θ), the oscillators themselves also influence each other's phase. The two state variables for the limit cycle oscillators are the Influence Function $X(\varphi)$, which represents "all effects by which an oscillator makes its presence and phase known to others", and the Sensitivity Function $Z(\varphi)$, which represents the "sensitivity to stimuli of some sort S with which we will perturb it". Using these two state variables, Winfree was able to simulate a population of oscillators, that had similar, but not necessarily the same, periods. These oscillators were attracting each other and became synchronized with a stable period as though it was one oscillator. With this intuition, Winfree was the first to suggest that the circadian clock consisted of a multitude of differently phased oscillators, that were synchronized in order to produce a unified output signal (Winfree, 1967).

A number of other studies followed this line of thought, where 'simple' oscillators were placed in a network and coupling was studied using the theoretical mathematical mechanisms of coupled oscillators (Pavlidis, 1971;Pavlidis, 1978a). The theory of coupled oscillators was discovered by the famous Dutch scientist Christiaan Huygens when looking at two pendulum clocks swinging in perfect synchrony, and is discussed in relation to circadian clocks by Strogatz and coworkers (Strogatz and Stewart,

1993;Mirollo and Strogatz, 1990;Strogatz, 2003). The study of coupled oscillators showed that a stable rhythm could arise from a population of less reliable oscillators (Enright, 1980a;Enright, 1980b).

The network models discussed use artificial oscillators that represent the neurons in the SCN. Furthermore, they use theoretical connection and synchronization schemes between the single units. The network models that follow gain realism. First, more realistic molecular models are introduced to represent the neurons in the network models. Second, the network topology of the SCN is taken into account in the coupling mechanisms of the SCN.

Bernard et al. (2007) have modeled SCN neurons in a similar fashion as the Goldbeter group. However, in their study, a coupling term was added to the equations of the oscillators, where the coupling was based on the concentration of one of the phosphorylation phases of the PER/CRY protein complex. The coupling between the oscillators was tested using three types of coupling: random coupling, nearest neighbor coupling and a coupling scheme based on the ventral-dorsal and left-right distinction of the SCN. Their main finding was that oscillators of which the rhythms would normally damp out, could remain rhythmic when they were coupled to other damped oscillators. The coupling between damped oscillators actually sustained the rhythmicity of the network (Bernard et al., 2007).

The work of Achermann and Kunz can also be seen as representatives of the models that add more realistic molecular models to the network models (Achermann and Kunz, 1999;Kunz and Achermann, 2003). However, the coupling schemes are still derived from mathematical constructs, and not so much from realistic coupling between SCN neurons. The models from Bernard et al and Achermann and Kunz use theoretical coupling patterns to describe the interaction between the single cells instead of more realistic coupling mechanisms between the neurons. Other models turned their focus on more realistic coupling schemes between the single cells.

Antle et al. (Antle et al., 2003;Antle et al., 2007) model the SCN as consisting of two regions, the ventral region and the dorsal region. The “gate cells”, situated in the ventral region of the SCN, synchronize the oscillator cells, which are situated in the dorsal SCN. An oscillator cell is modeled by

a polar parameterization of the Van der Pol equation, suggested by Forger and Kronauer (2002)

$$\frac{dr}{dt} = -\omega r \cos(\theta)^2[-1 + r^2 \cos(\theta)^2] \quad (14)$$

$$\frac{d\theta}{dt} = \omega[-1 + \varepsilon r^2 \cos(\theta)^3], \quad (15)$$

where

- the polar coordinate form uses an angle, θ, and a radius, r, to map a point's location relative to the origin
- ω is the frequency of the oscillator
- ε is the "stiffness" coefficient that determines how closely the oscillator mimics a cosine curve.

The gate cells in the ventral SCN reset an oscillator by pushing its phase closer to the average phase of the ensemble in a linear fashion. The resetting function has two parameters. The *slope* of the resetting function represents the strength of the resetting. A slope of 0 would bring every oscillator back to the gate point every time the gate fired; a slope of 1 would have no effect. The second parameter is the *point of intersection with null resetting function*, which determines what phases are advanced and what phases are delayed when the gate is triggered. Note that the oscillators themselves are not coupled in this model. Antle, et al. conclude that this model shows that gate cells, which are under the influence of light, can be important for creating synchronization between the oscillating cells in the SCN and different strengths of the gate cells can explain a decreased synchronization (Antle et al., 2003).

Gomes Cardoso, et al. defined a model that takes into account the biological realism in the coupling and especially in different SCN regions (Gomes Cardoso et al., 2009). The ventral region is an input region which sends output to the dorsal region, similar to the model of Antle, et al. (2003). The dorsal region is defined as a three-dimensional grid, which resembles the model of Achermann and Kunz (1999). In the dorsal region the neurons are connected to each other, in contrast to the Antle model, because in that model the dorsal neurons were not coupled to each other. The dorsal neurons

are able to modify each others frequencies because of this coupling (Gomes Cardoso et al., 2009).

Beersma et.al. (2008) extends the coupled oscillator studies by adding to the coupling mechanisms of the oscillators more realistic SCN neuronal properties, without trying to model precisely the cell itself. A cell can be actively firing or be silent. The exact mode of operation can be influenced by the light dark cycle and by other pacemaker cells. All cells are influencing all other cells. Using a simplified version of a single cell representation instead of a realistically feasible neuronal model, the authors are able to obtain SCN properties that arise purely from the network level (Beersma et al., 2008).

Many other models have been created in the field of circadian rhythms. This selection provides a sufficient overview of the different lines of research in modeling the biological clock. A number of modeling techniques have been discussed and different approaches have been mentioned. One can model one single neuron, or one can model the whole SCN. One can focus on realistic models of the neuron, or one can focus on coupling between neurons. Depending on the research question one approach is preferred over another.

2.9 Conclusions

The circadian clock is endogenously rhythmic which can be explained by a molecular feedback loop within neurons of the SCN. These endogenously rhythmic neurons are synchronized to each other to produce a rhythmic output pattern. Synchronization of the neurons can be explained by different coupling mechanisms between the neurons. The clock can be entrained to the environmental light-dark cycle and responds to seasonal differences in day length. Different functional regions can be distinguished in the SCN, which have a specific function in the entrainment of the clock. Within and between these regions, neurons may show different coupling mechanisms. To investigate the organization of the SCN and the coupling mechanisms between neuronal subpopulations, computer models and simulations can be employed to guide experiments and gain insight in possible working mechanisms.

Models are always based on reality. They are designed to provide answers to questions related to everyday life. However, it is not always necessary to create a model that captures as many aspects of reality as possible. Sometimes, a 'simple' model that connects to only one small property of reality is as good as any larger model that tries to explain many aspects of real life. An important criterion for the use of a model is that the model should be sufficient to address the research question at hand. Depending on the research question the complexity of the model and the simulations should be determined. The purpose of the simulations should be thoroughly considered. What is it that the simulation should do? Is it to show how a system works? Or should the simulation provide answers to certain specific questions?

One should always remember that simulations alone can not provide irrevocable evidence for the subject under investigation. However, if the boundaries are defined well, it is possible to find answers to a specific question. With the answers that are found, new questions arise. At least some of these questions need experimental testing. When a question is defined too strictly, it is not possible to answer questions that lie outside the model. If other questions need answers, such as the underlying mechanisms of certain phenomena, new models are required that are designed with close regard of the boundaries needed for that specific question.

If these constraints to modeling and simulation are taken into consideration, the results coming from simulations can provide interesting insights and can be very valuable to guide experiments and research. In the next chapters of this thesis, simple models are used to simulate attributes of the circadian timing system where the network organization of the SCN and the coupling between subpopulations of neurons is involved.

Chapter 3

Simulation of day length encoding

3.1 Introduction

To anticipate 24 h rhythms in the environment, organisms have innate circadian systems, or clocks, that have a genetic basis for rhythm generation (Takahashi et al., 2001;Reppert and Weaver, 2002). For the proper functioning of these circadian systems, they have to be synchronized, or entrained, to the daily external cycle. The most important synchronizing stimulus in the environment is light, rather than the change of temperature or other environmental stimuli (Meijer and Rietveld, 1989;Morin and Allen, 2006).

Seasonal changes in the environment are caused by the earths' rotation around the sun, resulting in changes in day length in the course of the year. Changes in day length are perceived by animals, and are used to determine the time of the year. Adaptations to the changing seasons can be observed in many different organisms, and are commonly referred to as 'photoperiodicity'. In mammals, information on day length is transmitted to and processed by the SCN. As a result, the SCN plays a crucial role in controlling both daily and seasonal rhythms (Mrugala et al., 2000;Sumova et al., 1995;Sumova et al., 2003). The rhythm generating capacity of SCN neurons is explained by a molecular feedback loop, in which protein

products inhibit the expression of specific clock genes (Kume et al., 1999;Reppert and Weaver, 2002;Hastings and Herzog, 2004). Rhythms in clock gene expression or in their protein products can be recorded within the SCN (Abe et al., 2002;Reddy et al., 2002;Hastings et al., 2003;Hastings and Herzog, 2004;Hamada et al., 2004;Nakamura et al., 2005;Nagano et al., 2003;Maywood et al., 2006). The rhythms show sinusoidal patterns, and for most (but not all) clock genes, expression is high during the day and low during the night.

Likewise, circadian rhythms can be recorded in electrical impulse frequency in the SCN (Gilette et al., 1993;Groos and Hendriks, 1982). The electrical impulse frequency of neuronal populations of the SCN is high during the day and low during the night. The electrical impulses are thought to be a major output of the SCN (Schwartz et al., 1987) and carry information on the time of day to other parts of the brain, including the pineal gland. Under long or short photoperiods, the waveform changes that are generated by the SCN show remarkable changes. In long days, gene expression profiles show long durations of elevated activity, and electrical activity patterns are broad, while in short days, the expression profiles and electrical activity patterns show narrow activity peaks (Mrugala et al., 2000;Schaap et al., 2003;Sumova et al., 1995;Sumova et al., 2003). Recordings of single cell electrical activity and of Per1 gene expression profiles have shown that neurons show phase differences (Brown et al., 2005b;Schaap et al., 2003;Yamaguchi et al., 2003;Quintero et al., 2003). Moreover, it has been shown that individual neurons of the SCN exhibit electrical activity patterns that are remarkably short as compared to the population waveform pattern.

We show that a broadening or narrowing of the multiunit pattern can be based on changes in phase differences between neurons, as well as on changes in the circadian pattern of individual neurons. However, these mechanisms give rise to differences in the maximal discharge level of the multiunit pattern, leading to testable predictions to distinguish between the two mechanisms. If single units broaden their activity pattern in long days, the maximum frequency of the multiunit activity should increase, while an

increase in phase difference between the single unit activity rhythms should lead to a decrement in maximum frequency.

It has been proposed that in short days, phase differences between neurons decrease, while in long days they increase. Recordings of mouse SCN neurons under short and long day length have confirmed these predictions. Long term recordings of the electrical activity patterns of single SCN cells have shown an increment in phase distribution among oscillating neurons in long days and a decrease in phase distribution in short days (VanderLeest et al., 2007). While the precise phase distribution between the neurons is significantly different between long and short days, the available data do not allow quantifying the distribution.

The simulations also show that coding for day length by an evening and morning oscillator is not self-evident and will only work under a limited set of conditions in which the distribution within each component and temporal distance between the components is taken into account.

In the present study, we combine the results from rat and mouse SCN recordings with simulation experiments, and investigate the influence of different phase distributions between the neurons on the population activity patterns of the rat and mouse SCN.

While our simulations were based on single cell and multiunit electrical activity patterns, they are also relevant for understanding the relation between single cell and population molecular expression profiles.

3.2 Methods

The simulations were aimed to evaluate the contribution of single clock neurons to the overall electrical output of the mammalian circadian pacemaker. Simulation software was implemented in Matlab, a high-level technical computing language and interactive environment (Matlab, 2007). The simulations involved the calculation of the multiunit activity pattern from single unit activity patterns. The multiunit activity pattern was simulated by distributing single unit activity patterns over the circadian cycle and then adding up the equally weighted activity of all single units. The intrinsic parameters of the simulation were the shape and width of the activity pattern of the single unit, the type of the distribution, the phase

difference of the single unit patterns over the cycle and the number of single units that constitute the multiunit pattern. We investigated the effects of parameter changes on the width of the multiunit activity pattern at the half maximum amplitude (c.f. Schaap et al., 2003). The amplitude of the simulated multiunit patterns was normalized to enable qualitative predictions, except for figures 3.7, 3.8 and 3.9, where quantitative changes in population pattern were examined. The results were compared with multiunit patterns recorded under three different photoperiods; short day length (LD 8:16), normal day length (LD 12:12) and long day length (LD 16:8). The single unit pattern as well as the distribution could independently be narrowed or broadened. The results could be graphically presented with or without photoperiod indication, single units, and an indicator of the width of the pattern.

We used different waveforms for the single unit activity patterns, or used measured single unit patterns (rat: Schaap et al., 2003; mouse: VanderLeest et al., 2007). The single unit activity patterns were established by calculating the mean single unit activity pattern from the different recorded units. These units had been recorded in acutely prepared slices with stationary electrodes. For this purpose, the peaks of all normalized single unit activity patterns were aligned. The effects of different single unit activity patterns and of different distributions between these neurons on the multiunit activity pattern were evaluated.

We used four different distributions in our simulations: a linear, normal, bimodal and trimodal distribution. The linear distribution was used in Schaap et al. (2003) and spreads the single unit activity patterns linearly over the light period with the peak of the first unit at light onset and the peak of the last unit at light offset (figure 3.1 D). In the normal or Gaussian distribution the single unit activity patterns were normally distributed over a certain time window within the circadian cycle, where the Gaussian distribution was characterized by $e^{-(x-\mu)^2/2\sigma^2}/(\sigma*\sqrt{2\pi})$ (figure 3.1 E). The distribution used in our simulation is not a proper Gaussian distribution, but its tails are cut off as we deal with a repetitive signal with a period of 24 hours. The σ could be changed from low values (narrow distribution) to high values (broad distribution). A bimodal distribution was used to simulate

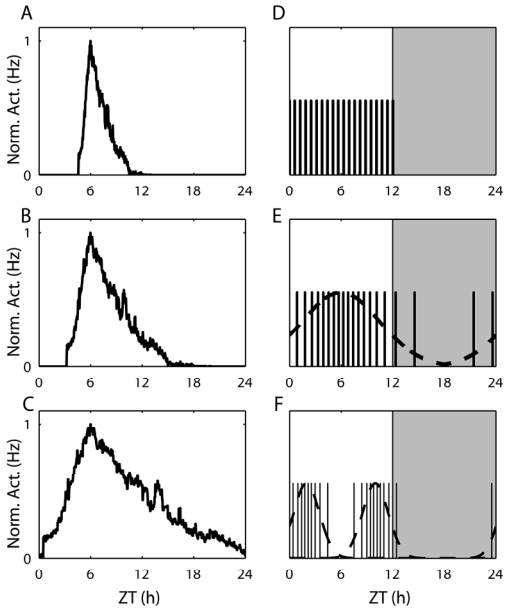

Figure 3.1 Single unit activity patterns and distributions. (A) A narrow single unit activity pattern, (B) a measured single unit activity pattern, and C a broad single unit activity pattern. The measured pattern is the average from 9 recorded single unit activity patterns. Patterns (A) and (C) are derived from the measured pattern (B) by modifying it to half or to twice its width. The maximum frequency of each pattern is normalized and is set to ZT 6. (D) – (F) Different distributions of peak times of single units. (D) A linear distribution in a normal photoperiod (LD 12:12). (E) A normal distribution over a 24-hour period. (F) A bimodal distribution with means at ZT 2 and ZT 10.

evening and morning oscillators (figure 3.1 F). This distribution has two components, and each of them was given either a Gaussian or a linear distribution. The first component was set around light onset and the second component around light offset. The distance between the components, measured in hours, as well as the distribution within the components could be manipulated. The trimodal distribution obtained an additional component at midday.

To account for changes in multiunit activity patterns that occur through seasonal changes, simulations were performed to investigate waveform changes in three different photoperiods. We investigated the effects of changing the phase relation between the single units in the linear, normal or bimodal distribution on the width of the multiunit pattern. In addition, we investigated the outcome of changes in single unit activity patterns. A change in waveform of single unit activity patterns was achieved by

narrowing the width by half or broadening it twofold (figure 3.1 A-C). In addition, the effects of a range of widths of single unit activity patterns on the multiunit pattern were investigated.

Multiunit activity patterns were quantified by their peak width. The peak width, or the duration of electrical activity, was defined as the time difference between the half-maximum amplitude of the rising and declining phase of the rhythm (figure 3.2). Mice and rats are nocturnal and therefore active during the night. The SCN electrical activity patterns of rodents show high activity during the day and low activity during the night. Thus, the half-maximum amplitude of the rising phase of the rhythm coincides with activity offset, and the half maximum of the declining phase with activity onset.

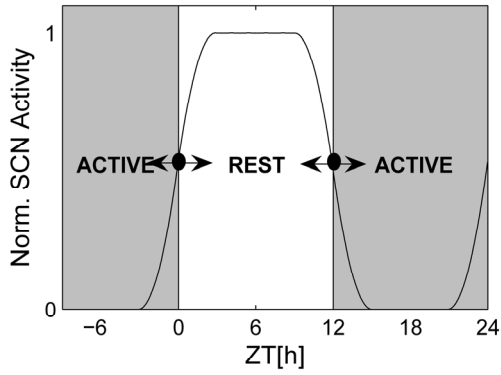

Figure 3.2 SCN electrical activity in nocturnal rodents. Rats and mice are active during the night, when the electrical activity of the SCN is low, and rest during the day, when the electrical activity of the SCN is high. The peak width, or duration of electrical activity, was defined as the difference between the half-maximum amplitude of the rising and the declining phase. For short days, the resting phase becomes smaller and the activity phase becomes longer, while for long days, the resting phase increases and the activity interval decreases. In the figure, the darker background denotes nighttime, while the white background denotes daytime.

3.3 Results

3.3.1 From single cell to multiunit pattern

Single unit activity patterns that have been measured in the rat and mouse are relatively narrow as compared to the population activity pattern. In rats, kept in 12 h light-12 h dark schedules, the mean width of a single unit activity pattern is 4.4 ± 0.6 h (see figure 2 A in Schaap et al., 2003). In mice, the mean duration of single unit activity was 3.48 ± 0.29 hr (n = 26) kept in short days (LD 8:16) and 3.85 ± 0.40 hr (n = 26) kept in long days (LD 16:8) (VanderLeest et al., 2007). It has been shown that neurons show differences in phase (Brown et al., 2005b;Schaap et al., 2003), and that their summed activity pattern accounts for the ensemble behavior of the population.

We simulated multiunit patterns from measured single unit patterns that either were or were not distributed over the circadian cycle. When the single units are not distributed and are all active at the same time, the obtained multiunit pattern is narrow (figure 3.3 A).

When, on the other hand, single units are distributed in phase, a broader multiunit activity pattern is obtained (figure 3.3 B). This broader pattern resembles the multiunit activity pattern that is measured with stationary electrodes in rat slices (figure 3.3 C) (Brown et al., 2005b;Schaap et al., 2003;Gilette et al., 1993;Prosser, 1998;Yannielli et al., 2004;Groos and Hendriks, 1982). To investigate the influence of the number of recorded neurons on the multiunit activity pattern, we varied the number of neurons in the simulation. At first, an arbitrary number of 10 single unit activity patterns were distributed over the day (figure 3.4 A). This results in a multiunit activity pattern with a width of 13.12 h, which is similar to data from slice recordings, although there are more fluctuations in the signal. An increase in the number of units renders a smoother multiunit activity pattern that becomes slightly more narrow (figure 3.4 A-C).

Different distributions of single unit activity patterns can all lead to multiunit activity patterns that resemble recorded patterns. A Gaussian distribution ($\sigma = 180$) results in a multiunit activity pattern with a width of 12.21 h (figure 3.4 D). A bimodal distribution, with the mid of the first component at ZT3 and the mid of the second component at ZT9 (each with σ

= 135), renders a peak width of 12.05 h (figure 3.4 E). Finally, a trimodal distribution with the mid of the 3 components at ZT2, ZT6, and ZT10 (each with σ = 135) renders a peak width of 12.38 h (figure 3.4 F). We conclude that for all distributions, solutions exist that lead to a realistic multiunit pattern.

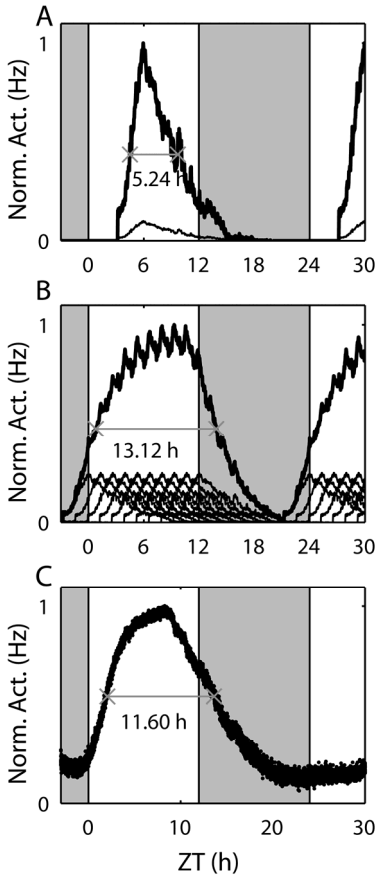

Figure 3.3 Multiunit activity pattern recording and simulation based on the single unit activity patterns as used in figure 3.1 *B*. (A) Single unit patterns with their peaks in electrical activity at the same time (ZT 6). An added multiunit pattern of an arbitrary number of 10 neurons is shown. The single unit patterns are indicated at the bottom. The resulting multiunit pattern is narrow as compared to the recorded pattern of (C). (B) Single unit patterns distributed over the light period. The added multiunit pattern of an arbitrary number of 10 neurons that are linearly distributed over the light period is shown, with the single units indicated at the bottom. The resulting multiunit pattern broadens and resembles the recorded activity pattern. (C) Example of a multiunit pattern in the rat SCN slice recorded with a stationary electrode. Slices were acutely prepared from rats kept in LD 12:12. The simulated multiunit pattern can be compared to the measured patterns with respect to the width, which is measured at the half maximum level of the pattern.

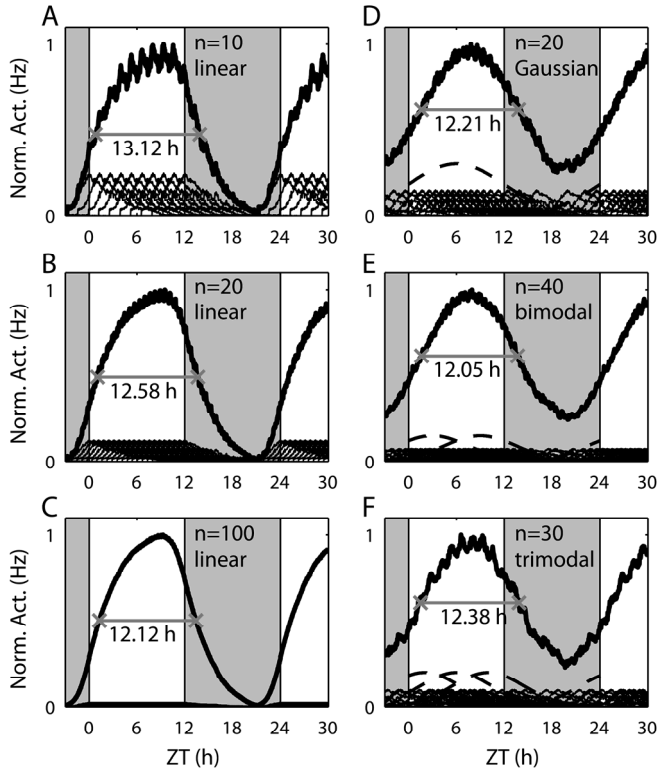

Figure 3.4 Multiunit activity pattern simulation for different numbers of single units and for several distributions. In (A)-(C) single units are linearly distributed over the light period. In (A) the summed activity of 10 single units is simulated, in (B) 20 units are simulated and in (C) 100 units. The data indicate that an increment in the number of neurons affects the variability in the multiunit pattern, but not the waveform. In (D)-(F) the single units are distributed using different distributions. (D) shows 20 single units that are distributed using a normal (Gaussian) distribution over 24 hours. The dashed line shows the Gaussian distribution according to which the single units are distributed. In (E) the single units have a bimodal distribution with the mid of the first component at ZT 3 and the mid of the second component at ZT 9. The dashed lines show the Gaussian distribution of the two components. (F) shows a trimodal distribution with the mid of the three components at ZT 2, 6 and 10. The data show that the multiunit waveform can be obtained by three temporal clusters of neurons. The data indicate that the multiunit waveform does not necessarily reflect the underlying distribution of single units.

It appeared difficult to predict the underlying distribution of single units on the basis of the recorded multiunit activity pattern (figures 3.4 and 3.5). A bimodal distribution of single units can result in a bimodal multiunit pattern, if the peaks are at ZT3 and ZT9 (figure 3.5 A) and if the distribution within each component is rather narrow. It can also result in a unimodal multiunit

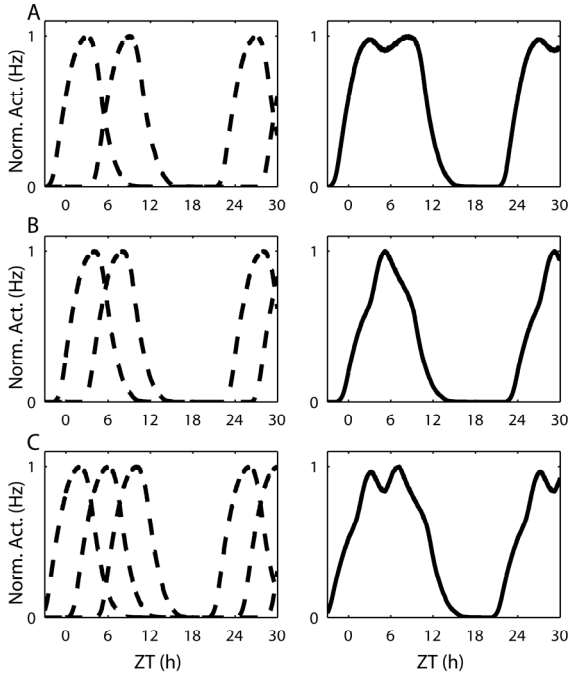

Figure 3.5 Multiunit waveforms do not reflect the underlying distribution of single units. On the left hand side the distribution is shown of the subpopulations, on the right hand side the multiunit pattern resulting from this distribution is shown. (A) Two multiunit activity patterns of different subpopulations of neurons that are far apart in time result in a bimodal multiunit activity pattern. (B) Two multiunit activity patterns that are closer to each other result in a multiunit activity pattern with one peak. (C) Three multiunit activity patterns of different subpopulations may result in a multiunit activity pattern with two peaks. The data indicate that the multiunit activity pattern does not necessarily reflect the underlying distribution of subpopulations or single units.

pattern if the peaks are closer together (i.e., at ZT4 and ZT8; figure 3.5 B) or if the distribution within each component is broader. A bimodal multiunit pattern can also be obtained by an underlying distribution of 3 subpopulations (figure 3.5 C).

Multiunit activity patterns are not only determined by the distribution of neurons but also by the circadian pattern of individual cells. Simulated discharge patterns show that the shape of single unit activity patterns affects not only the multiunit activity pattern, but also the peak time of the multiunit pattern. If the single unit activity pattern is characterized by a steep activity onset, and a slow activity offset, the multiunit activity pattern shows the

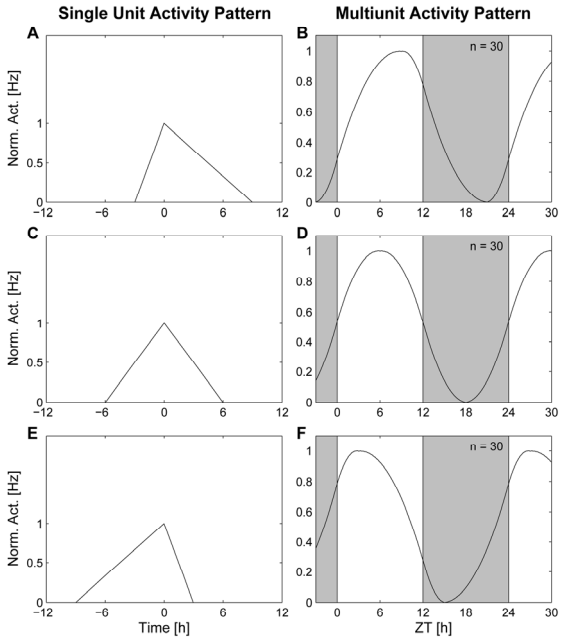

Figure 3.6 Single unit activity pattern shape can affect the shape of the normalized multiunit activity pattern. Three different artificial single unit activity shapes (A), (C), (E)) are used to obtain different multiunit activity patterns (B), (D), (F). To obtain the multiunit activity pattern, 30 single unit activity patterns were distributed according to a linear distribution in a 12h:12h light-dark schedule. The multiunit activity patterns on the right result from the corresponding single unit waveform on the left.

opposite waveform and displays a slower onset and a faster offset (figure 3.6 A and B). A symmetrical single unit pattern leads to symmetrical population patterns (figure 3.6 C and D).When, vice versa, a single unit pattern has a slow onset and a fast offset, the resulting multiunit pattern has a steep onset and a shallow offset (figure 3.6 E and F).

3.3.2 Mechanisms for photoperiodic encoding

It is well known that a multiunit pattern is narrow in a short photoperiod and broadens when the photoperiod increases (Jagota et al., 2000;Schaap et al., 2003). We explored changes in the width of the single unit activity pattern and their effect on the broadness of the multiunit activity pattern. For this purpose, artificial single unit patterns were narrowed (by 50%) or broadened (doubled) while their phase distribution was kept constant. The width of the multiunit activity pattern was not changed significantly by this manipulation

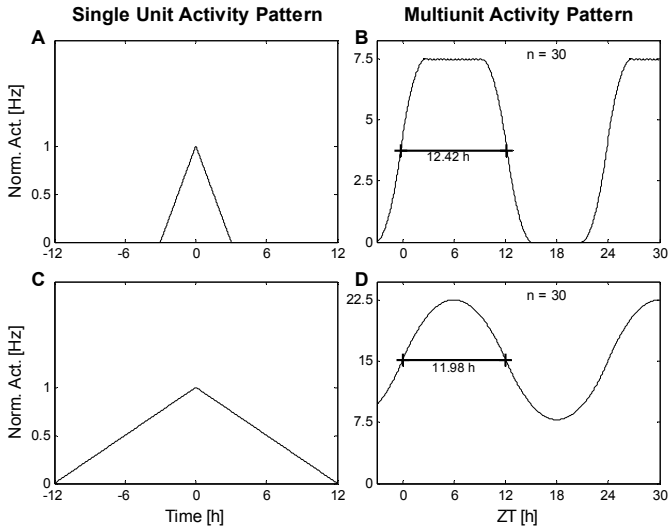

Figure 3.7 The influence of single unit activity width on the width of the multiunit activity pattern. One narrow artificial single unit activity pattern (A) and one broad pattern (C) are used to obtain multiunit activity patterns by distributing the single unit patterns according to identical linear distributions over 12 h. The upper right panel (B) shows the normalized multiunit activity pattern resulting from the distribution of 30 single unit patterns as shown in (A). The lower right panel (D) shows the normalized multiunit activity pattern resulting from distributing 30 single unit activity patterns as shown in (C).

(figure 3.7). For a linear distribution, broadening the single unit activity pattern, counterintuitively, even leads to a narrower peak. For narrow single units, a peak width of 12.42 h was obtained, while for broad single unit patterns, the multiunit peak width was 11.98 h.

When the phase distribution between neurons was changed, the width of the multiunit pattern altered significantly. For narrow distributions, a mean population peak width of 8.88 h was found, while for broad distributions, a peak width of 15.62 h was obtained (figure 3.8). A change in single unit activity pattern, in combination with a change in phase distribution, appeared to result in substantial effects on the population waveform as well. For narrow single unit activity patterns, in combination with narrow distributions of the neurons, we observed that the multiunit peak width was strongly compressed to 8.25 h, while the combination of a broad single unit pattern with a broad distribution resulted in a broader multiunit peak of 11.98 h (figure 3.9).

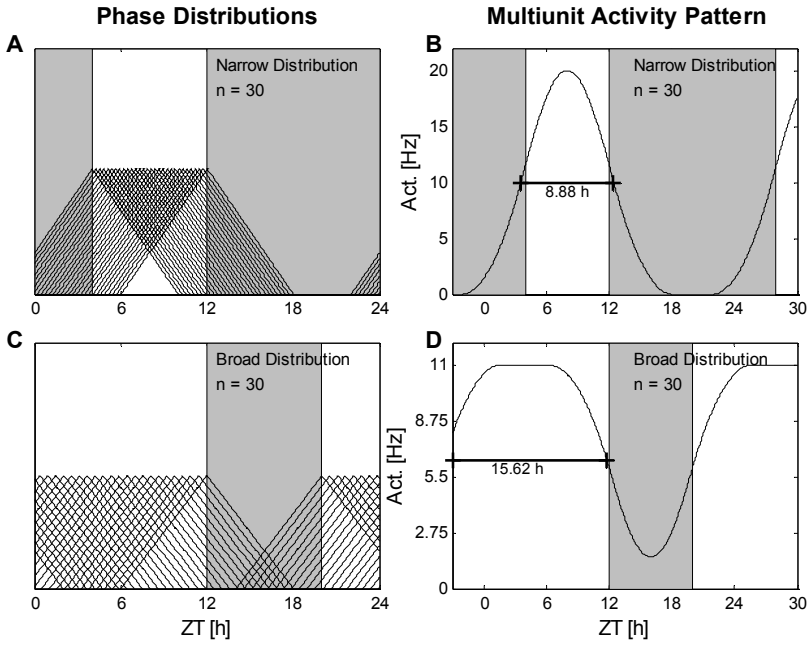

Figure 3.8 The influence of the phase distribution of single unit patterns on the width of the multiunit activity pattern. One narrow linear phase distribution (8 h) (A) and one broad linear phase distribution (16 h) (C) are used to obtain multiunit activity patterns. The single unit patterns in (A) and (C) are identical. The upper panel (B) shows the multiunit activity pattern resulting from the distribution of 30 single unit patterns shown in (A). The lower panel (D) shows the multiunit activity pattern resulting from the distribution of 30 single unit patterns shown in (C).

Experimentally measured data show that the mean width of a multiunit pattern in a short photoperiod (LD 8:16) is 11.07 h, and in a long photoperiod (LD 16:8), it is 14.62 h in rats (from Schaap et al., 2003). The difference between a long and short photoperiod is somewhat more than 3.5 h (figure 3.10 A). Next to the simulations that were done with artificial single unit activity patterns, we examined the effects of changes in the width of the measured single unit pattern from rats on the width of the multiunit pattern. The single unit activity width ranged from near 0 up to 12 h (figure 3.10 B). The results show that, counterintuitively, changes in single unit activity patterns can not code for changes in multiunit pattern (measured at halfmaximum amplitude) when single units are linearly distributed in phase.

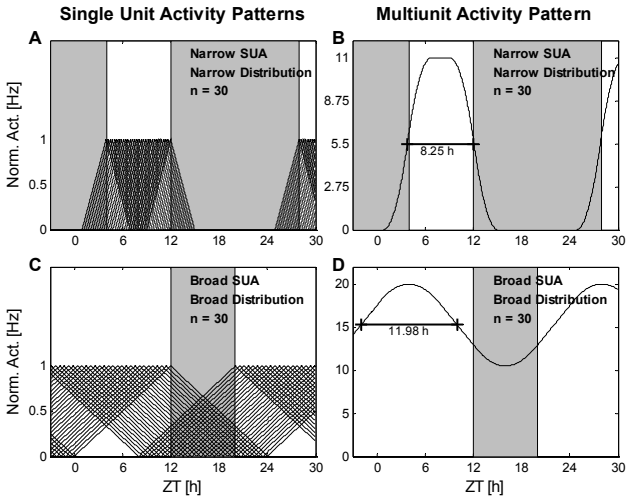

Figure 3.9 The influence of the combination of phase distribution of single unit patterns together with single unit width on the width of the multiunit activity pattern. A narrow linear phase distribution, distributing 30 narrow artificial single unit activity patterns over 8 hours (A) is used to obtain a multiunit activity pattern (B). This corresponds to a short day length. A broad linear phase distribution which distributes 30 broad single unit activity patterns over 16 hours (C) results in the multiunit activity pattern of (D). This corresponds to a long day length

Instead, the linear distribution resulted in a decrease in multiunit pattern width when the single units became broader. For instance, a single unit pattern with a width of 0.5 h resulted in a multiunit width of 12.65 h, while a single unit with a width of 10.5 h resulted in a multiunit width of 12.25 h for a given linear distribution. The Gaussian distribution showed a slight increase in multiunit width when the single unit pattern was broadened. The predominant increase in multiunit width occurred when a single unit width of about 2 h (multiunit pattern width of 9.65 h) was lengthened to a single unit width of about 6 h (multiunit pattern width of 11.08 h). This change in single unit waveform resulted in an increase in multiunit width of less than 1.5 h.

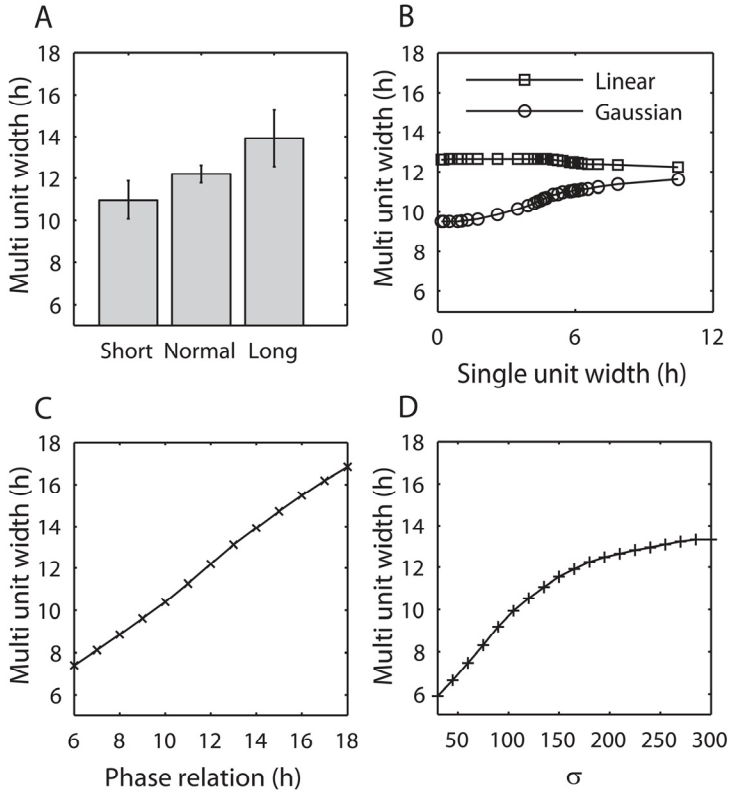

Figure 3.10 Photoperiod encoding using single unit pattern width or phase distribution. (A) Experimental data from the rat SCN slice (± SEM) shows that in a short photoperiod, the width of the multiunit pattern is narrower than in a long photoperiod (Schaap et al., 2003). (B) summarizes the effect of a change in width of the single unit activity pattern on the width of the simulated multiunit pattern. On the x-axis the width of the single units at halfmax is shown. The linear distribution shows that a narrow single unit pattern results in almost the same simulated multiunit pattern width as a broad single unit pattern. The normal distribution shows that a narrow pattern results in a somewhat smaller multiunit width than a broad pattern. (C) summarizes the effect of a change in phase relation of single unit patterns on multiunit activity width for linear distributions. The x-axis indicates the range of the single units: in LD 12:12, the peaks of the single units are distributed over the 12 hour light phase, in LD 16:8, the units are distributed over 16 hours of light (see figure 3.5 C). (D) shows the effect of changes in a normal (Gaussian) distribution on multiunit activity width using different values for σ. It is concluded that changes in phase relation can cause large changes in multiunit width, while changes in single unit activity patterns have only minor effects.

A range of changes in phase relationship between single unit patterns that are linearly distributed over the photoperiod resulted in considerable differences in the width of the multiunit pattern (figure 3.10 C). For instance, when distributed over 8 h, the multiunit pattern width was 8.85 h, and when

distributed over 16 h, the multiunit pattern width was 15.49 h. This difference was about 6.5 h. For a Gaussian distribution, the σ indicates the width of the distribution. When a range of σ's was used to alter the phase relationship between single units for the Gaussian distribution, significant differences in the width of the multiunit pattern were obtained (figure 3.10 D). For instance, when σ = 105, the multiunit width was 9.95 h., while σ = 270 resulted in a multiunit width of 13.22 h. The difference between these two values is approximately 3.2 h.

Figure 3.11 shows measured single unit activity patterns in mice for short days and for long days. There were no significant differences between the average peak width of the mean neuronal discharge patterns under long and short days (figure 3.11 A and B). However, the patterns were broader during daytime than during the night, both for short and for long day length (figure 3.11 C–F; see also VanderLeest et al., 2007).

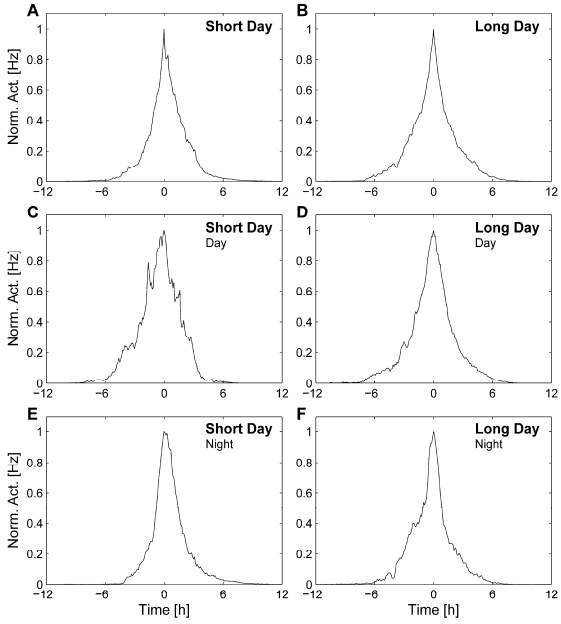

Figure 3.11 Six average single unit patterns from mice measured in short and long days (taken from VanderLeest et al., 2007). The normalized average single unit activity patterns of mice are shown, for short and for long day lengths. The width of the single unit patterns averaged over 24 hour for short days is 3.24h (A) and for long days 3.47h (B). The widths of the average single unit patterns that were measured exclusively during daytime were, for short days 4.01 h (C) and for long days 3.44 h (D). The widths of the average single unit patterns measured during the night were 2.80 h (E) and 3.14 h (F) for short and long days respectively.

We used these measured patterns to simulate encoding for day length in the mouse SCN. When the same linear distribution was applied to the single unit discharge patterns, measured under short and long days, the resulting multiunit activity pattern was not significantly different (figure 3.12 A and B). When the distribution was altered, on the other hand, significant changes in multiunit patterns were observed. A more narrow distribution was required to mimic narrow multiunit activity patterns, such as those recorded under short days, while a broadening of the distribution was required to mimic long day length patterns (figure 3.12 C and D).

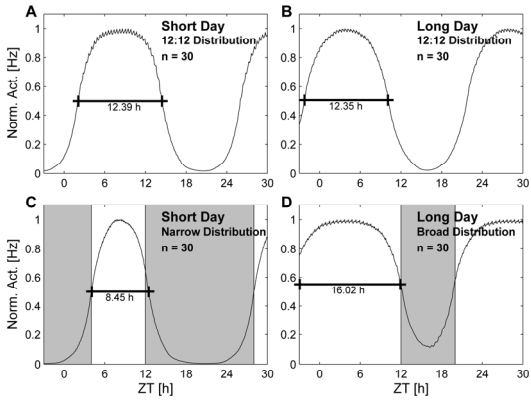

Figure 3.12 The influence of averaged single unit activity patterns of mice for short and long day length on the multiunit activity pattern. (A) Multiunit activity pattern with a width of 12.39 h is obtained by distributing 30 average single unit patterns for a short day length (see figure 3.11 A) according to a linear distribution over 12h. (B) A multiunit activity pattern of comparable width (12.35h) is obtained by distributing 30 average single unit activity patterns for a long day length (see figure 3.11 B) according to the same linear distribution as used in (A). These simulations did not result in multiunit patterns that carry day length information. (C) A narrow distribution of 30 average single unit patterns for a short day length (see figure 3.11 A) distributed over 8h results in a narrow multiunit activity pattern (8.45h). (D) A broad linear distribution of 30 average single unit activity patterns for a long day length (see figure 3.11 B) distributed over 16 h results in a broad multiunit activity pattern (16.02 h). All multiunit patterns are normalized.

3.3.3 Photoperiodic encoding by 2 populations

Bimodal distributions were characterized by the temporal distance between the two components and by the distribution of neurons within each of the components. We analyzed changes in distance between the two components (figure 3.13 A-D) and found that these lead to changes in multiunit patterns (figure 3.13 E-H).

The pattern broadens if the components move away from each other, but when moved even further, the multiunit pattern shows two peaks. For narrow single unit distributions within a component, the system codes for photoperiod in the way expected: if the components are more separated, the multiunit activity pattern becomes broader (figure 3.14). This is true both for narrow normal distributions with σ values of 90, 120, and 150, which are relatively low (figure 3.14 A), as well as for narrow linear distributions of 8 and 10 h (figure 3.14 B). For broad distributions within a component (i.e., normal distributions with σ values of 180 and 210 or linear distributions of 14 and 16 h), the system codes for day length opposite to the expectation: if the components are more separated, the multiunit activity pattern becomes narrower. To verify this, simulations were performed using the width of the population pattern at a fixed level of 8 Hz and at halfmaximum amplitude. The results demonstrated that the summed waveform becomes narrower irrespective of the method used for determining the width (figure 3.15). If the components are separated 6 h, the width of the multiunit activity pattern is approximately 12 h, independent of the single unit distribution that is used for each component.

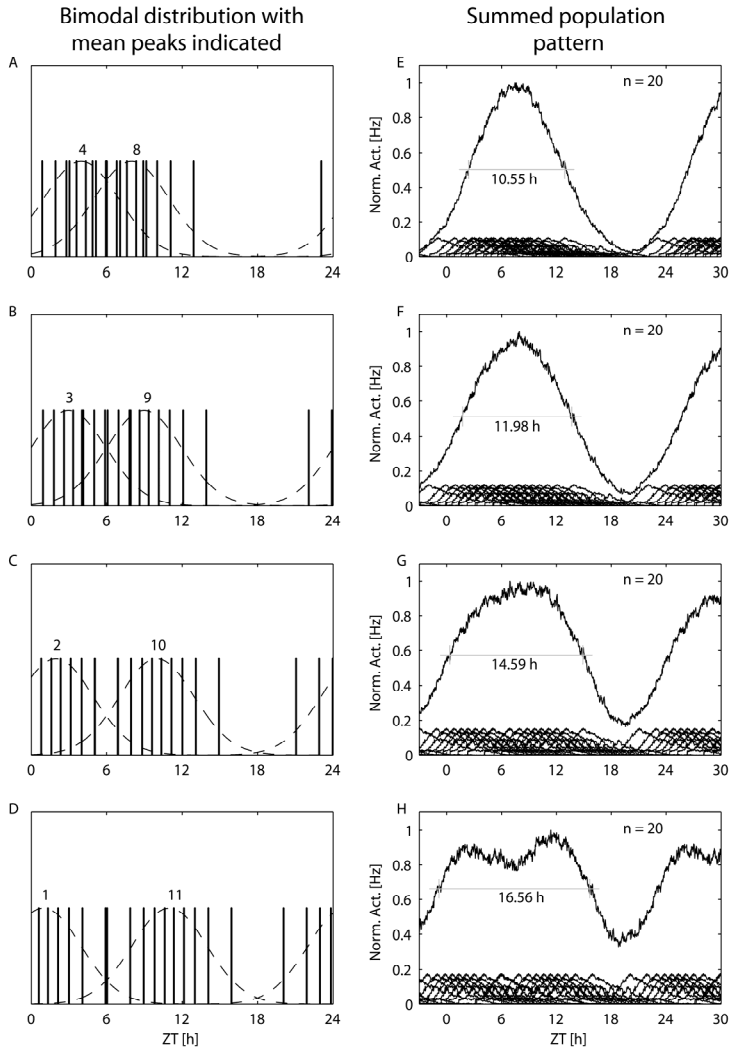

Figure 3.13 (A)-(D) Distribution of the two components in the circadian cycle. Two clusters in the bimodal distribution placed at different distances from each other. In (A), the two components are four hours apart, in (B), they are 6 hours apart, in (C) the components are 8 hours apart and in (D) the two components are 10 hours apart. The numbers indicate the mean peak time for each component. The vertical lines indicate peak times of single units. The dashed lines indicate the distribution of single units within each cluster. The σ used for all the bimodal distributions is 90. (E)-(H) Multiunit activity patterns based on bimodal distributions used in (A)-(D). In (E), the two components are four hours apart, in (F), they are 6 hours apart, in (G) the components are 8 hours apart and in (H) the two components are 10 hours apart. We can see in (H) that if the clusters are too far apart, double peaks arise in the multiunit activity pattern. We conclude that a bimodal distribution can account for changes in multiunit patterns as observed under different photoperiods.

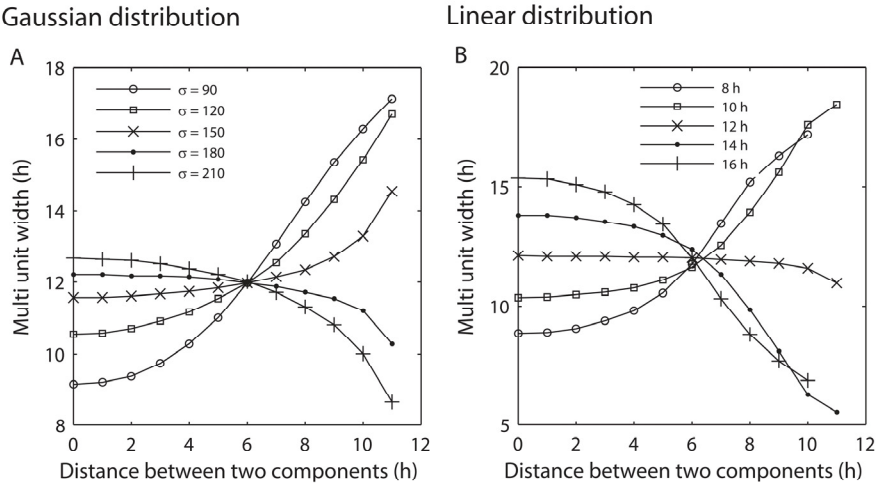

Figure 3.14 Effects of distance between components on multiunit width. On the x-axis the temporal distance between both components is plotted, on the y-axis the width of the multiunit activity pattern is plotted in hours. (A) Multiunit activity pattern width using a normal distribution within the components. The different σ values that are used represent the width of the Gaussian distribution that is used. A narrow Gaussian distribution has a small σ, while a broad distribution has a large σ. (B) Multiunit activity pattern width using a linear distribution for the single units within each component. The different lines represent different widths of these distributions. It can be observed that if the distance between both components is 6 hours, the width of the multiunit activity pattern is always approximately 12 hours. This is irrespective of the distribution that is used. For narrow distributions, the model codes for photoperiod in the way expected: if the components are more separated, the multiunit activity pattern becomes broader. This is the case in the normal distribution as well as in the linear distribution. For broad distributions, the model counter intuitively codes for photoperiod exactly opposite to the narrow distributions: if the components are more separated, the multiunit activity pattern becomes narrower.

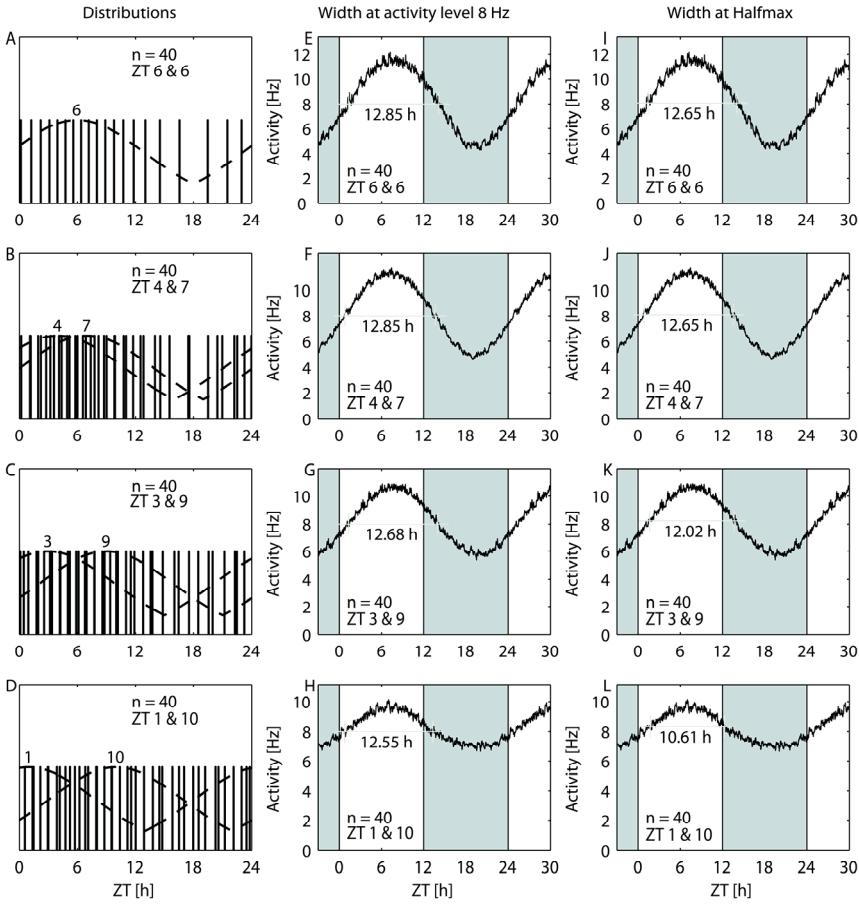

Figure 3.15 Distribution of the two components in the circadian cycle and their effect on the population width. (A)-(D) Two clusters in the bimodal distribution are placed at different distances from each other. In (A), the two components are on top of each other, in (B), (C) and (D), the components are 3, 6 and 9 hours apart respectively. The vertical lines in (A)-(D) indicate peak times of single units. The dashed lines indicate the distribution of single units within each cluster. The σ used for all the bimodal distributions is 210 which is a broad distribution. (E)-(H) Multiunit activity patterns based on bimodal distributions used in (A)-(D), measured at a constant height of 8 Hz. (I)-(L) Multiunit activity patterns based on bimodal distributions used in (A)-(D), measured at half maximum height. It is obvious that the summed waveform is narrower, at half maximum width, and also at a particular activity level, when the two components are further apart

3.4 Discussion

3.4.1 Population patterns caused by distribution of neurons

In this study, we have simulated multiunit signals taken from distributed and nondistributed single units. The outcomes of the simulations were compared with obtained experimental multiunit patterns. These recorded patterns were very precise and enabled us to evaluate them carefully for the presence of multiple components and the width of the multiunit pattern. The data show that realistic multiunit patterns can only be obtained when single units are distributed over the circadian cycle, in agreement with Schaap et al. (Schaap et al., 2003), who applied a linear distribution. In this study, the single units were distributed according to a linear, a Gaussian, a bimodal, and a trimodal distribution. We show that the outcome of all these simulations can render multiunit patterns that resemble the experimentally recorded patterns. In other words, we show that solutions are possible for all distributions.

In the current simulations, we use a simplified model containing identical single unit activity patterns. In reality, this may not be the case. The SCN is a heterogeneous structure, with respect to, among others, cell type, receptor density, neurotransmitter content, and afferent and efferent pathways (Morin and Allen, 2006). A major differentiation appears to exist between the vasoactive intestinal polypeptide (VIP)-containing cells in the ventral SCN, which receive retinal afferents and the vasopressin-containing cells in the dorsal SCN (Moore and Silver, 1998;van den Pol, 1980). It may well be that heterogeneity relates to differences in single unit activity patterns or that within particular regions of the SCN, units show different circadian profiles. This can not be incorporated in the present simulations but is an interesting possibility for future simulations, if experimental data will point in this direction. Despite the present uncertainty about the differences in single unit activity patterns within the SCN, it has become clear that all recorded single unit activity patterns are considerably narrower than the multiunit pattern and show differences in phase (Schaap et al., 2003;Brown et al., 2005b). These narrow single unit patterns, as well as the phase differences among the neurons, were the major and sole assumption for the present simulations.

Note that single unit activity patterns from isolated neurons may deviate from patterns in a network, not only with respect to their cycle-to-cycle precision (Herzog et al., 2004;Honma et al., 1998) but also with respect to the broadness of their activity patterns. The present simulations were not designed to provide insight in coupling mechanisms (i.e., phase response relations) between neurons (see Kunz and Achermann, 2003) but aimed to provide insight in the relation between the behavior of individual neurons and the measured population activity. The starting point in these simulations is the recorded activity pattern of a neuron in a network that had presumably been shaped by the interactions with other neurons.

The simulations indicate that the phase distribution of single unit activity patterns can not be derived from the multiunit activity pattern. For instance, a bimodal distribution of single units may show up as a bimodal multiunit pattern if the components are temporally far enough apart but may show up as a unimodal distribution when closer in phase. We also showed that a trimodal distribution can result in bimodal multiunit patterns. This shows that single unit recordings are required to establish how the SCN multiunit patterns are determined by the individual oscillatory cells, their individual patterns, and their phase relation.

In the rat, Schaap et al. (2003) showed a mean single unit activity pattern that is a-symmetrical, with a steep rising phase and a slower declining phase. This pattern results at the population level in a pattern that is gradually increasing and rapidly decreasing. This summed activity pattern may contrast the primary expectation, but is in fact consistent with multiunit activity patterns that have been described for the rat (Meijer et al., 1997;Schaap et al., 2003).

While the present simulations were based on electrical activity recordings, the simulations also have relevance for other population measurements such as gene expression profiles, transmitter concentrations, and so on. It will be important to establish whether molecular expression profiles of individual neurons resemble the population pattern or show short periods of enhanced expression within the 24 h cycle, with peaks at different phases of the circadian cycle. The observation that neurons show out of phase oscillations in Per1 (Quintero et al., 2003;Yamaguchi et al., 2003) may

indicate that phase differences also exist at the molecular level and may play a significant role in adjustments of molecular cycles to different environmental conditions.

When the number of neurons is increased in the simulations, the width of the multiunit pattern remains relatively stable. However, when more neurons are incorporated, the multiunit pattern becomes smoother and more precise. Mathematical modeling of multiunit activity in neuronal networks has shown that an increment in the number of neurons results in increased precision (i.e., decrease in day-to-day variability) at the multiunit level (Enright, 1980b). Noteworthy, increased precision in the latter model results from a stochastic process in which the ensemble pattern of imprecise neurons renders accuracy at the network level.

Herzog et al. (2004) and Honma et al. (1998) confirm that single neurons have imprecise periods but also state that precision is enhanced when neurons synchronize in a network, such as in a slice. Quintero et al. (2003) found in slices that a variation in period exists between neurons but are uncertain about differences in period within a neuron. Yamaguchi et al. (2003) suggest that intrinsic network properties could give rise to fixed phase relations between neurons. However, intrinsic network properties may also result in variable phase relations (i.e., when coupling is weaker or when afferent pathways are stimulated). The variations in period, either between or within neurons, may underlie the observed phase differences between SCN neurons (Schaap et al., 2003;Brown et al., 2005b). In our simulations, single units were given a fixed period, and as a result, they peak at a fixed phase of the circadian cycle. However, the outcome of the simulations would be similar if an earlier neuron on day 1 becomes a later neuron on day 2 while another neuron behaves vice versa, as long as the overall phase distribution between neurons is preserved.

3.4.2 Photoperiodic encoding

The observed phase differences between individual discharge patterns prompted us to investigate the role of phase differences in photoperiodic encoding processes within the SCN. A priori, one may expect that the waveform changes of the SCN under long and short photoperiod reflect a

change in individual discharge patterns. As an alternative, one may propose that population waveform changes are caused by differences in phase distribution between oscillating neurons, while individual patterns do not change. We investigated these most extreme alternatives in a series of simulation studies.

Changes in the broadness of single unit discharge patterns were realized by decreasing the peak width to 50% of its initial value, or by doubling the width of the peak. The results indicated that these substantial changes in individual discharge patterns have little effect on the half-maximum electrical activity level. For linear distributions of neurons, this manipulation resulted, in fact, in a counterproductive effect on the population waveform, and the half-maximum discharge pattern narrowed as a consequence of the broadening of the individual discharge pattern. Although the linear distribution is unlikely in a biological process, it could represent a multitude of components within the SCN that are evenly distributed over the subjective day. For normal distributions, this manipulation resulted in a minor increment in peak width. This counterintuitive result is explained, in part, by the increment in activity during the trough of the electrical activity pattern. This issue raises the question how the output signal of the SCN is actually read by downstream brain areas that receive the information. In other words, are downstream areas sensitive to changes in electrical activity pattern, and is the half maximum an indicator of the functional output signal, or alternatively, are these areas sensitive to the absolute discharge rate that is produced by the SCN. While changes in the electrical activity pattern were not effective in changing the broadness of the population signal at half-maximum discharge levels, they did increase the broadness of the peak at a fixed discharge rate. It will be of great importance to investigate, in vivo, by simultaneous SCN and behavioral recordings, how SCN electrical activity relates to behavioral activity levels.

While single unit activity waveform changes were not effective to change the broadness of the electrical activity pattern at half-maximum levels, changes in phase relation were most effective. Widening the phase relation in a linear phase distribution resulted in an increase in population peak width at half-maximum discharge levels (i.e. from 12.35 h to 15.62 h), while a

decrease in phase relation resulted in a decrease in peak width (to 8.88 h). When absolute discharge levels were investigated, this manipulation was equally effective and broadness of the peaks under short, normal and long photoperiod were 8.9 h, 12.4 h and 16.5 h respectively.

Thus far, all conclusions were based on normalized discharge patterns, in which the maximum frequency was equaled to 1. When we analyze the discharge levels quantitatively and study changes in discharge levels that follow from different parameter settings, we observe that for phase changes between the single units, the maximal frequency of the multiunit pattern decreases somewhat in a long day length and increases in a short day. For instance, in figure 8, the multiunit activity for long day lengths decreases to about 55% of the activity for short day lengths. These effects should be measurable and are, in fact, consistent with multiunit recordings in the rat by Schaap et al. (Schaap et al., 2003).

Changes in width of the single unit activity pattern lead to major changes in total SCN activity (figure 3.7 A and B). These changes in impulse frequency are not apparent from recordings in rats and hamsters (Mrugala et al., 2000;Schaap et al., 2003). However, as the number of counted neurons also depends on spike trigger settings and electrode characteristics, this conclusion needs further confirmation.

Although our simulations indicate that changes in phase distribution are an effective way to code for photoperiod, they do not exclude the possibility that coding for photoperiod involves a combination of the two processes, i.e. a change in individual waveform patterns, and a change in phase distribution among the neurons. Simulation studies show that a combination of these manipulations, also result in waveform changes at the population level. A decrement in phase relation, together with a decrement in single unit peak width results in a narrow population electrical activity peak. An increment in phase relation together with an increment in single unit peak width causes an increased peak width, and a considerable decrease in the amplitude of the rhythm, due to a substantial rise in the trough. As the compression and decompression of the population discharge pattern was already observed by a change in phase distribution alone, we conclude that the change in single unit activity width is of minor importance for the system to code for

photoperiod, but that large changes in single unit activity patterns may also occur. While changes in broadness of individual discharge patterns play a minor role for the waveform of the population signal, changes in phase distribution appear to be essential in coding for day length.

The present results are important for the design of future experiments. When photoperiodic encoding results from adaptations in single unit activity, relatively large changes in single unit activity patterns are predicted. These should be easy to record, and the number of neurons or animals that should be recorded from need not be large. Moreover, multiunit activity patterns should not only broaden in long day lengths, but the maximum frequency should also increase. If alterations in phase distributions are the mechanism for photoperiodic encoding, the frequency of the multiunit activity peak in long days should decrease. In addition, single units should reveal a larger distribution in phase. It is difficult to predict how many recordings will be required to confirm the latter point.

Experimental recordings of single SCN neurons of the mouse have been performed after the animals were entrained to long (LD 16:8) and short (LD 8:16) light dark cycles. This procedure resulted in changes in multiunit waveform patterns in slices containing the SCN, and in vivo recordings showed that these photoperiod-induced changes remained consistent for at least 4 days after release in constant darkness (VanderLeest et al., 2007). Single unit activity recordings revealed little difference between the duration of electrical activity patterns of single neurons under long and short days (3.47 h and 3.24 h respectively). While we can not exclude that an increase in the number of recorded neurons would reveal differences in individual waveform changes, we stress that small changes are not sufficient to result in the substantial population discharge patterns that are recorded in rats, hamsters and mice (recording studies: Mrugala et al., 2000;VanderLeest et al., 2007;Schaap et al., 2003). We can also not exclude that specific subsets of neurons exist within the SCN that do follow the photoperiod, and that we have missed in our recordings. Finally, we can not exclude that other parameters, such as gene expression profiles, do change with photoperiod. For instance, some genes may reflect the electrical activity pattern of the SCN as a whole, and may therefore follow the population discharge pattern.

While all these uncertainties exist, the recording studies in mice revealed unequivocally that electrical activity patterns in mouse from long and short days show clear differences in phase relation. In long days, a wide distribution of phases was observed, with many neurons that peaked also in the 'silent' phase of the cycle (i.e. the subjective night), while in short days the neurons showed a much tighter synchrony in terms of their phase differences. The small phase differences in short days result not only in narrow population activity patterns, but also in an increment in circadian amplitude. Vice versa, an increase in phase difference results not only in a broadening of the multiunit activity pattern. These effects of long and short day on circadian amplitude have been described for different clock genes, and for rat electrical activity rhythms (Schaap et al., 2003;Sumova et al., 1995;Sumova et al., 2003).

The simulations of the present study show how the measured single unit activity patterns may contribute to the population signal under short and long day lengths. In these simulations, we incorporated the finding that in long day length, the distribution is significantly larger (VanderLeest et al., 2007). We applied a linear distribution and a normal distribution to the measured neuronal discharge patterns, and investigated the outcome for the population discharge pattern. We choose for these distributions as insufficient single units have been recorded to characterize and quantify the distribution of neurons within the SCN (n = 26 under both photoperiods), and we believe that a multitude of these numbers would be required to describe this distribution. In fact, our finding may still be consistent with unimodal (Yamaguchi et al., 2003), bimodal (Jagota et al., 2000;Pittendrigh and Daan, 1976b) or trimodal (Quintero et al., 2003;Meijer et al., 1997) distributions, and for all of these distributions there is evidence in the literature.

The pineal gland is considered to play an important role in photoperiodic time measurement. The circadian oscillator in the SCN is connected to the pineal gland via a multisynaptic neural pathway (Moore, 1996). The hormone melatonin is secreted by the pineal and its synthesis is stimulated by the SCN (Goldman, 2001). The melatonin production is low during the day and high during the night. This inverse relation between the length of the day and the duration of melatonin secretion is found in many mammals and

during nighttime, the melatonin production can be suppressed by light (Nelson and Takahashi, 1991). The duration of the melatonin production serves as a photoperiodic message, as the length of the day is encoded in the melatonin signal and decoded in the target tissues of the hormone. The signal is compressed during long summer days and decompressed during short winter days. Our present simulations were based on recordings in C57 mice. These mice have no melatonin which raises the question whether C57 mice are a good model to study photoperiodicity. In experiments where the pineal gland is removed, a loss of melatonin leads to the inability of the reproductive system and body fat regulatory systems to discriminate between long and short days. However, entrainment of circadian rhythms to cycles of light and darkness proceeds in the absence of melatonin (Goldman, 2001). We observed that C57 mice responded to the photoperiod with a change in their behavioral activity pattern, as well as with a change in their SCN electrical activity rhythms. We believe therefore that photoperiodic changes in behavioral activity are independent from melatonin, but are correlated with the waveform of the SCN.

3.4.3 Bimodal distributions

The two-component structure of the SCN pacemaker, also called E (evening) and M (morning) oscillators, plays a significant role in a vast amount of literature in the field of circadian rhythms (Pittendrigh and Daan, 1976b;Daan and Berde, 1978;Daan et al., 2001;Hastings, 2001;Illnerova and Vanecek, 1982;Sumova et al., 1995). For this reason, we also explored bimodal distributions in our simulations. In terms of our current work, the two-oscillator model is a specific version of a model in which phase distribution determines day length encoding. We found that bimodal distributions can encode for day length, but that this is not trivial. Instead, and to our surprise, two components can code for day length only when certain conditions are met. The first is evidently that the two components should move within the right boundaries. While small movements yield no effect on multiunit waveform, the pattern becomes bimodal when the components are moved too far apart.

The system will only function properly if not only the distance between the components is taken into consideration, but also the distribution within a component. The latter restriction has not been acknowledged before. Only if both components have relatively small distributions of single units can the resulting multiunit pattern encode for day length. If the distributions of single units are broad for both components, moving the peaks of the two components apart results, against the expectation, in a narrower multiunit pattern. Additional simulations showed that the summed waveform is more narrow, not only at half maximum width, but also at a particular activity level (data not shown). In a bimodal distribution, neurons within each component are commonly distributed according to a Gaussian distribution. We also used a linear distribution of neurons within each component and show that this leads to the same results. We conclude that two components can code for day length when specific conditions are met. Hence, the two-oscillator model is a possible but not self-evident option for day length encoding. Note that the temporal distribution within the SCN may or may not be related to a spatial distribution. There may be two areas with out-of-phase neurons, depending on the environmental condition (anterior-posterior: Hazlerigg et al., 2005; dorsal-ventral: Albus et al., 2005;de la Iglesia et al., 2004). Bimodality in phase may theoretically also arise in a more diffuse way in which earlier and later neurons are intermingled in the SCN.

In conclusion, it has been observed that single unit activity patterns deviate from the population pattern of the SCN (Schaap et al., 2003;Brown et al., 2005b). This implies that that single units do not mirror image the population activity pattern. To understand the relation between single and multiunit data, simulations are conspicuously suited. A simulation model in which it is possible to simulate a multitude of possible configurations can help in understanding the multi oscillator structure of the SCN.

Chapter 4

Phase resetting caused by rapid shifts of small population of ventral SCN neurons

4.1 Introduction

Jet lag is often experienced as a disruption of day to day rhythms. The symptoms associated with jet lag are fatigue, reduced alertness and concentration, fragmented sleep, premature awakening, excessive sleepiness, and a decrement in performance (Waterhouse et al., 2007;Sharma, 2007). The symptoms can be caused by shift work, sleep disturbance or by acute time zone transitions caused by transatlantic flight (Reddy et al., 2002). Jet lag is attributed to slow adaptation of the circadian pacemaker, as well as to an unequal speed in the resetting of bodily functions (Takahashi et al., 2002).

In mammals, the suprachiasmatic nuclei (SCN) of the anterior hypothalamus drive daily rhythms. By means of a transcriptional and translational negative feedback loop, individual neurons of the SCN have endogenous circadian rhythms (Reppert and Weaver, 2001;Welsh et al., 1995). The individual neurons of the SCN synchronize in certain, not fully identified ways to produce a precise circadian rhythm at the tissue level (Enright, 1980a;Aton and Herzog, 2005;Colwell, 2005). The SCN receive information from the environmental light-dark cycle via specialized photoreceptors and pathways (Moore and Lenn, 1972;Morin and Allen,

2006). Under influence of light, the SCN synchronizes to the 24 hour environmental cycle (Quintero et al., 2003;Yamaguchi et al., 2003;Schaap et al., 2003;Brown et al., 2005a;Rohling et al., 2006b;VanderLeest et al., 2007).

Following a shift of the light-dark cycle, the circadian system requires several days to readjust to the new cycle. It is well known that adjustment of the circadian clock takes longer for eastbound flights, causing advances of the light-dark cycle, than for westbound flights, which cause delays.

Previous real-time electrical-activity measurements in SCN slices following a 6 hour delay of the light-dark cycle revealed bimodal patterns, with one shifted and one unshifted component (Albus et al., 2005). It appeared that the ventral part of the SCN corresponded with the rapidly shifting component while the dorsal region corresponded with the unshifted component (Albus et al., 2005). The aim of the present study is to provide a quantitative analysis of the observed bimodal electrical activity pattern.

We performed electrical activity recordings in SCN slices following a shift of the light-dark cycle and confirmed the presence of bimodal electrical activity patterns. Analysis of the bimodal activity records shows that the unshifted component is relatively broad and the shifted component narrower. Computer studies, including curve fitting analysis, show that the number of action potentials that contribute to the shifted component is a small fraction of those that contribute to the unshifted component. Subpopulation analysis confirms these findings, and shows strong synchronization in peak phase in the shifted component but not in the unshifted component. We propose that phase shifts are brought about by an initial rapid shift of a relatively small subpopulation of neurons within the SCN.

4.2 Methods

4.2.1 In vitro electrophysiology

All experiments were performed under the approval of the Animal Experiments Ethical Committee of the Leiden University Medical Center. Male wildtype Wistar rats (Harlan, Horst, The Netherlands) were individually housed in cages that were equipped with a running wheel and

entrained to a 12:12 light-dark cycle. Food and water were available ad libitum. When the animals were properly entrained, the light-dark schedule was delayed by 6 hours by delaying the time of lights-off (Albus et al., 2005). After subsequent exposure to one complete shifted light-dark cycle, the animals were killed by decapitation at the time of lights off. Brains were rapidly dissected from the skull and coronal hypothalamic slices (~400 µm thickness) containing the SCN were prepared and transferred to a laminar flow chamber within 6 min after decapitation. Slices were perfused with oxygenated artificial cerebrospinal fluid (ACSF) and kept at a temperature of 35°C. The slice was kept submerged and was stabilized with an insulated tungsten fork. We used one slice per animal.

The slices settled in the recording chamber for ~ 1 h before electrode placement. Recording electrodes were placed in the ventral and dorsal SCN in order to obtain multiunit discharge activity patterns from both SCN regions simultaneously. Action potentials were recorded with 90% platinum 10% iridium 75 µm electrodes, amplified 10k times and bandpass filtered (300 Hz low, 3 kHz high). The action potentials crossing a preset threshold well above noise (~5 µV) were counted electronically in 10s bins by a computer running custom made software. Time of occurrence and amplitudes of action potentials were digitized and recorded by a data acquisition system (Power1401, Spike2 software, CED, Cambridge, UK) and stored for offline analysis.

4.2.2 Analysis of in vitro electrophysiology

Multiunit activity data that showed two peaks on day 1 after the delay were used for analysis. The recordings were smoothed using a penalized least squares algorithm (Eilers, 2003). The data from dorsal and ventral SCN were pooled. The widths for both peaks of the bimodal pattern were determined at the height of the trough between both peaks. A straight line was drawn from the trough between the two peaks to the opposing slope of the peak to determine the width of the peak. To allow for comparison between different experiments, we also calculated the relative peak width. The difference in absolute and relative peak widths was tested for statistical significance with independent t tests ($p < 0.001$).

4.2.3 Subpopulation studies

Activity of neuronal subpopulations in the SCN was analyzed using MATLAB (Matlab, 2007). Subpopulations in the multiunit recordings were constructed on the basis of spike amplitude, and correlated with distance to electrode tip. The amplitude data were divided into 50 equally sized bins reaching from a low spike threshold level, representing a large number of neurons, to the highest threshold including only a few units (Schaap et al., 2003). Population and subpopulation activity were smoothed and the peak times of the different subpopulations were determined relative to the time of the trough between the shifted and the unshifted component in the multiunit activity recording. All experiments were aligned to the time of the troughs.

4.2.4 Peak fitting

To determine the relative contribution in electrical activity for each component, the area under the curve was determined for each component using manual curve fitting and automatic curve fitting procedures (Igor: http://www.wavemetrics.com and Origin: http://www.originlab.com). We fitted one peak for each component in the electrical activity multiunit pattern. In the manual curve fitting method we manually determined the peak for each component in the multiunit activity pattern. We defined a start time and an end time of the peak. Then we counted the number of action potentials in the region from the start time until the end time of the peak. The number of action potentials found for each peak represents the area for each component (see also figure 4.3). For each component the component peak area was taken as a relative measure of the total area for both components. This relative number for each component was taken as a measure for the relative amount of action potentials contributing to the component.

For automatic peak fitting, mathematical techniques were used to determine the relative contribution of the area under both components. Using the multi-peak fitting algorithm in Igor (http://www.wavemetrics.com) the peaks were fitted automatically. The results were confirmed with the multi-peak fitting algorithm of Origin (http://www.originlab.com).

For each bimodal activity pattern, area approximation was performed by fitting two or more Gaussian functions to the smoothed signal. Usually, these

Gaussian functions are added to a baseline. In figure 4.3 B for example, the two Gaussian functions which describe the smoothed signal must be added to a baseline. In figure 4.3 B, the baseline is set at a constant level $f(x) = 135$. If no baseline function was used in the fitting procedure, the fitting algorithm often added an extra Gaussian function which served as a baseline. Three types of baseline functions were used. The first baseline function was a constant level ($f(x) = a$), the second a linear function ($f(x) = a + bx$) and the third baseline function was a cubic function ($f(x) = a + bx + cx^2 + dx^3$). No quadratic function was used because the results were very similar to either the linear or the cubic function. In addition to fitting the complete curve, we also fitted a part of the smoothed signal that only contained both components. The resulting Gaussian functions that best described the two peaks of the components were selected, using the lowest chi-square test statistic and the lowest Akaike Information Criterion (AIC) value. The area for the selected peaks was subsequently determined and then regarded relative to the total area for both components. These relative values were taken as an indication for the relative number of action potentials contributing to each component.

The Gaussian function describing the component peaks was characterized as follows

$$y = \frac{A}{w}\sqrt{(\pi/2)}e^{-2(\frac{x-x_c}{w})^2}, \qquad (1)$$

where A represents the area under one Gaussian, w characterizes the width of the Gaussian function, and x_c represents the time of the peak of the Gaussian function.

4.2.5 Simulation studies

Simulations were done in the Matlab programming environment (Matlab, 2007) using the model that was described in chapter 3, section 3.2. Two components were simulated at the average ZT times of the unshifted and shifted component (ZT 9 and ZT 13, ZT before the shift). The multiunit activity pattern was derived from the activity patterns of the two components. Each component was composed as an ensemble of neurons, by distributing a number of single unit activity patterns according to the

following Gaussian distribution $e^{-(x-\mu)^2/2\sigma^2}$. The single unit pattern was obtained by taking the average electrical activity of recorded single unit patterns, as described in (VanderLeest et al., 2007;Rohling et al., 2006a). The number of neurons and the width of the distribution could be adjusted for each component separately. Sigma (σ) of a distribution is a measure for the width of a Gaussian distribution, a high sigma reflecting a broad distribution and a small sigma indicating a narrow distribution.

4.3 Results

Albus et al. (2005) witnessed two components in the multiunit activity pattern after a 6 h delay of the light-dark cycle. One component was situated in the ventrolateral region of the SCN, while the other resided in the dorsomedial region. The two components could be identified by two separate peaks of electrical activity in multiunit recordings. On day 1 after the delay, the two peaks were already clearly distinguishable. Additional electrophysiological experiments have been carried out to obtain a sufficient amount of data for the quantitative analysis of the observed bimodal pattern.

The experiments for day one after the delay used in Albus et al. (2005) were pooled with the new experiments. From all experiments, 13 showed two components in the recording. Looking at these examples there was a clear tendency that the peak of the shifted component was more narrow than the peak of the unshifted component (figure 4.1). First, we confirmed the difference in the shift of the two components, as found in Albus et al. (2005) (figure 4.2 B). Then, the width of the peaks at the level of the trough between both peaks was measured (figure 4.2 A). The width of the shifted component was significantly narrower than the width of the unshifted component ($p < 0.001$; figure 4.2 C), and this was also true when the relative widths were compared ($p < 0.001$).

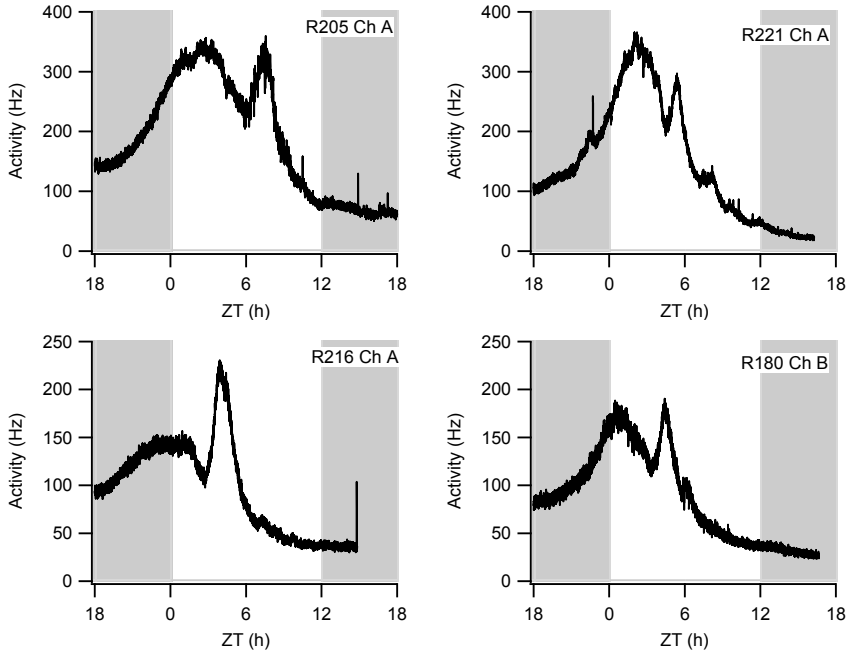

Figure 4.1 Four examples of recordings showing two components. Multiunit electrical activity recordings clearly showing two peaks in electrical activity. The shifted light-dark schedule is depicted with gray indicating the night. The left peak in each recording is unshifted component, while the right peak is the shifted component.

Next, we manually fitted the smoothed patterns to determine the area under the curves for both components and calculated the relative contribution of each (figure 4.3 A). The results were a rough estimate of the area for each curve and showed that the area of the unshifted component was about 70% and the area of the shifted component about 30% (figure 4.3 C).

In the manual fits, the shape of the curve was not considered, which puts a bias on the smaller shifted component. To avoid this bias, we fitted two or more Gaussian functions to the smoothed pattern using the automatic fitting procedures. The best fit was used and the Gaussian curves for both components were analyzed (figure 4.3 B). The areas for both components were again determined relative to each other. The first component was almost 80%, while the area of the second component was 20% (figure 4.3 D).

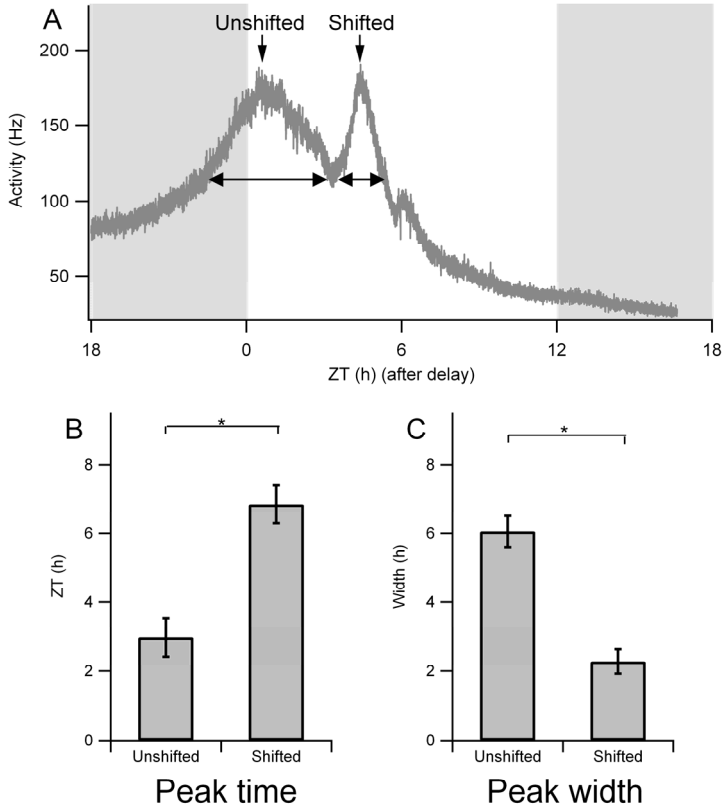

Figure 4.2 Width and time of peak for both components. (A) Raw multiunit activity recording following a shift of the light-dark cycle. After smoothing of the data, the trough between both components was determined as well as the peak times. Subsequently, the width of the unshifted and the shifted component was determined by drawing a horizontal line from the trough to the opposing slope of the component's peak. (B) The peak time for the shifted component occurred at ZT 3.0 ± 2.0 h, while the unshifted component peaked at ZT 6.8 ± 2.0 h. The ZT refers to the shifted Zeitgeber time. The difference in peak times was statiscally significant ($p < 0.01$). (C) The width of the peak of the unshifted component was 6.1 ± 1.6 h, while the shifted component had a peak width of 2.3 ± 1.3 h. This was also significantly different ($p < 0.01$).

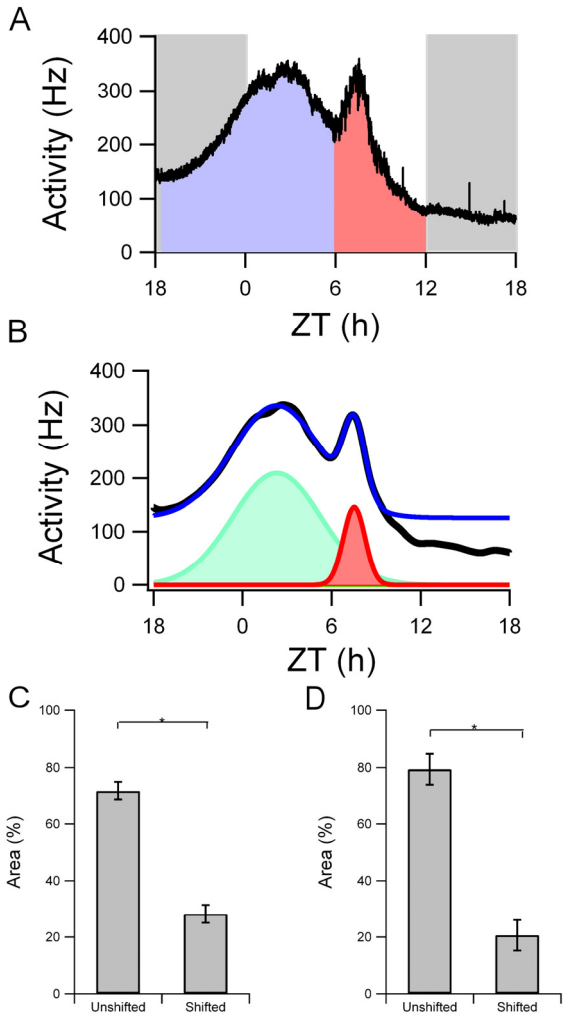

Figure 4.3 Relative number of action potentials contributing to each component. The area under the curve for each component was taken as an indication for the amount of action potentials contributing to each component. (A) The total area under each of the components was used to determine the relative number of action potentials contributing to each component. (B) Mathematically fitting Gaussian functions to the smoothed multiunit activity pattern also gave an indication of the area under each component peak. (C) The area under the unshifted component as determined in (A) was about 70% of the total area, while the area under the shifted component was 30%. (D) For mathematical fitting, about 80% of the relative area under both components was covered by the unshifted component and 20% was covered by the shifted component.

Finally, we used a subpopulation analysis to determine the number of subpopulations in the unshifted and shifted component. Subpopulation analysis shows the time of the peak of subpopulations in the recording. The peak times of these subpopulations were determined relative to the time of the trough between both components. The subpopulation analysis shows that more subpopulations were present before the trough than after the trough (figure 4.4). Before the trough, a total number of 37 subpopulations were observed and after the trough 12 subpopulations were observed. The distribution of the subpopulations found before the trough is significantly broader than after the trough ($p < 0.05$).

From these results it seems that only a relatively small group of neurons shifts immediately after a 6-hour phase delay. The group of shifted neurons also appears to have a narrower phase distribution as compared to the unshifted group. To obtain more insight in the mechanism that can explain this phenomenon, simulations were performed.

In the simulations, the multiunit pattern shows a bimodal pattern if the width of the shifted component was considerably smaller than the width of the unshifted component (or vice versa). Also, in the case of the two components that are separated only by 4 hours, the number of neurons contributing to the shifted components had to be less than the number contributing to the unshifted component (or vice versa). When these prerequisites were met, a bimodal multiunit activity pattern was obtained (figure 4.5 A and B). When the distribution of the shifted component is narrowed, the number of neurons contributing to the shifted component can be varied slightly, although they should not be more than 30% of the total amount of neurons. This small variability in the amount of neurons in the shifted component produces different shapes of bimodal peaks (figure 4.5 C and D), that can also be found in the experimental data (figure 4.1). If the number of neurons contributing to the shifted component is about 20% of the total amount of neurons a bimodal shape in the multiunit activity pattern is found where the height of the peak of the shifted component is similar to that of the unshifted component (figure 4.5 D). However, if the percentage is higher, the height of the shifted peak immediately increases substantially as opposed to the unshifted one (figure 4.5 C).

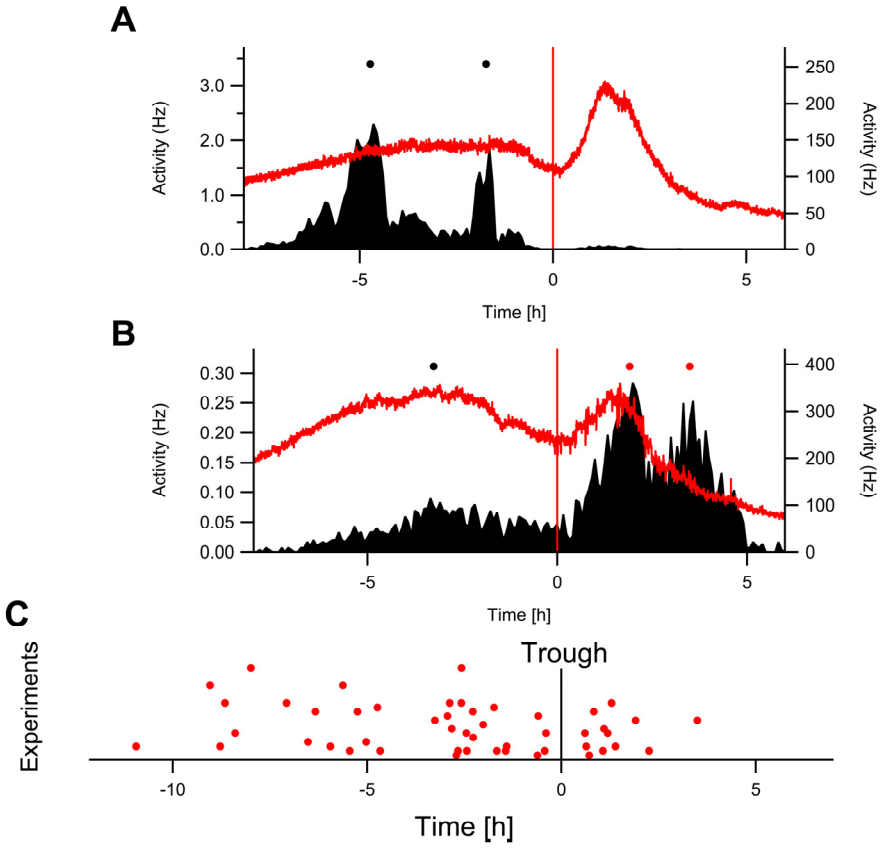

Figure 4.4 Subpopulation analysis of the shifted electrical activity profile. (A and B) The multiunit activity pattern (right axis) and subpopulations (left axis) for the same recording. The peak times of the subpopulations were determined by smoothing the electrical activity pattern. The dots denote the times of the peaks of the subpopulations. The subpopulation analysis was performed for all bimodal recordings and for all experiments the peak times were aligned to the trough (C). The number of subpopulations found in the unshifted component was higher than that in the shifted component (80 % versus 20 % respectively). Furthermore, the subpopulations of the unshifted component show a much broader distribution than the subpopulations of the shifted component.

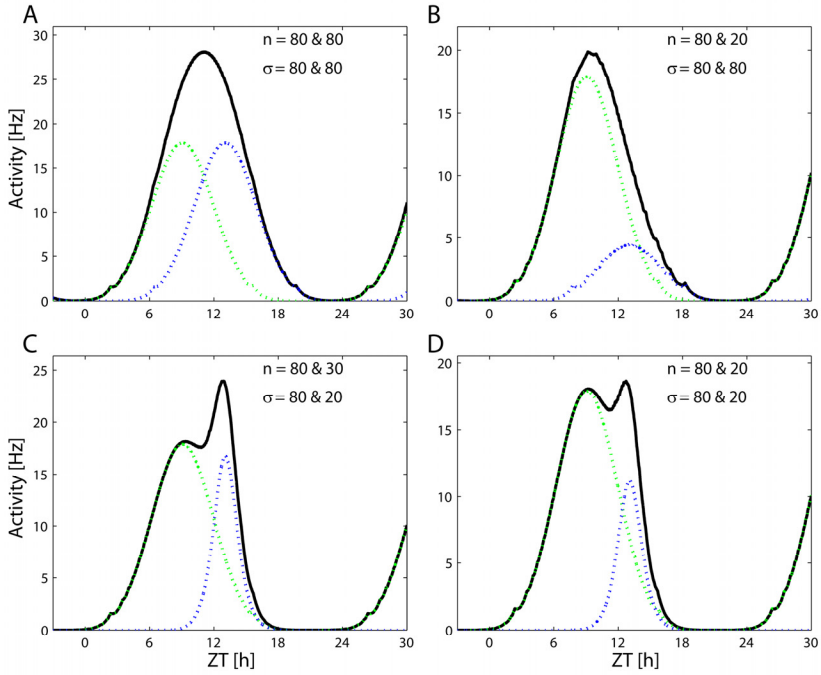

Figure 4.5 Simulations of electrical activity patterns with two components. Each graph shows the resulting multiunit pattern of two components that are placed at ZT 9 and ZT 13. Each component contains a number of neurons and these neurons are distributed according to a Gaussian distribution that has a certain width (indicated by σ: a lower value leads to a narrow distribution). (A) Both populations have an equal number of neurons and the same distribution. This leads to a single peak in the multiunit activity pattern. (B) The number of neurons in the second component is decreased, still resulting in a unimodal multiunit pattern. (C and D) The distribution of the shifted component is narrower. This leads to a bimodal multiunit pattern. If the number of neurons in the unshifted component is 80% and in the shifted component 20%, the obtained multiunit activity pattern resembles recorded bimodal multiunit activity patterns. (C). If the number of neurons is increased only by a small amount, we see that the second peak rapidly becomes higher (D). We have also seen this in one of the recordings (figure 4.1 C).

While we can not be certain of other mechanisms that might be involved in the shift of the light-dark cycle for different parts of the SCN, we have shown that the unshifted component is broader than the shifted component. The unshifted component also contributes more to the total activity of the multiunit pattern than the shifted component, and the number of subpopulations is higher in the unshifted component. The subpopulations in the shifted component are more clustered in phase.

4.4 Discussion

New experiments were performed to explore the mechanisms involved in the dissociation of neuronal subpopulations in the SCN after a phase delay of 6 hours. At day one after the shift, two components could be identified in the electrical activity pattern. First, we analyzed these bimodal patterns by measuring the width of both components and observed that the width of the unshifted component was substantially broader than the width of the shifted component. The width of the unshifted component was almost three times as broad as the width of the shifted component.

Then, we calculated the relative contributions of each component to the ensemble pattern by the use of curve fitting methods and a subpopulation analysis. We found that only a small percentage (20-30 %) of the total number of action potentials shifted immediately after the delay of 6 hours, while the larger part of the action potentials contributed to the unshifted component. The data suggest that only a small number of the total population of neurons shifted immediately following the delay.

Using simulations, we investigated how the activity patterns for two subpopulations can lead to bimodal ensemble patterns. In simulation studies, discussed in chapter 3 (sections 3.3.3 and 3.4.3), it was found that the width of the distributions for each component had to be narrow and the components had to be sufficiently separated in time to render a bimodal pattern. In the present study, our simulations show that also the relative number of neurons is of importance. Our simulations show that bimodal patterns in multiunit activity only arise when two conditions are met. First, the width of the distribution of the shifted component is maximally 25 % of the distribution width of the unshifted component. Second, the number of neurons contributing to the shifted component is maximally 25 % of the amount contributing to the unshifted component. If these conditions are not met, the multiunit activity pattern shows only one peak.

Some of our recordings showed one peak in electrical activity. This does not necessarily reflect a unimodal distribution of the contributing neurons. As shown in figures 4.5 A and B, bimodal distributions can result in unimodal multiunit activity patterns. For the unimodal recordings, the distribution of the shifted component may have been broad or the

components were not separated enough in time (see chapter 3, sections 3.3.3 and 3.4.3). Either case results in a unimodal multiunit activity pattern.

In a previous paper, Albus et al (2005) found that the two concurrent peaks in the in vitro electrical activity measurements could be located in the ventral and dorsal SCN. The ventral SCN is shifted immediately to the new phase, while in the dorsal SCN the shift is completed only after 6 days. We expect that the small group of rapidly shifting neurons is located in the ventral SCN.

In the current study we restricted ourselves to phase delays. Phase advances of the circadian system are known to be more complex, and require more time, than phase delays. In vitro electrical activity measurements in the rat SCN, following 6 hour phase advances showed an immediate shift of about 3 hours, but after 6 days the phase was at the old regime again (no phase shift persisted: Vansteensel et al., 2003). In vivo electrical activity showed no phase shift after a phase advance, indicating that perhaps the dorsal SCN does not shift and keeps the ventral SCN from shifting too (Vansteensel et al., 2003). When dorsal and ventral SCN in vitro after an advance where measured, there was indeed a difference in the phase shift: the ventral SCN shifted more quickly than the dorsal (Albus et al., 2005). This indicates that also for advances the dorsal and ventral region of the SCN shift at a different pace, causing dissociation within the SCN.

In molecular studies, different clock genes have been assessed following a phase delay or advance of the light-dark cycle. The expression of Per1 showed a rapid phase shift immediately after a delay or an advance (Reddy et al., 2002;Nagano et al., 2003;Yamazaki et al., 2000;Vansteensel et al., 2003). However, in different regions of the SCN, the response was different. In the ventral part of the SCN the shifts were immediate, while in the dorsal part the shift took longer (Nagano et al., 2003). Even within the ventral and dorsal regions, differences in phase shifting capacity of Per1 were found, where lateral cells shifted more rapidly than medial cells (Nakamura et al., 2005). Furthermore, an advance was more difficult than a delay (Nagano et al., 2003;Nakamura et al., 2005). Per2 expression showed the same characteristics as Per1 (Reddy et al., 2002;Nagano et al., 2003). This

indicates that also in gene expression a dissociation exists between the ventral and the dorsal SCN.

Apart from regional differences there are differences in the adaptation rate of certain clock genes. During phase delays, the Cry1 gene expression was synchronized to the expression of Per1 and Per2 (Reddy et al., 2002). Following phase advances the Cry1 gene expression rhythm became out of phase with the expression of Per1 and Per2 genes (Reddy et al., 2002). CRY1 protein levels followed the Cry1 gene expression profiles for phase delays (Nagano et al., 2003). This might indicate a special role for Cry1 in the phase resetting properties of the SCN, which differs between delays and advances.

In conclusion, we propose that phase shifts are brought about by an initial rapid shift of a relatively small subpopulation of neurons within the SCN. This group resides most probably in the ventral part of the SCN. Coupling between the shifted and the unshifted population of SCN neurons is asymmetrical, as the shifted neurons exert a strong phase shifting effect on the unshifted neurons. This causes a complete shift of the SCN which is realized after several cycles.

Chapter 5

Phase shifting of circadian pacemaker determined by SCN neuronal network organization

5.1 Introduction

The daily revolution of the earth causes 24 hour cycles in the environmental conditions, while the annual cycle of the earth moving around the sun brings about seasonal changes. In mammals, a major pacemaker for circadian rhythms is located in the suprachiasmatic nuclei (SCN) of the anterior hypothalamus (Ralph et al., 1990). The SCN are synchronized to the environmental light-dark cycle via the retina. Light information reaches the SCN directly via the retino-hypothalamic tract, which innervates the SCN with glutamate and pituitary adenylate cyclase activating peptide containing fibers (Morin and Allen, 2006). Synchronization to the environmental light-dark cycle is based on a time-dependent responsiveness of the SCN to light, which is most easily demonstrated in "perturbation experiments" in which animals are kept in constant darkness and subjected to discrete pulses of light. Light pulses presented during the early night induce phase delays of the rhythm, while at the end of the night, they induce advances. The characteristic phase dependent light responsiveness is a prerequisite for animals to entrain to the environmental cycle, and is a common property of many organisms (Pittendrigh et al., 1984).

The maximum advancing and delaying capacity depends strongly on the photoperiod to which animals are exposed. This finding has received surprisingly little attention, given the robustness of the photoperiodic modulation and potential functional significance. For instance, in rodents, the phase shifting effects of a 15 min light pulse on behavioral activity rhythms are about 2-3 fold larger in short winter days than they are in long summer days (Pittendrigh et al., 1984). One possibility is that increased light exposure in long days desensitizes the system to light at the level of the retina (Refinetti, 2002). Recently, it has become known that the organization of the SCN shows plasticity under influence of changes in day length (Schaap et al., 2003;Johnston et al., 2005;Rohling et al., 2006b;Inagaki et al., 2007;VanderLeest et al., 2007;Naito et al., 2008). The variation in light response over the seasons could therefore also result from different response properties brought about by plasticity within the SCN itself. Behavioral and electrophysiological experiments were performed and evidence was found that the phase shifting magnitude is determined by the SCN, rather than by the light input pathway (VanderLeest et al., 2009). The large phase shifts observed in high amplitude rhythms in short days versus the small shifts in long days lead them to propose that synchronization among individual oscillator components enhance the phase resetting capacity. This chapter is a more detailed description of the simulations that supported the study showing that the phase resetting capacity of the SCN is altered by the degree of synchronization between the different pacemaker neurons.

5.2 Methods

5.2.1 Ethics statement

All experiments were performed in accordance to animal welfare law and with the approval of the Animal Experiments Ethical Committee of the Leiden University Medical Center.

5.2.2 Behavioral experiments

Mice (C57BL6) were kept under long (16 h light, 8 h dark) and short (8 h light, 16 h dark) photoperiods for at least 30 days in clear plastic cages

equipped with a running wheel. The animal compartments are light tight and illuminated by a single white fluorescent "true light" bulb with a diffuse glass plate in front. The light intensity at the bottom of the cage was ~180 lux. Running wheel activity was recorded with Actimetrics software and the onset of activity was determined and defined as circadian time 12 (CT 12). After at least 30 days in the light regime, the animals were released into constant darkness (DD). On day 4 in DD, the animals received a 30 min white light pulse (180 lux) at a specific CT. We have previously shown that after 4 days in constant darkness, photoperiodic effects on behavioral activity and on SCN waveform are still fully present (VanderLeest et al., 2007). For each animal in the compartment, the average onset of activity was calculated and the CT of the light pulse was determined. Running wheel activity was recorded for another 14 days after the light pulse. The phase shifts were calculated by comparing activity onset in DD before and after the light pulse. The circadian times at which the light pulses were given were binned in 3 h intervals.

5.2.3 In vitro experiments

Animals were housed under long and short photoperiods, as described before, for at least 30 days. Prior to the in vitro experiment, the animals were transferred to a dark compartment for 3 days. Onset of wheel running activity was determined over these 3 days and decapitation and subsequent dissection of the brain was performed at the end of the resting period of the animal (CT 12). Slices of 400 µm were prepared with a chopper and were transferred to a laminar flow chamber that was perfused with warmed (35°C) ACSF within 6 min after decapitation (Schaap et al., 2003). The pH was controlled by a bicarbonate buffer in the ACSF and was maintained by gassing the solution and blowing warmed humidified O_2 (95%) and CO_2 (5%) over the slice. The slice was kept submerged and was stabilized with an insulated tungsten fork.

The slices settled in the recording chamber for ~1 h before electrode placement. Action potentials were recorded with 90% platinum 10% iridium 75 µm electrodes, amplified 10k times and bandpass filtered (300 Hz low, 3 kHz high). The action potentials crossing a preset threshold well above noise

(~5 μV) were counted electronically in 10 s bins by a computer running custom made software. Time of occurrence and amplitudes of action potentials were digitized by a CED 1401 and stored for off-line analysis. To induce a phase shift, the recording chamber was perfused with ACSF containing 10 or 25 μM N-methyl-D-aspartate (NMDA) for 30 min. The timing of the NMDA application was in accordance with the light pulse presentation in the behavioral experiments: The slices were prepared on day 3 in DD and on the fourth night in DD the NMDA pulse was applied at CT 15. The estimation of CT 15 was done one the basis of the activity onsets of the animals in DD, on the days preceding the preparation of the slice.

5.2.4 Data analysis

Electrophysiological data was analyzed in MATLAB using custom made software as described earlier (VanderLeest et al., 2007). The time of maximum activity was used as marker for the phase of the SCN and was determined on the first peak in multiunit activity, both for control and experimental slices. Multiunit recordings of at least 24 h, that expressed a clear peak in multiunit activity, were moderately smoothed using a least squares algorithm (Eilers, 2003) and peak time, half maximum values and amplitude were determined in these smoothed recordings.

For a more detailed analysis of rhythm amplitude, we used the stored times of the occurrence and amplitudes of the action potentials. This analysis allows for an off-line selection of the size of the population of neurons that contributes to the electrical activity rhythm, through a selection of voltage thresholds (see also Schaap et al., 2003 and VanderLeest et al., 2007). In this way, we could describe the circadian activity pattern of larger or smaller subpopulations of SCN neurons. This analysis was performed in slices from long and short day animals, and allowed to compare rhythm amplitudes in both groups with an equal number of action potentials that contributed to the recording over the same time interval (c.f. figure 5.4). The thresholds were determined so that each trigger level includes 10^5 more spikes than the previous level. For all experiments the deviation from the aimed number of action potentials selected for was < 5%.

Statistical analyses were performed in Origin 7 (OriginLab Corporation) and Excel (Microsoft). All values are stated as average ± standard error of the mean (s.e.m.). Whenever the calculated value is the result of a difference between groups, such as in the calculation of in vitro phase shifts, variances were considered unequal, rendering a conservative test. P-values were calculated with a two sided t test and were considered to be significant when $p < 0.05$.

5.2.5 Simulations

Simulations of a phase response curve (PRC) for short day length and long day length were performed in MATLAB by distributing 100 normalized artificial single unit phase response curves over the day. Two types of single unit PRCs were used (figure 5.1). The first PRC consisted of a 12 h dead-zone (where no phase responses can be induced) and a 12 h sinusoidal responsive part, in accordance with the type 1 light pulse PRC (Johnson, 1999). The other single unit PRC was in accordance with a type 0 light pulse PRC, consisting of a 12 h deadzone followed by an exponential function with an asymptote at CT18, and a maximum shift of 12 h (Johnson, 1999). The distributions that were used for long and short day lengths were taken directly from experimentally described subpopulation distributions in long and short photoperiods (see figure 5.6 A and VanderLeest et al., 2007). The peak times of these subpopulations were used to fit a distribution curve. This curve was used to distribute 100 single unit PRCs over the circadian day. In addition, simulations were performed using single unit PRCs without a deadzone (see figure 5.7 B) (c.f. Ukai et al., 2007).

We have measured the area under the curve, which is the surface of the delay and advance part of the PRC. The surface is an indication for the phase shifting capacity of the circadian system. The equation for this calculation is the first integral of a curve over a certain interval: $\int_a^b f(x)dx$ or $\sum |y| \times \Delta x$ for discrete functions, where the absolute value of y is multiplied by the width on the x-axis.

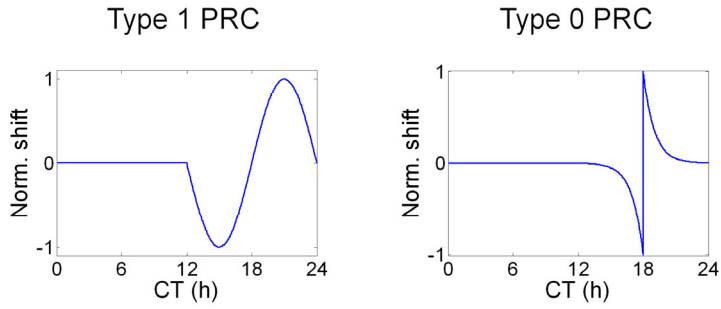

Figure 5.1 Single unit phase response curves. Type 1 and type 0 normalized artificial single unit phase response curves (PRCs) were used in the simulations. The type 1 PRC consists of a 12 h dead-zone (where no phase responses can be induced) and a 12 h sinusoidal responsive part (Johnson, 1999). The type 0 single unit PRC consisted of a 12 h dead-zone followed by an exponential function with an asymptote at CT18, and a maximum shift of 12 h.

5.3 Results and discussion

Behavioral experiments established phase shifting effects of light under long and short photoperiods (light:dark 8h:16h and 16h:8h). The phase shifting effects were determined by light pulses given at different phases of the circadian cycle (figure 5.2). Maximum delays were observed for pulses given 3 hours after activity onset in both animals from short days (shift: -2.68 ± 0.19 h, n = 6) and animals from long days (shift: -0.62 ± 0.28 h, n = 5). The magnitude of the delays was significantly larger for animals in short days than for animals in long days ($p < 0.001$). Light pulses towards the end of the night produced small phase advances which were not significantly different between the groups (short day advance: 0.61 ± 0.26 h, n = 8; long day advance 0.50 ± 0.11 h, n = 9; $p > 0.6$) (VanderLeest et al., 2009).

Experimental results show that the difference in shift between long and short day animals is not attributable to a difference in photic sensitivity of the circadian system (VanderLeest et al., 2009). VanderLeest et al. (2009) also tested whether the phase shifting capacity of the circadian system under long and short photoperiods is determined by the SCN itself, rather than by sensitization or desensitization of retinal input. The SCN was tested in vitro using NMDA pulses (figure 5.3 and 5.4). The NMDA receptor is of crucial importance in mediating phase shifting by light and application of the

glutamate receptor agonist NMDA to brain slices in vitro generates phase shifts of the circadian rhythm resembling photic phase responses (Colwell et al., 1991;Ding et al., 1994;Shibata et al., 1994). The absence of a difference in the magnitude of the NMDA response underscores that the phase shifting capacity is determined by the SCN itself and shows that the same increase in neuronal activity of the SCN results in a different phase shifting response (VanderLeest et al., 2009).

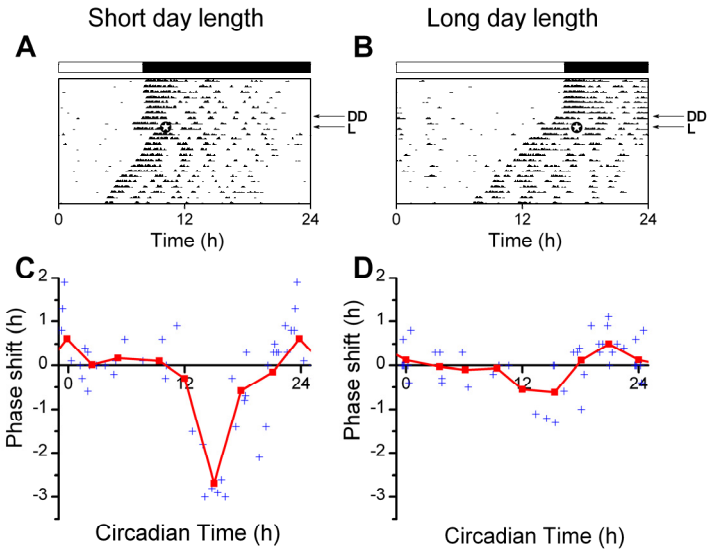

Figure 5.2 Phase shifts of wheel running behavior in mice induced by 30 minutes light pulses. Examples of wheel running actograms from animals kept in short (A) and long photoperiods (B). The top bar indicates the light-dark schedule before transfer to continuous darkness (DD, indicated with an arrow), days are plotted underneath one another. A light pulse was given on day four in DD (L, indicated with an arrow), 3 hours after activity onset (indicated by ✪ in the actogram). Activity onset was defined as circadian time 12. Phase response plots to 30 minute light pulses in short (C) and long (D) photoperiod. Phase responses are plotted as a function of the time of the light pulse. Individual phase shifts are indicated by a plus symbol. The results were grouped in 3 h bins centered at CT 0, 3, 6, 9, 12, 15, 18 and 21. The average phase responses of the light pulses are indicated by squares and connected with a solid line. The time of maximal delay is at CT 15 for both long and short photoperiods and is significantly different between both day lengths ($p < 0.001$). The large magnitude of the delays observed in short days is consistent with other studies (Pittendrigh et al., 1984;Refinetti, 2002).

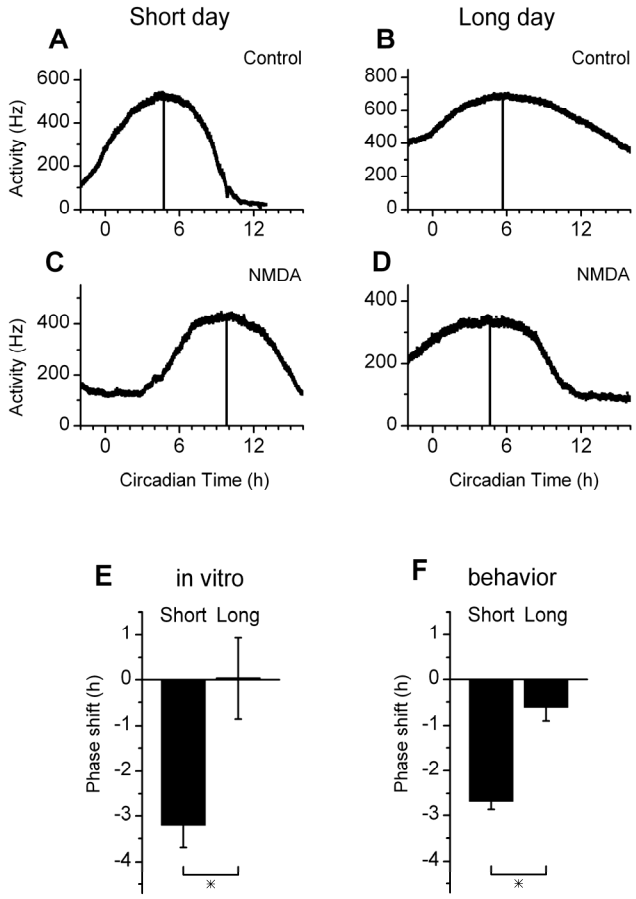

Figure 5.3 Phase shifts of multiunit electrical activity rhythms in brain slices from mice kept on a short and long photoperiod. Examples of extracellular multiunit recordings from the SCN in mice kept on a short photoperiod (A, C) and on a long photoperiod (B, D). Action potentials were counted in 10 s bins, and are plotted as a function of circadian time. NMDA pulses were given 3 hours after the activity onset, at CT 15, both in slices from short (C) and long (D) day animals. These pulses induced a delay in the peak time of the rhythm in slices obtained from short day animals. Peak times are indicated by a vertical line. (E) Delays obtained at CT 15 from short day animals were significantly larger than delays obtained from long day animals. The magnitude of the delay after an NMDA pulse at CT 15 was significantly different between day lengths ($p < 0.01$). (F) The magnitude of the behavioral delay was not different from the delay observed in vitro, for both day lengths (Short day in vitro vs. behavior $p > 0.3$, Long day in vitro vs. behavior, $p > 0.4$).

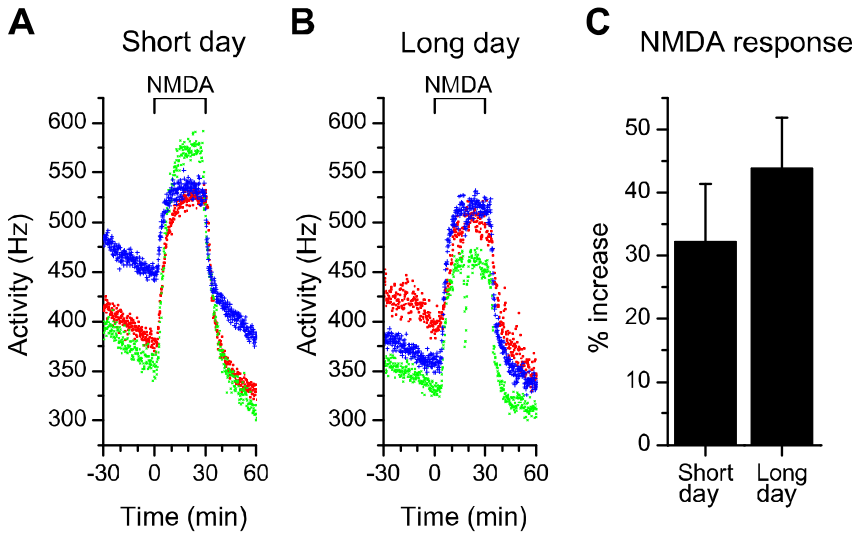

Figure 5.4 Acute NMDA responses in multiunit electrical activity. (A, B) NMDA (10 μM) induced an increase in firing rate as recorded by extracellular multiunit electrodes. The magnitude of the NMDA response is similar in slices from long and short day animals and in both photoperiods, a plateau was reached during the application. (C) The magnitude of the acute response to NMDA, measured as the relative increase in discharge rate, was not different between day lengths ($p > 0.3$).

The question arises what mechanism in the SCN underlies the photoperiodic modulation of phase shifts. Recently it has become clear that photoperiodic encoding by the SCN (Mrugala et al., 2000;Sumova et al., 2003) is accomplished through a reconfiguration of cellular activity patterns (Schaap et al., 2003;Hazlerigg et al., 2005;Inagaki et al., 2007;VanderLeest et al., 2007;Naito et al., 2008). In long days, the activity patterns of single SCN neurons are spread in phase, rendering a broad population activity pattern, while in short days, the neurons oscillate highly in phase, which yields a composite waveform with a narrow peak (Schaap et al., 2003;VanderLeest et al., 2007). Molecular studies have shown regional differences in gene expression patterns that increase in long days and decrease in short days (Hazlerigg et al., 2005;Inagaki et al., 2007;Naito et al., 2008).

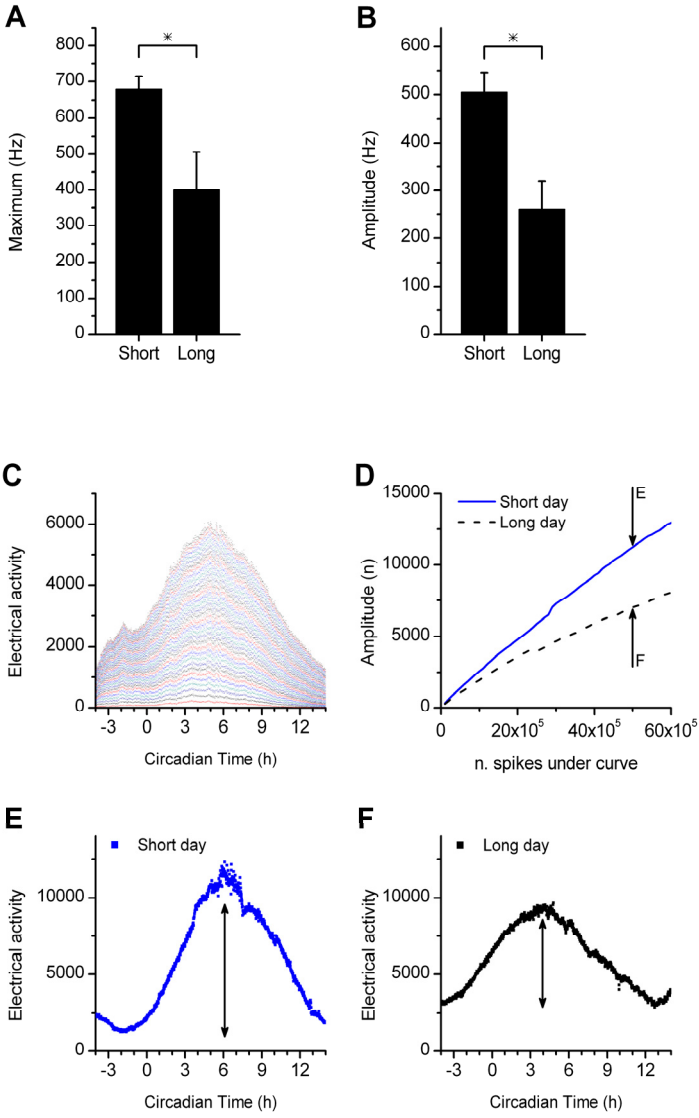
A
Maximum (Hz)
800
700
600
500
400
300
200
100
0
Short
Long
B
Amplitude (Hz)
600
500
400
300
200
100
0
Short
Long
C
Electrical activity
6000
4000
2000
0
-3
0
3
6
9
12
Circadian Time (h)
D
Amplitude (n)
15000
10000
5000
0
Short day
Long day
E
F
0
20x10^5
40x10^5
60x10^5
n. spikes under curve
E
Electrical activity
10000
5000
0
Short day
-3
0
3
6
9
12
Circadian Time (h)
F
Electrical activity
10000
5000
0
Long day
-3
0
3
6
9
12
Circadian Time (h)

Figure 5.5 Amplitude of the electrical activity peak in short and long days. (A) Maximal firing frequency recorded in slices from animals maintained in short and long days ($p < 0.05$). (B) Amplitudes of the rhythm, defined as the difference between maximal and minimum firing level in long and short day groups were significantly different ($p < 0.01$). (C) Subpopulation analysis, in which each line represents an increase of a total number of 10^5 action potentials recorded under the curve. Action potentials were counted in 60 sec bins. (D) Amplitude of electrical activity rhythms, for different numbers of action potentials included in the recording. The amplitude of the electrical activity in the short day group is larger than the amplitude in the long day group, for recordings with an equal number of action potentials. For 50×10^5 action potentials (indicated by arrows), examples of electrical activity patterns are indicated in E and F. The difference in amplitude between long and short days becomes larger with an increasing number of action potentials under the curve. (E, F) Examples of a recording in short and long days, with an equal amount of action potentials contributing to the electrical activity pattern.

Theoretically, it follows from such a working mechanism, that the amplitude of the rhythm in short days is larger than the amplitude in long days. That is, when neurons overlap in phase in short days, the maximum activity of each neuron will be at similar phases, leading to a high frequency in multiunit activity due to the summed activity of overlapping units during the peak, while during the trough, non-overlapping units lead to low activity (Rohling et al., 2006b). VanderLeest et al. (2009) measured the frequency of the multiunit activity of SCN neurons in long and short day slices and found that indeed, the maximum discharge levels are higher in short day animals (figure 5.5). A general assumption in the field of circadian rhythm research is that high amplitude rhythms are more difficult to shift than low amplitude rhythms (Pittendrigh et al., 1991), which stands in contrast to our present findings. To critically test the observed amplitude differences, VanderLeest et al. (2009) analyzed the amplitude under long and short days in more detail, by an off-line analysis of subpopulation activity. This allowed them to compare subpopulation activity rhythms, with an equal number of action potentials contributing to the circadian waveform. The results showed that in short days, the amplitude of the rhythm was larger than in long days for any given number of spikes in the recording (figure 5.5).

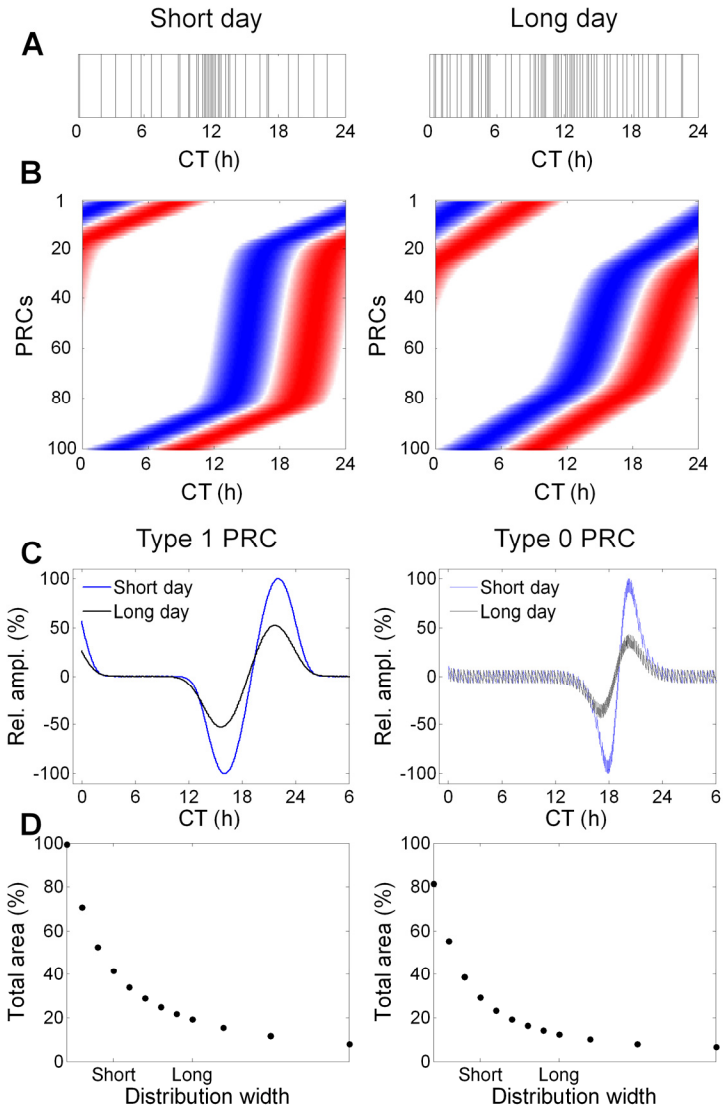
A
Short day
Long day
0
6
12
18
24
CT (h)
B
PRCs
1
20
40
60
80
100
C
Type 1 PRC
Type 0 PRC
Short day
Long day
Rel. ampl. (%)
100
50
0
-50
-100
D
Total area (%)
Short
Long
Distribution width

Figure 5.6 Short and long photoperiod PRCs obtained from simulations. (A) The distributions for short and long day subpopulations were taken from (VanderLeest et al., 2007). Each vertical line represents the peak time of a subpopulation of neurons. (B) A fitted curve through the long and short day length distribution was used to distribute 100 single unit PRCs. The y-axis represents differently phased single unit PRCs, distributed according to the fitted curve. The blue part of each line represents the delay part of the single unit PRC, the red part represents the advance part of the single unit PRC. The left side shows the distribution for short days and the right side shows the distribution for long days. (C) The resulting simulated PRCs for short and long days using type 1 single unit PRCs (left) or type 0 single unit PRCs (right). The long day PRCs show a lower amplitude than the short day PRCs (see also figure 5.7). (D) The area under the curve of the PRC decreases exponentially when the phase distribution of the neurons increases. The area is given relative to the area under the curve when all single unit PRCs coincide, which leads to a maximum amplitude of the PRC of the ensemble, and a maximal working area. On the x-axis, the observed distributions for the short and long day lengths are indicated. The left side shows the results for type 1 single unit PRCs, the right side for type 0 single unit PRCs. The results indicate that the area under the curve for short days is about two times larger than for long days, consistent with experimental results (see also figure 5.8).

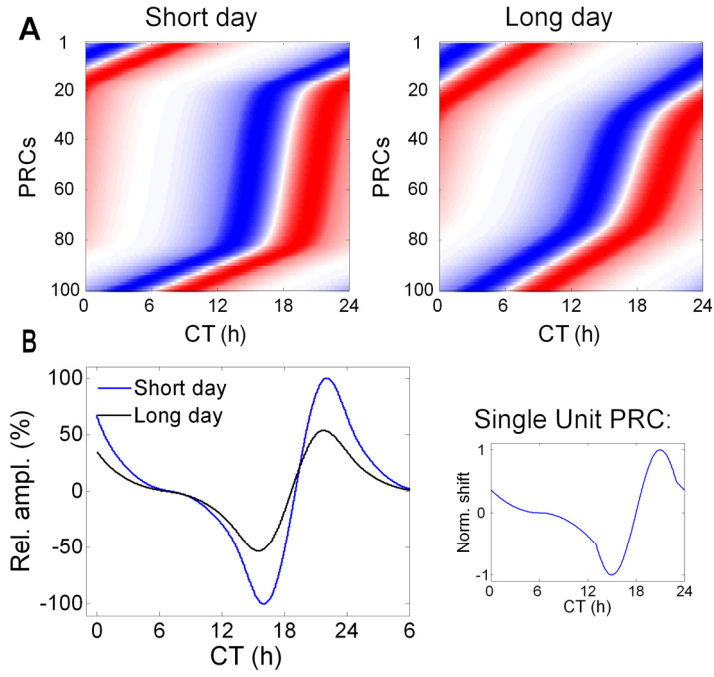

Figure 5.7 Simulating short and long day PRCs. Single unit PRCs without a dead zone (Ukai et al., 2007) were used for the simulations. (A) Distribution of 100 single unit PRCs, with the delay part in blue and the advance part in red. The left side shows the distribution for short days and the right side shows the distribution for long days. (B) The resulting long and short day PRCs show large shifts for short days and smaller shifts for long days. The right side shows the single unit PRC that was used in these simulations.

These findings contradict a long standing dogma in the field of circadian rhythms that the magnitude of a phase shift is inversely related to the amplitude of the rhythm, i.e. that it is more difficult to shift high amplitude rhythms than low amplitude rhythms. This dogma is based on the theory of limit cycle oscillators, where a perturbation of similar strength changes the phase of an oscillator with low amplitude more than one with higher amplitude, because the perturbation represents a larger fraction of the radius of the circle (Aschoff and Pohl, 1978;Winfree, 2000). The question is how to explain our current findings.

Both molecular and electrophysiological studies have provided evidence that photoperiodically induced waveform changes observed at the population level (Sumova et al., 2003;Mrugala et al., 2000) are caused by a reconfiguration of single cell activity patterns (Schaap et al., 2003;Hazlerigg et al., 2005;Inagaki et al., 2007;VanderLeest et al., 2007;Naito et al., 2008). In short day length single units oscillate highly in phase while in long days they are more spread out over the circadian cycle. Because in short days the phase distribution among neurons is narrow, light information will reach SCN neurons at a similar phase of their cycle. When the distribution is broad, however, light information reaches neurons at different phases of their cycle. We performed simulations both with type 1 and with type 0 PRCs in the distributions. When distributing 100 type 1 PRCs, the magnitude for the long day length PRC is 52.5% of the magnitude for the short day length PRC; for type 0 PRCs, this ratio is 43% (figure 5.8). The simulations revealed that irrespective of the type of single unit PRC, a broad distribution of cellular oscillations, corresponding to long days, results in a low amplitude PRC of the ensemble, and a narrow distribution, corresponding to short days, results in a high amplitude PRC of the ensemble (figure 5.6 and 5.7). These results were independent of the number of single unit PRCs that were used in the simulations, although small deviations occurred for low numbers ($n < 40$). The simulated differences in the magnitude of the shifts resembled the experimentally obtained data (figure 5.8).

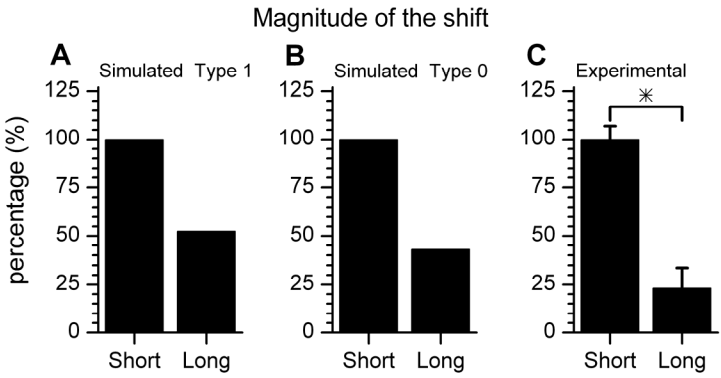

Figure 5.8 Magnitude of the light induced phase shift. (A) Experimentally obtained subpopulation distributions (VanderLeest et al., 2007) were used to distribute 100 type 1 single unit PRCs. The results revealed high amplitude phase shifts for short days and low amplitude shifts for long days. Short day shifts were normalized to 100%, long day shifts were plotted relative to this value. (B) The same procedure was followed for type 0 single unit phase response curves. (C) For comparison, the experimentally obtained phase shifts in running wheel activity are depicted with the shift in short days normalized to 100% ($p < 0.001$).

We have also measured the area under the curve for long and short day length PRCs for both the simulations and the experimentally obtained data (figure 5.9). The area under the simulated long day PRC curve is about 50% of the area under the short day PRC. This was true for both types of single unit PRCs that were used to construct the ensemble PRC. For type 1 single unit PRCs, the area under the curve of the simulated long day PRC was 55.9% of the area under the curve of the short day PRC. For type 0 single unit PRCs, the area under the curve of the simulated long day PRC was 53% of the short day PRC. The results from these simulations were independent of the number of single unit PRCs and in accordance with the experimentally obtained data (figure 5.9).

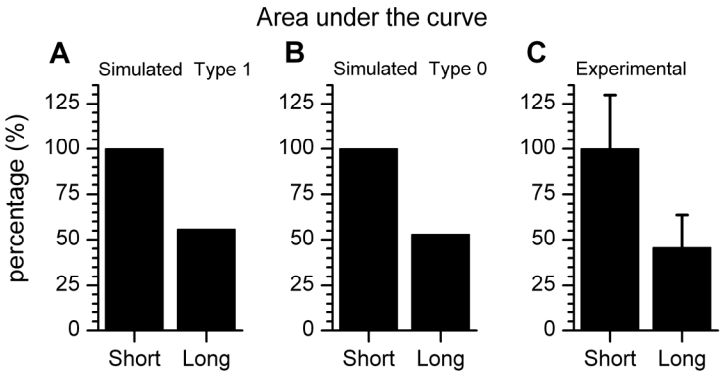

Figure 5.9 Area under the phase response curve. (A) Quantitative analysis of the PRC based on type 1 single unit PRCs by a measurement of the area under the curve. For short days, the area was normalized to 100% and for long days, the area was plotted as a fraction of this value. (B) The same procedure was repeated for type 0 single unit PRCs. (C) The relative area under the curve from experimentally obtained behavioral PRCs. The area under the PRC in long day length is 45% of the normalized area in short day length.

In summary, our findings indicate that the phase shifting capacity of the SCN expressed in long and short day length is retained in the SCN in vitro, offering an attractive model for future investigation. Our data also show that the inverse relation between the phase shifting capacity and the amplitude of the rhythm may not hold for neuronal networks in which neurons oscillate with different phases. We have shown that such networks respond in fact opposite, and show a maximum phase shifting capacity when the rhythm amplitude is large, and a smaller response when the amplitude is low. The data provide a clear example that neuronal networks are governed by different rules than single cell oscillators. To predict the phase response characteristics of the SCN network, we have taken into account the phase distribution among the single cell oscillators. We realize that a more accurate prediction of the properties of the network can be obtained when the interactions between the single cell oscillators are incorporated (Johnson, 1999;Indic et al., 2007;Beersma et al., 2008). In the past few years a number of synchronizing agents have been proposed such as VIP, GABA, and gap junctions (Colwell et al., 2003;Aton et al., 2005;Welsh, 2007;Albus et al., 2005;Long et al., 2005;Colwell, 2005), and it would be interesting to determine their role in photoperiodically induced changes in the phase

resetting properties of the SCN. Our findings may be relevant not only for the photoperiodic modulation of the phase shifting capacity of the circadian system, but may have broader implications and be relevant also to observations of reduced light responsiveness and reduced circadian rhythm amplitude in the elderly.

Chapter 6

Asymmetrically coupled two oscillator model of circadian clock in the SCN

6.1 Introduction

The biological clock acts as a physiological pacemaker, generating an endogenous rhythm that is circadian, i.e. these endogenous rhythms have an approximate length of 24 hours. To anticipate the daily light-dark (LD) cycle correctly, the pacemaker must be entrained to the environmental LD cycle. The period of the endogenous rhythm of the circadian pacemaker is usually denoted by τ and can be measured when all environmental conditions are kept constant. When the organism is placed in complete darkness (DD), such that no periodic LD cycle is present, the organism shows a behavioral *free-running* rhythm: it shows a rhythmic behavioral cycle with a period length of τ hours (notwithstanding small daily perturbations). Entrained to an environmental LD cycle with a period of T hours, the period of the pacemaker is changed by an amount of τ - T hours. While the length of the light and dark duration contributing to each day depend on the season, the daily environmental LD cycle on earth is characterized by T = 24 hours.

An animal's behavioral cycle is usually divided into a period of activity and a period of inactivity, coinciding with subjective day and subjective night. This holds in a LD schedule as well as under free-running conditions.

The endogenous cycle, with a period of τ hours, is often expressed in *circadian time* (CT). The free-running period is defined to be 24 circadian hours, such that each circadian hour amounts to τ/T physical hours, consequently in the environmental LD cycle, a circadian hour equals $\tau/24$ physical hours. The start of the subjective night is defined at circadian time 12 by convention (Pittendrigh and Daan, 1976a). The LD cycle to which the pacemaker is entrained is called a *Zeitgeber* (german for "time provider") (Aschoff, 1965b), and the 24 hours of its environmental cycle define the so-called *Zeitgeber time* (ZT).

Entrainment to the environmental LD cycle is causally linked to light input coming from the retina through a specialized photic entrainment pathway, the retino-hypothalamic tract (RHT) (Nelson and Takahashi, 1991;Meijer, 2001). At different times of the subjective cycle, the organism's susceptibility to this light input differs. Light pulses given during subjective day cause little or no phase shift, while light pulses of the same intensity and duration given during subjective night cause large phase shifts (Daan and Pittendrigh, 1976). If the magnitude of the phase shifts is determined for different circadian timepoints, distributed over the circadian day, a so-called *phase response curve* (PRC) can be constructed (see figure 6.1) (Daan and Pittendrigh, 1976;Pittendrigh, 1981b;Nelson and Takahashi, 1991).

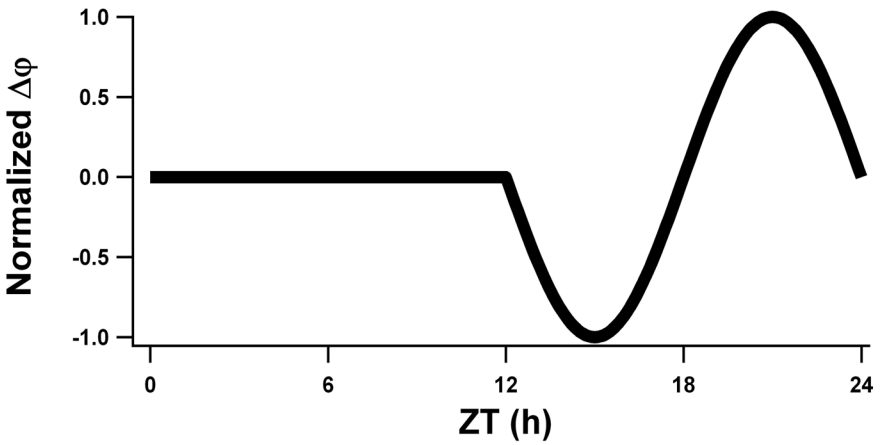

Figure 6.1 Mathematical approximation of a typical phase response curve (PRC). This PRC will be used in the mathematical analysis described in this chapter.

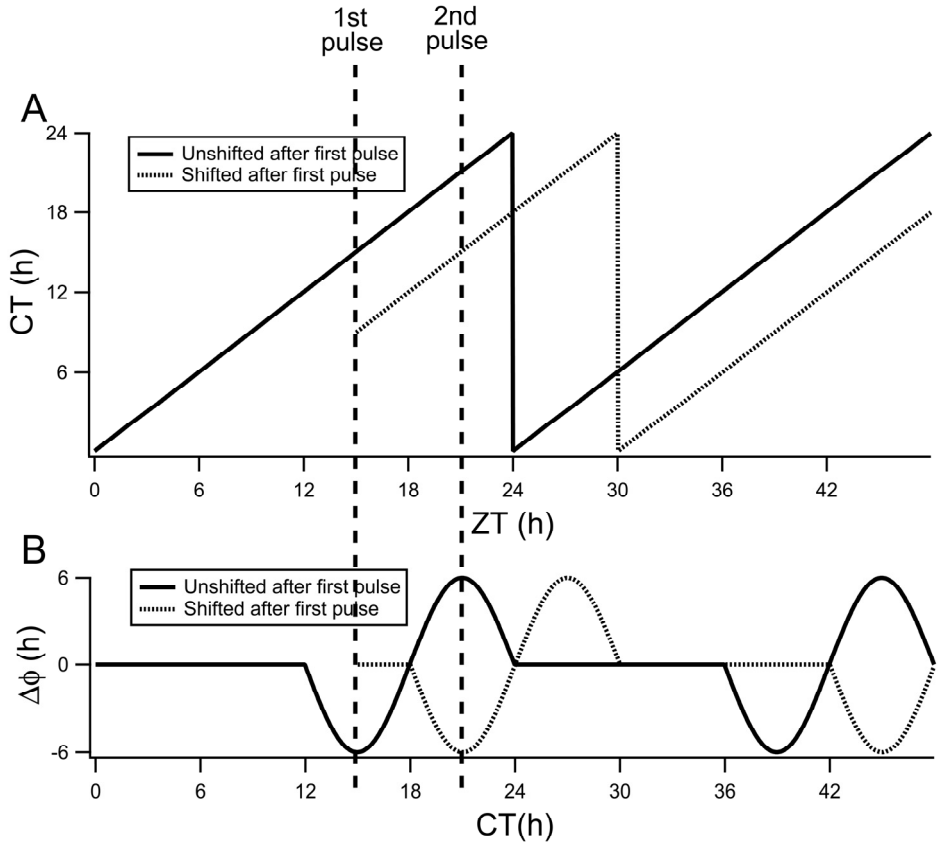

Figure 6.2 Mechanism for two-pulse phase shift experiment. (A) shows the phase of the internal clock of the organism (CT) with respect to the external time (ZT), where the internal period of the organism in this example is 24 h. (B) shows the PRC of the organism, given in CT. The first light pulse is given at ZT 15. The second pulse is given at ZT 21. The solid lines represent the case when the organism is unaffected by the first light pulse. The dotted lines represent the case when the organism instantaneously shifted its internal phase (CT) after the first pulse. To know if the organism instantaneously shifted its phase or not, one only needs to check what happens after the second light pulse. If the organism did not shift instantaneously, the effect of the second pulse would be an advance of the internal phase of the organism by 6 hours, as can be read from the solid PRC in (B). If the animal did instantaneously shift, the organism would delay its phase by 6 hours.

Some studies have reported that the oscillator resets essentially instantaneously after been given a light pulse (Pittendrigh, 1981a;Meijer and de Vries, 1995;Watanabe et al., 2001;Best et al., 1999). Pittendrigh was the first to show this instantaneous shifting of the pacemaker with a series of two-pulse phase shift experiments in *Drosophila* (Pittendrigh, 1981a). A phase delay (or advance) inducing pulse is followed by a second ('tester')

pulse every hour after the first pulse, for a full 24 hours. The delay (or advance) reconstructed from the behavior after the tester pulse agrees with the shift that would be the result if the shift of the first pulse has already been taken into account. Thus the effective PRC that governs the phase shift of the pacemaker with respect to the tester pulse is considered to be the PRC of the shifted pacemaker resulting from the first pulse, rather than the PRC of the unshifted pacemaker. Other studies found similar results for *Neurospora* (Crosthwaite et al., 1995), for mice (Sharma and Chandrashekaran, 2000), and for Syrian hamsters (Elliott and Pittendrigh, 1996;Best et al., 1999;Watanabe et al., 2001).

Behavioral recordings however show that the shift is not immediate. If a single light pulse is given somewhere during the subjective night of the organism, it takes some cycles before the behavior of the organism shifts its phase completely. These cycles are called transient cycles. They only last a few cycles. For phase advances, transient cycles typically last longer than for phase delays (Waterhouse et al., 2007). This phenomenon is associated with jet lag.

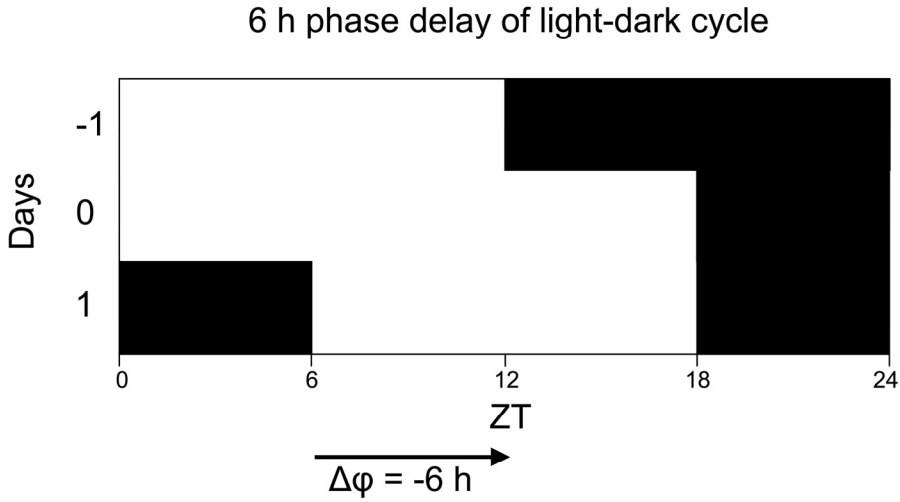

Figure 6.3 Protocol for a 6 hour phase delay of the light dark cycle. At the day of the phase shift, the light period is extended by six hours. On the day following the shift the light period starts six hours later than in the previous light dark cycle. Such a six hour phase delay results in a shift of -6 hours. In the protocol used by Albus et al. (2005), the following days were in constant darkness. In the protocols used by Reddy et al. (2002) and Yamazaki et al. (2000), the new light dark regime was continued.

The seemingly incompatible findings of an instantaneously shifting SCN on the one hand and the existence of transient cycles on the other hand led Pittendrigh to believe that such transients reflect the motion of a second slave oscillator that gradually relaxes to a steady-state phase relationship with respect to the primary (reset) pacemaker (Pittendrigh, 1981a). Watanabe and colleagues have also speculated on a secondary downstream oscillatory system, either inside or outside the SCN (Watanabe et al., 2001). Inside the SCN two regions can be distinguished, the ventral region, where the environmental light information enters the SCN, and a dorsal part, which contains the majority of output fibers from the SCN to other body parts.

Albus and co-workers showed that after a 6 hour delay of the LD cycle (see figure 6.3) the ventral and the dorsal part of the SCN shift at a different pace (Albus et al., 2005). The ventral part shifts immediately to a newly imposed light dark cycle, while the dorsal SCN requires about 6 days to regain a steady state phase relationship with the new light dark cycle. In table 6.1 the quantitative results from this experimental study are shown. In this study, we have built a mathematical model for this mechanism of dissociating regions of the SCN (figure 6.4).

The model described in this chapter is based on the two oscillatory regions in the SCN, the ventral and the dorsal regions. Other models describe the SCN either by one limit cycle oscillator (Wever, 1965;Wever, 1972;Kronauer et al., 1982;Kronauer, 1990) or by a large group of identically coupled limit cycle oscillators (Winfree, 1967;Pavlidis, 1971;Pavlidis, 1978a;Achermann and Kunz, 1999;Bernard et al., 2007).

Day	$\Delta\varphi$ component 1 (h)	$\Delta\varphi$ component 2 (h)
1	-6.2 ± 0.6	-1.8 ± 0.6
3	-7.9 ± 0.8	-2.8 ± 0.8
6	-6.0 ± 0.7	

Table 6.1 Average phase shifts and standard error of the means of the ventral and dorsal component of the SCN at day 1, day 3 and day 6 after a phase delay of 6 hours of the light dark cycle (taken from Albus et al., 2005).

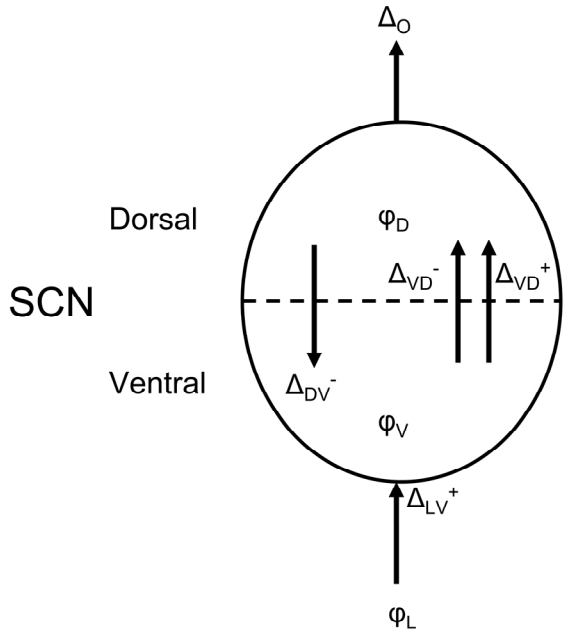

Figure 6.4 Model for the SCN, distinguishing a dorsal and a ventral part in the SCN with mutual interactions. φ_L = phase of external light-dark cycle, φ_V = phase of ventral SCN, φ_D = phase of dorsal SCN, Δ_O = influence of SCN on behavior, Δ_{LV}^+ = influence of light on (ventral) SCN, Δ_{VD}^+ = excitatory influence of ventral SCN on dorsal SCN, Δ_{VD}^- = inhibitory influence of ventral SCN on dorsal SCN, Δ_{DV}^- = influence of dorsal SCN on ventral SCN (based on Albus et al., 2005).

These models regard the SCN as a homogeneous structure. However, the SCN is not homogeneous. Different regions are described that seem to have different functional significance (ventral-dorsal: Albus et al., 2005;Nagano et al., 2003;de la Iglesia et al., 2004;Yan and Silver, 2004;Yan and Silver, 2002;Nakamura et al., 2005; rostral-caudal: Hazlerigg et al., 2005; anterior-posterior: Inagaki et al., 2007) and different types of neurons underlie heterogeneity in function. A model that focuses on regional differences is the 'Gates and Oscillators' model of Antle et al. (2003). In this model, a non-oscillating entity, the 'gate', imposes external influences on the oscillating unit, which comprises of numerous individual non-coupled limit cycle oscillators. The 'gate' drives the phase of all oscillators towards a mean phase. Other models that take heterogeneity into consideration are described by Gomes Cardoso et al. (2009) and Vasalou et al. (2009).

For our model a precise mathematical formulation is given in terms of a system of two asymmetrically coupled ordinary differential equations

(ODE). This mathematical model is fit to the experimental results from the phase delay experiments described in Albus et al. (2005), and the results of the mathematical modeling studies are compared to the experimental results. After the model was fit to the experimental results described in Albus et al. (2005), this parameterized model was used with the protocols as described in Reddy et al. (2002) and Yamazaki et al. (2000), and the results from the model were compared to the experimental results of those studies. We show that this model of two interacting oscillators can qualitatively describe the dynamics of a phase shift.

6.2 Mathematical model

The model we consider is depicted in figure 6.4. Light information mainly enters the SCN in the ventral region. The ventral SCN induces an excitatory phase shifting effect on the dorsal SCN, as well as a, much smaller, inhibitory effect (Albus et al., 2005). A small inhibitory phase shifting effect goes from the dorsal to the ventral SCN region.

The dynamical variables are the phases for the ventral and the dorsal region of the SCN, in the model represented by φ_1 and φ_2 , respectively. These phases represent the activity of the neural network in the corresponding SCN region. Under constant environmental conditions this activity follows a fixed periodical pattern with an intrinsic period τ, measured in 24 hours of CT, and the two phases are therefore measured in CT as well. In electrical activity measurements, the maximum activity of the sinusoidal function is reached at CT 6 (Schaap et al., 2003;VanderLeest et al., 2007).

The day-night rhythm is included in the model as an additional dynamical variable φ_0, with an angular speed of 1. The angular speed contrasts with that of φ_1 and φ_2, where the difference between CT and ZT results in a slightly deviating angular speed of ξ_1 and ξ_2, which are relative to the intrinsic periods τ_1 and τ_2 for both regions. The LD cycle is described by a 12 hour light period and a 12 hour dark period. To simplify the model, we also assume that the ventral and dorsal regions have similar activity patterns: a 12 hour active phase and a 12 hour inactive phase.

The influence functions are based on phase shifts to light, which are described by PRCs. A light PRC was used for the influence of light to the ventral SCN. A phase resetting function between ventral and dorsal SCN has not been measured experimentally. For this reason we used PRCs with the same shape as light PRCs for the phase resetting between ventral and dorsal SCN. The normal PRCs for light pulses were used for the positive effects, while PRCs for dark pulses where used for the negative connections. The dark pulse PRC shows phase resetting from CT 0-12 and has a deadzone from CT 12-24, opposite to the light pulse PRC.

We assume that the PRCs describe the instantaneous effect of a light pulse on the internal clock. In principle, the PRCs contain all the necessary information to model the system under study, without knowing the actual underlying mechanisms. We consider a continuous ODE model with coupling via empirically measured PRCs. The actual PRCs are themselves modeled by simple analytical curves (figure 6.1).

The light-induced PRCs have a deadzone during the subjective day, while the dark-pulse PRCs have a deadzone during the subjective night. In the deadzone, no shifts in phase are imposed. Together with the fact that the PRCs can only cause phase shifts in the target area if the stimulating region is in its active phase, a phase response curve can be created for the different regions (figure 6.5 C). Figure 6.5 shows the PRCs and responses (right-hand terms) of the system for fixed phase differences, where the ventral region is shifted by 3 hours and the dorsal by 4 hours with respect to the LD cycle. Figure 6.5 A shows the activity patterns of light, the ventral and the dorsal SCN. In figure 6.5 B, the PRCs are shown for the targeted regions that are under the influence of the activity periods directly above them in figure 6.5 A. The responses in figure 6.5 C are of the targeted areas, so left is the response of the ventral SCN to light, in the middle the response of the dorsal SCN to the both the excitatory and the inhibitory influences from the ventral SCN, and on the right the response is shown of the ventral SCN to the dorsal SCN.

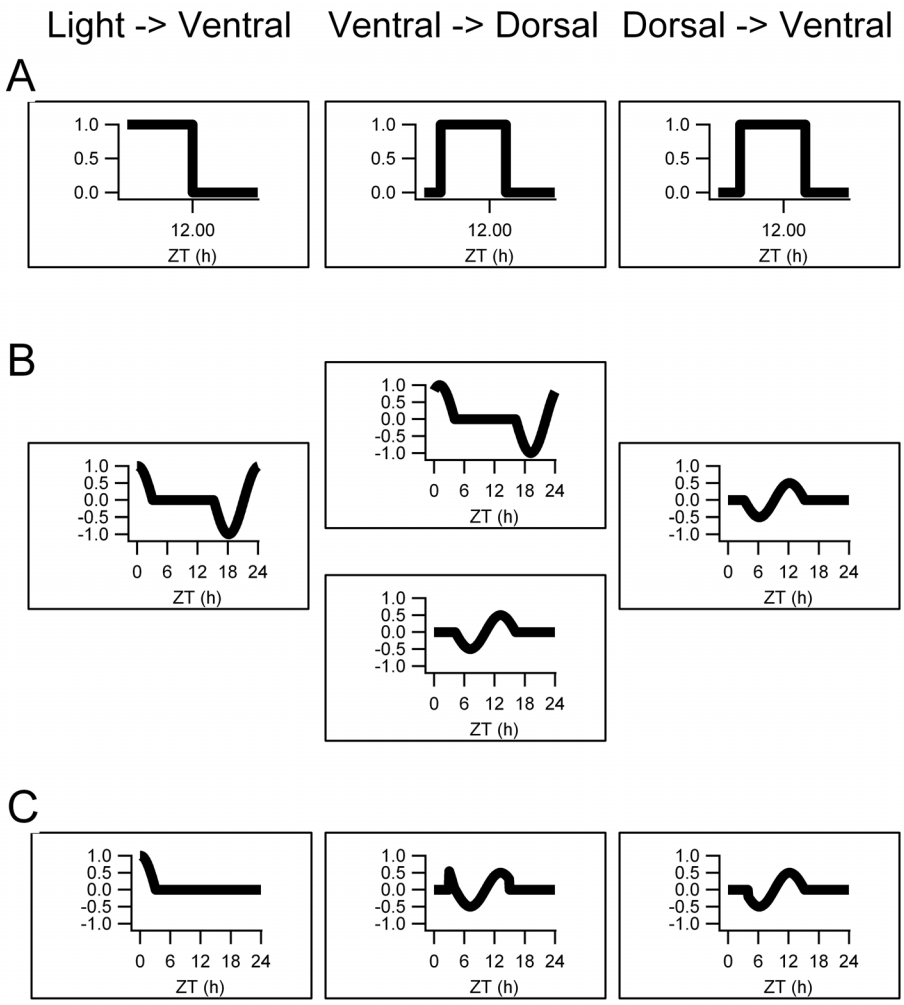

Figure 6.5 PRCs and response functions for fixed phase differences. The ventral SCN has a phase difference of 3 h with respect to physical time (ZT), and the dorsal SCN has a phase difference of 4 h. (A) shows the periods of activity of light, the ventral SCN and the dorsal SCN, respectively and they act as stimulating regions. (B) shows the PRCs of the targeted regions. On the left the PRC is shown of the ventral SCN when stimulated by light input. The middle two figures show the PRCs of the dorsal SCN for the positive and the negative reaction to the influence of the ventral SCN. On the right the ventral SCN under (negative) influence of the dorsal SCN is shown. The negative PRCs have been scaled by a factor of 1/2 to illustrate that these are usually much smaller than the others. (C) shows the actual phase response of the targeted area under influence of the activity rhythm of the stimulating regions. On the left the response of the ventral SCN to light is shown. The middle figure shows the dorsal response to the ventral stimulation and the right figure shows the ventral response to the dorsal input.

The model is described by the following set of ODEs

Light: $$\frac{d\varphi_0}{dt} = 1 \quad (1)$$

Ventral Oscillator: $$\frac{d\varphi_1}{dt} = \xi_1 + k_1 P(\varphi_0)\Delta_{01}(\varphi_1) + k_3 P(\varphi_2)\Delta_{21}(\varphi_1) \quad (2)$$

DorsalOscillator: $$\frac{d\varphi_2}{dt} = \xi_2 + k_2 P(\varphi_1)\Delta_{12a}(\varphi_2) + k_4 P(\varphi_1)\Delta_{12b}(\varphi_2), \quad (3)$$

where Δ_{ij} is the PRC of the *j*-th oscillator with regard to the *i*-th stimulus, $P(\varphi_i)$ is the activity of this stimulus, $k_i > 0$ are the coupling strengths and $\xi_i = \tau_i/24$ is the relative period of the endogenous oscillators, with respect to ZT. The PRCs and activities are explicitly given by

$$P(\varphi) = \begin{cases} 1 & \text{if } 0 \le \varphi \le 12 \\ 0 & \text{otherwise} \end{cases}, \quad (6)$$

where all phases are to be interpreted modulo 24 (hours), and the response functions

$$\Delta_{01}(\varphi_1) = -\sin(2\chi\varphi_1) \cdot (1 - P(\varphi_1)) \quad (7)$$

$$\Delta_{21}(\varphi_1) = -\sin(2\chi\varphi_1) \cdot P(\varphi_1) \quad (8)$$

$$\Delta_{12a}(\varphi_2) = -\sin(2\chi\varphi_2) \cdot (1 - P(\varphi_2)) \quad (9)$$

$$\Delta_{12b}(\varphi_2) = -\sin(2\chi\varphi_2) \cdot P(\varphi_2), \quad (10)$$

where $\chi = 2\pi/24$. Furthermore we will assume that the inhibitory influences are much smaller than the excitatory influences: $k_4 \approx k_3 \langle\langle k_2 \approx k_1$.

A phase difference for the oscillators is determined on the basis of the deviation in external time (ZT) for the internal phase of the oscillator at CT 6 (figure 6.6). If the animal's behavior is synchronized with physical time, then $\varphi_2 \approx \varphi_1 \approx \varphi_0$, and $\varphi_2 = 6$ (maximal activity) occurs at $\varphi_0 = 6$ (noon). The phase difference is then 0. In entrained conditions, the difference remains 0 (figure 6.6 A). If the oscillator is free-running, having a τ which is not 24 h, the phase of the oscillator starts to deviate from the 24 h cycle. The ZT at which the oscillator arrives at its intrinsic maximum activity level, which is at CT 6, is becoming earlier for $\tau < 24$ h (figure 6.6 B) or later for $\tau > 24$ h.

Figure 6.6 C shows that this deviation becomes larger every day. Note that the figure runs downwards. Day 1 is at the top of the figure while the last day is at the bottom of the figure. This resembles the way behavioral activity is usually plotted.

After a shift of the LD cycle, the oscillators will start having a phase difference. The model will cause the oscillators to shift their phase towards the new LD cycle. The phase shift of the oscillator is determined by the difference in its phase (at CT 6) in real hours (on the ZT timescale) before and after the shift of the oscillator.

6.3 Fitting the model

We used the experimental data of Albus et al. (2005) to fit the model, minimizing a global error criterion. The model fitting consists of a number of steps. In the first step, random parameter values are chosen uniformly from intervals described in Muskulus and Rohling (2009). If the parameterized model satisfies the conditions for free-running and entrainment to a LD cycle, a simplex algorithm (Nelder and Mead, 1965) is invoked to optimize the parameter values with respect to a global error criterion. The error criterion is based on the following constraints:

1. stable free-running period for a τ = 23.8 h, which is an approximation of the average endogenous period for a rat;
2. stable entrainment to an external period of T = 24 h;
3. experimentally obtained data after a phase delay of 6 h, as described in Albus et al. (2005) (see table 6.1).

In step 3 the model is integrated six days under the phase shift protocol described in Albus et al. (2005), starting at day 0. The peaks of the ventral and dorsal phases, i.e., the times ZT when the internal phases CT exhibit a value of 6 hrs, were recorded for each of the three days for which experimental data points were obtained: one, three, and six days after the shift of the LD cycle. The root-mean-square error of the deviation of these values and the values obtained in step 1 and 2 from the target values determines the value minimized by the simplex algorithm. More detailed information on weighting of the values is described by Muskulus and Rohling (2009).

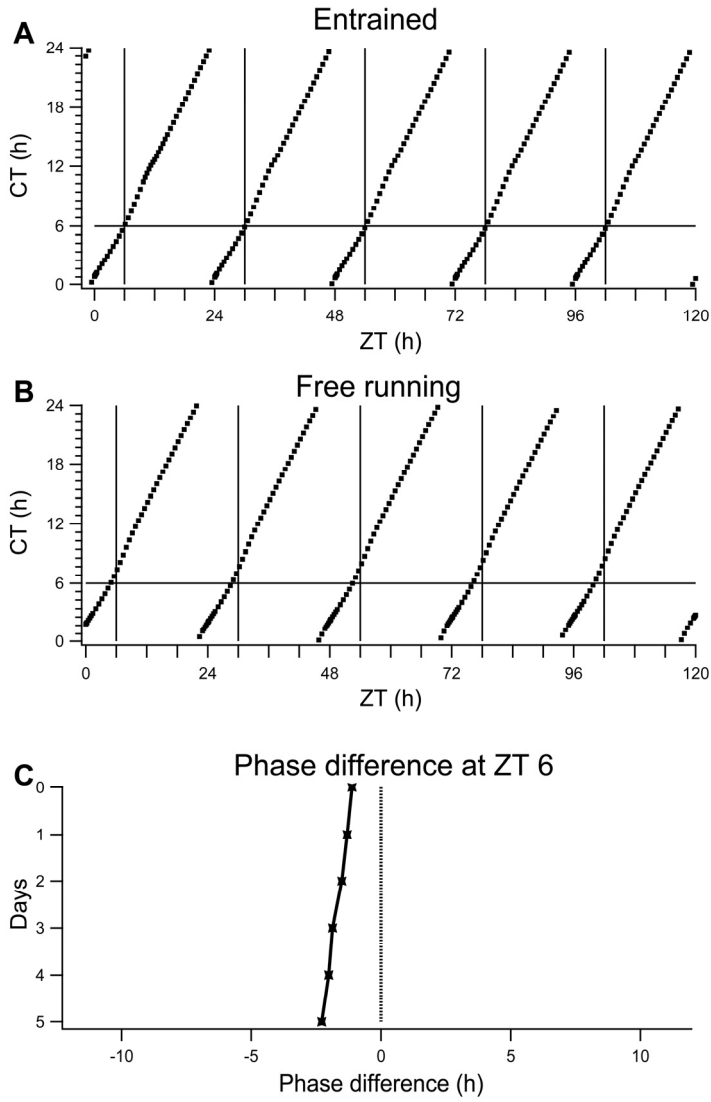

Figure 6.6 Numerical solution of model equations. (A) In entrained conditions the phase of the oscillator (in CT) is stable at ZT 6 of the Zeitgeber, for every successive cycle. In the remainder of the 24h, the phase may diverge from the Zeitgeber phase, but the internal phase CT 6 always coincides with ZT 6. (B) In free-running conditions, the internal phase of the oscillator diverges from the initial phase at ZT 6. Every cycle, the internal phase CT 6 is at an earlier Zeitgeber (ZT) phase, which means that this oscillator has a free-running period that is somewhat shorter than 24 h. (C) The phase diversion as described in (B) is plotted as a diversion from the stable 24 h entrained state (the dotted line). The timeline is running downwards, so day one is at the top of the figure and the last day at the bottom.

The ten sets of parameters that had the lowest error functions were selected (see Muskulus and Rohling, 2009) and used in the simulations described below. The following parameters sets were used for the different simulations (table 6.2):

Para-meters	**Delay experiments of Albus et al, 2005**	**Delay experiments of Reddy et al., 2002 and Yamazaki et al. 1999**	**Advance experiments of Reddy et al., 2002**
k_1	1.3139	1.1357	1.8927
k_2	0.7966	1.0396	1.0734
k_3	0.2289	0.3048	0.2276
k_4	0.0096	0.1514	0.0087
ξ_1	1.0186	1.0309	1.0189
ξ_2	0.9948	1.0032	0.9940

Table 6.2 Parameter sets used in the different simulations. These parameters are taken from the ten sets of parameters having the lowest error functions (see Muskulus and Rohling, 2009).

6.4 Results of the numerical simulations

We used the experimental data of Albus et al. (2005) to validate the model. As seen from this data (table 6.1), the ventral oscillator in the model adapts quickly to the change in daylight regime, whereas the dorsal oscillator needs more days. In figure 6.7 the shift in phase for the ventral and dorsal part of the SCN-model is shown together with the experimental results.

The simulation data for the ventral SCN shows a fast shift, which resembles the fast shift seen in the experimental data. The experimental data shows some kind of 'overshoot' at day 3 after the shift, for it has shifted 7.9 h while the light dark cycle shifted only 6 hours. The shift of the ventral SCN at day 6 after the shift was again 6 hours, equal to the shift of the external cycle. In the simulation data an 'overshoot' is visible, but it is not as big as seen in the experimental data. Also at day 6 after the shift, the simulation data is still shifted more than 6 hours. When the simulation is continued in DD, according to the protocol, it becomes clear that at day 10 after the shift of the light dark cycle the system starts to show free-running behavior (figure 6.8). At day 14 after the shift of the light-dark cycle the

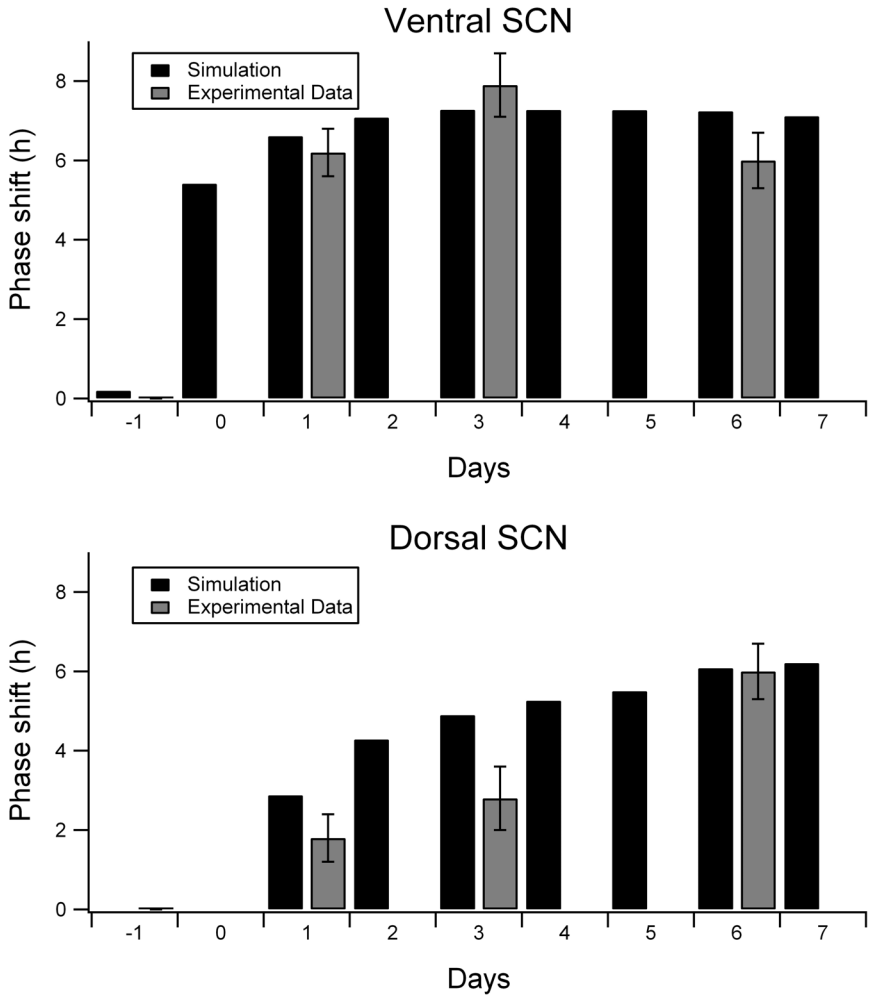

Figure 6.7 Phase shift after a phase delay of the Zeitgeber of 6 h given at day 0. The simulation data is shown from one day before the phase shift until seven days after the shift. The experimental data from table 1 is plotted as a reference for both the ventral and dorsal SCN.

ventral SCN in the simulation arrives at a 6-hour shift. From this day onwards it continues its free-run.

In the simulations, the dorsal SCN shifts more gradual than the ventral SCN, in accordance with the experimental data. The simulation data for the dorsal SCN has a greater shift in the first days compared to the experimental data, but 6 days after the shift of the light dark cycle the shift in hours was comparable to the experimental data. When the simulation was continued in DD for more than 6 days, it appeared that the dorsal SCN continued for a

few days with an overshoot similar to the ventral SCN, but less pronounced. Probably due to the influence of the ventral SCN in the simulations, which shifted more than 6 hours, the dorsal SCN in the simulations was also pulled to shift more than 6 hours. Around day 13 after the shift of the light dark cycle, the dorsal SCN in the simulations only shows free-running behavior (data not shown, but is similar to figure 6.8).

Summarizing the results, the dorsal oscillator adapts more slowly to the new regime than in the experimental data, and although the ventral oscillator shows an overshoot that was also found in the experimental data, the model is generally less pronounced than the experiment. Nevertheless, the model captures the adaptation to the new LD regime in a qualitatively correct way.

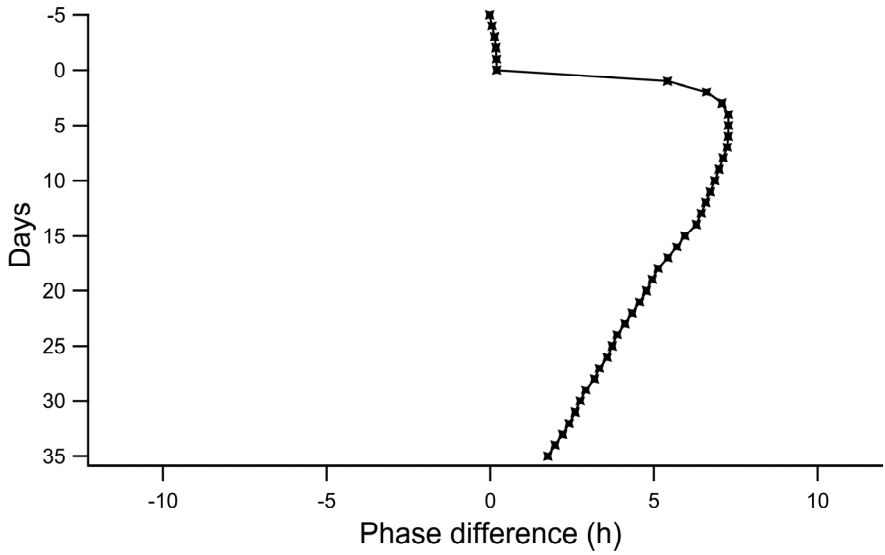

Figure 6.8 Long-term phase shift behavior of the ventral SCN after a delay of 6 hours according to the protocol defined in Albus et al. (2005). Note that the timescale is running downwards, where the first day is at the top of the figure and the last day at the bottom. At day 0, the phase of the LD cycle was delayed by 6 h. The days before the shift (denoted by negative numbers) the SCN was in entrained conditions and no deviation in phase was present. After the phase shift, the ventral SCN shifted quickly to the new light-dark regime. At day 2 after the delay, the conditions were changed to constant darkness. From day 10 after the shift, the ventral SCN starts to show free-running behavior. The period is somewhat less than 24 hour, causing the ventral SCN to advance its phase every day.

Consequently the model has been subjected to phase shifting protocols from other authors (Reddy et al., 2002;Yamazaki et al., 2000). In these protocols the new LD cycle continues, which means that the system is not expected to go into a free-run. The results are shown in figure 6.9.

The experimental data from Reddy et al. (2002) reflects a phase shift in behavioral activity of mice, while the experimental data from Yamazaki et al. (2000) shows a phase shift in Per1 expression in SCN cultures. While both dorsal and ventral SCN together determine the output of the SCN, our simulation data indicates that the dorsal SCN better corresponds to the behavioral data. At day 1, 6 and 7 after the shift of the LD cycle, the results of the dorsal SCN from the model are within the range of the standard deviation of the experimental data of Reddy et al. (2002), while at days 2-5 after the shift, the simulated dorsal SCN shifted a little less pronounced. The model captures the data of Reddy et al. (2002) in a qualitatively correct way. In the study of Yamazaki et al. (2000) only days 1 and 6 after the shift of the LD cycle were measured. For both days, the result of the dorsal SCN from the model is within the range of the standard deviation for that experiment. We can conclude that our model, which was fitted to data from a different phase shifting protocol, is able to simulate experimental data from other phase delay studies.

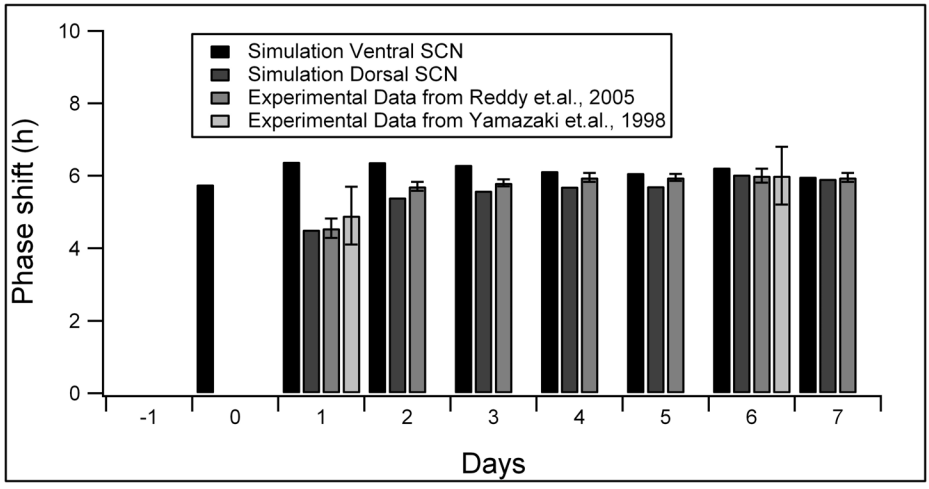

Figure 6.9 Phase shift after a phase delay of the Zeitgeber of 6 h given at day 0. The simulation data is shown from one day before the phase shift until seven days after the shift, following the phase shifting protocol used by Reddy et al. (2002);Yamazaki et al. (2000). The behavioral data from Reddy et al. (2002) and Yamazaki et al. (2000) are plotted as a reference.

In the simulations from the protocol of Albus et al. (2005), where the animals were put in constant darkness after one day in the new light dark regime, both oscillators started to show free-running behavior after 10-13 days, which means that by that time the effects of the phase shifts were complete. In the protocols as used in Reddy et al. (2002) and Yamazaki et al. (2000), where the animals remained in the shifted light dark regime for a longer period, no free-running is observed, but stable entrainment to the new light dark regime is established after 4-6 days, which adheres nicely to the experimental results (data not shown).

Additionally, the model is tested with experimental data obtained after 6 hour advance shift of the LD cycle. Figure 6.10 shows that after a phase advance, following the protocol used by Reddy et al. (2002), the simulated dorsal SCN shifts more slowly compared to delay data, which reflects the commonly known fact that phase advances are more difficult than phase delays. Although the experimental data in Reddy et al. (2002) shifts faster than advance of the simulated dorsal SCN, the error of the model is not big. Note that the model is tuned for the Albus delay protocol data (Albus et al., 2005), which may indicate that the model is applicable in a broader context than only for phase delays.

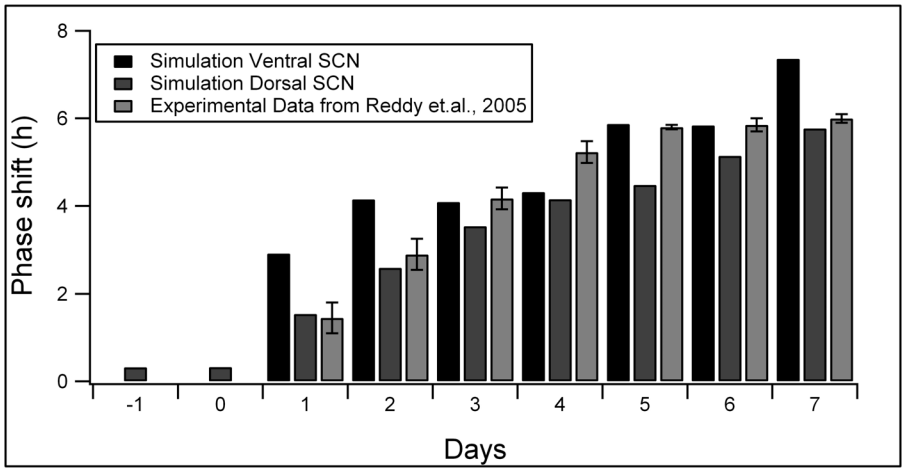

Figure 6.10 Phase shift after a phase advance of the LD cycle of 6 h given at day 0. The simulation data is shown from one day before the phase shift until seven days after the shift, following the phase shifting protocol used by Reddy et al. (2002). The behavioral data from Reddy et al. (2002) are plotted as a reference.

6.5 Discussion

The model described in this chapter is based on two regions in the SCN, the ventral and the dorsal region. It is the first model that considers both regions to be oscillators. The two oscillating regions interact with each other using non-uniform coupling mechanisms, and are self-organizing according to their coupling strengths under the influence of an external light dark regime. The model was able to qualitatively simulate different phase shifting studies.

The model was able to simulate the phase shifting results described in Albus et al. (2005); Reddy et al. (2002);Yamazaki et al. (2000). The parameters in the model were fit to the results from Albus et al. (2005), which appeared to be demanding for this model. It is difficult to find parameter values that accurately copy the experimentally obtained phase shift values. This could indicate that the current model is too simple to describe the system and needs more parameters to obtain a more precise match with the experimental data. It could also indicate that the simplifications in the current model are responsible for the deviations. A simplification that can cause the results of the model to deviate from the experimental results is that the activity rhythms for the light dark cycle, but also for the activity of the ventral and dorsal SCN, are modeled as on-off functions. In reality the rhythms in the SCN show slowly rising and falling slopes, creating a more sinusoidal activity function.

The model presumes instantaneous shifting, without any delay. Although it is known that the phase shifting effects of light are instantaneous in the SCN (Pittendrigh, 1981a;Meijer and de Vries, 1995;Watanabe et al., 2001;Best et al., 1999), it is not known if these phase shifting effects reflect the behavior of the complete SCN or only of a part of the SCN (Vansteensel et al., 2008). It is considered likely that only the light-sensitive part of the SCN shifts immediately (Vansteensel et al., 2008). This light-sensitive part may correspond to a subset of ventral SCN neurons. In two-pulse studies, only this light-sensitive part may shift immediately after the first pulse, and may shift again according to the shifted PRC following the second pulse. In *Neurospora* the shift was complete within 0.75 h (Crosthwaite et al., 1995), in *Drosophila* within 3 h (Pittendrigh, 1981a), in hamsters and mice within 2 h (Best et al., 1999). Future research is needed to determine if the phase

shifting for the different regions to light and to each other is indeed instantaneous or not.

Similar to describing the phase shifting effects of light on the SCN, we can describe phase shifting effects between regions in the SCN by a PRC. As opposed to a light-pulse PRC, a PRC for the coupling between regions in the SCN has not been determined experimentally. In the model described in this chapter, the coupling between the ventral and dorsal regions of the SCN is characterized by excitatory and inhibitory influences. The excitatory influences coincide with stabilizing effects to reach an equilibrium state and the inhibitory influences coincide with destabilizing effects. Different types of cells may be responsible for the excitatory and inhibitory effects between the ventral and dorsal SCN. As cells may have a sensitive period in which they are able to shift their phase (Beersma et al., 2008) the different cell types responsible for excitatory and inhibitory influences may be sensitive to phase shifts at different times. In the current model, the cells responsible for excitatory influences are sensitive to a shift in phase during the night, while the sensitive period for the cells responsible for inhibitory influences is during daytime. The PRCs that describe the phase shifting effects for the excitatory and inhibitory influences between the ventral and dorsal SCN are both characterized by a 12 h sinusoidal function together with a null-response in the deadzone. These PRCs may deviate from the real PRCs that describe phase shifting effects between the ventral and dorsal SCN, but these differences may only be of a quantitative nature, because every PRC is characterized by a delaying part and an advancing part, which are limited to a sensitive period. These various simplifications of the model may therefore not result in qualitatively different models. However, it may influence the phase shifting pace of the ventral and dorsal regions in the SCN. Future research on the coupling mechanisms between the ventral and dorsal regions is needed to resolve the mechanisms that underlie the exchange of phase information between these regions. This will improve the model and provides a better understanding of the functional significance of the ventral and dorsal region of the SCN.

Our model shows that an exact mathematical model comprising of two interacting, non-uniformly coupled oscillators, representing SCN regions,

can qualitatively describe experimentally obtained data for phase shifting attributes of the SCN. The model describes the phase shifts of the ventral and dorsal region of the SCN in response to each other and to the LD cycle. The results indicate that in the SCN different functional regions may exist each consisting of groups of cooperating neurons. These regions are interacting with each other, in the sense that they exchange phase information. The present results emphasize that phase shifting properties of the SCN emerge primarily at the network level by the communication between the ventral and dorsal region.

Chapter 7

Summary, conclusions and future work

In this thesis, computational models were created to investigate the biological clock in mammals, and more specifically the organization of the suprachiasmatic nuclei (SCN) and the coupling mechanisms between subpopulations of the SCN.

In mammals a circadian clock is located in the SCN. The animal can anticipate daily and seasonal rhythms in the environment because it is governed by an endogenous clock. At the molecular level, a transcriptional and translational feedback loop in SCN pacemaker cells generates an endogenous rhythm that is approximately 24 hours. To adjust to the environmental conditions, the clock must be able to synchronize, or entrain, to the daily light-dark cycle. To produce a concerted rhythmic output pattern, the clock cells within the SCN need to synchronize to each other as well as to the daily light-dark cycle. Coupling between the neurons is the mechanism to realize synchronization between the different cells.

Chapter 2 of this thesis provides an overview of different coupling mechanisms that are present in the SCN. The communication of phases between regions in the SCN may rely on different neurotransmitters, such as VIP or GABA. GABA can synchronize populations of neurons to each other, such as the dorsal and ventral region of the SCN. Within a region, VIP and gap junctions may be especially important coupling mechanisms. Thus, VIP

may synchronize cells within the dorsal or ventral region, while GABA may act as a synchronizer between these regions. Gap junctions may strengthen very specific groups of neurons in their coordinated output. No doubt the real situation will be more complex than this presentation. The exact nature of these coupling mechanisms is presently a major focus of many research lines in the field of circadian rhythm research, as it has become increasingly clear that coupling of clock neurons contributes strongly to the function of the SCN pacemaker to control daily and seasonal rhythms.

Different modeling studies of the circadian timing system and the SCN in particular have already been performed. An overview of the main directions of modeling studies of the biological clock is presented in chapter 2. In the first models, the clock was modeled as a single entity using a limit cycle oscillator. One limit cycle oscillator appeared to be unable to describe all the dynamic properties of the clock, which gave rise to two-oscillator models. In these models, the two oscillators were coupled and in the interaction between the oscillators some dynamic properties of the clock could be explained. As scientific knowledge in clock research progressed, it became increasingly clear that the circadian system is a heterogeneous system containing endogenously oscillating pacemaker cells. These findings resulted in two types of models. Some models focused on the modeling of the endogenous pacemaker cell and the generation of circadian rhythms itself. These models were based on molecular findings, such as the transcriptional/translational molecular feedback loop. Other models directed their research towards the network properties of the SCN. These models focused on the heterogeneous nature of the SCN and often presumed simple oscillatory units. The network properties of the SCN appear to be just as important for the control of circadian rhythms as the endogenous generation of rhythms by pacemaker cells.

When the molecular models and the network models are combined, the resulting models may become complex which makes the models hard to understand. At present, both type of models separately seem more to function satisfactorily to answer specific questions. This thesis demonstrates that simple models at the neuronal network level can provide interesting scientific results, and that models do not need to become very complicated to

produce scientifically interesting insights. The use of simple models is justified, if the model is able to provide a satisfying answer to the research question posed. The research question should be well defined in terms of the results intended and the boundaries for which the results are valid. The model should provide an answer that is sufficient, but that is also understandable. The modeling studies are especially useful if they lead to counterintuitive results.

An example of a useful simulation model is described in chapter 3. The model was based on previous experimental results from our laboratory, where it was found that very small populations of neurons could not produce an electrical activity pattern that resembled the multiunit electrical activity pattern, in width as well as in smoothness of the pattern. In support of this it was found that electrical activity patterns for single units, which may be regarded as the smallest possible population of neurons, have peaks that are narrower than the multiunit peak. The times of maximal single unit peak activities varies strongly and are distributed over the light-dark cycle. Finally, it was also shown that, by distributing single unit patterns over the day, and computing the total sum of the activity patterns, a feasible multiunit activity pattern could be obtained. This pattern could be altered by changing the width of the distribution of neurons, in this way simulating long and short day length.

The model described above can be summarized as follows. Single unit patterns have short electrical activity patterns. By themselves, single unit patterns can not account for a pattern as broad as recorded multiunit activity patterns in rats and mice. However, when the single unit patterns are active at different times of the day, the summed activity pattern of all single unit patterns resembles the recorded multiunit patterns. The question then is: how are the single units divided over the circadian cycle, or, in other words, what distribution can be used to distribute the single units in such a way that the added activity of all single units creates a realistic multiunit pattern?

In chapter 3, this research question was used to create a simulation model in which single unit activity patterns were distributed over the circadian cycle and accumulated to produce a multiunit activity pattern. Different single unit patterns were used and each pattern could be narrowed or

broadened. Four different distributions were tested: linear, Gaussian, bimodal and trimodal. The distributions could also be narrowed or broadened.

Using this simple simulation model, questions could be answered about how the different distributions and the changes in single unit activity patterns can alter the multiunit activity pattern. The results show that in order to obtain a realistic multiunit pattern, the single units had to be distributed in phase. It appeared also that all distributions tested can lead to a realistic multiunit pattern.

On the basis of the simulations it was predicted that changes in the width of the distribution of the single cells is necessary to account for photoperiodic encoding, even though changes in single unit activity may play an additional role. It was shown that changes in single unit patterns alone are not large enough to account for the multiunit pattern changes that are recorded in long and short day lengths. In contrast, minor changes in phase distribution between the neurons, are capable of encoding for day length.

On the basis of these findings some testable predictions are presented: if the mechanism for photoperiod encoding depends on changes in single unit patterns, the single unit activity patterns should show relatively large changes in the duration of electrical activity and the maximum frequency of the multiunit patterns should increase in long day lengths, if the distribution of the single units was kept constant. If photoperiod is encoded in the SCN by changing the distribution of neurons over the 24 h day, the frequency of the multiunit activity peak should decrease in long day lengths and single units should show a broader distribution. With this finding a way was found to distinguish between the two alternative models by simply measuring the multiunit electrical activity peak. Importantly, it was not necessary to measure the single units.

Experimental studies using extracellular electrophysiological recordings in-vitro showed that the shapes and widths of the single unit patterns in long and short days do not significantly differ. In chapter 3 these recorded single unit patterns are employed to show that changing the phase distribution between neurons can result in changes in multiunit pattern.

This simulation study is just one example of a simple model which provides interesting scientific results. These results could be obtained by a sharp focus on one specific mechanism of the SCN and by asking very specific questions about this mechanism. The model included only those mechanisms of the real system that were of importance for these specific questions. Within these well defined boundaries, the simple model could present some unsuspected and testable results.

In chapter 4 a study has been conducted to investigate the regional organization of the SCN. After a delay of 6 hours in the environmental light-dark cycle, a dissociation between the ventral and the dorsal region of the SCN was observed. At day one after the shift of the light-dark cycle, the ventral SCN immediately shifted to the new light-dark regime, while the dorsal SCN completed the shift of its phase only after 6 days. In the electrical activity patterns measured on the first day after the shift of the light-dark cycle two peaks could be identified. The electrical activity recordings were analyzed using different techniques, such as curve fitting and a subpopulation analysis. To investigate the properties of two subpopulations of neurons that are separated in time, a simple model was created. The simulations showed that only when the size of one of the populations was small and the distribution in that population narrow, a bimodal pattern could arise in the ensemble pattern. It appeared from the study that only a small number of the total population of neurons shifts immediately after a delay in the light-dark cycle. It is proposed that phase shifts are brought about by an initial rapid shift of this relatively small subpopulation of neurons within the SCN. This group is expected to be located in the ventral part of the SCN, given the fast shifts of the ventral SCN. Coupling between the shifted and the unshifted population of SCN neurons is asymmetrical, as the shifted neurons exert a strong phase shifting effect on the unshifted neurons. This causes a complete shift of the SCN which is realized after several cycles.

In future studies it should be realized that the different regions of the SCN, such as the ventral and dorsal region, may also be heterogeneous. The simulation studies that were performed indicated the existence of a small subpopulation of neurons which eventually brings about a shift in the

complete SCN. Experimental research can direct its search towards finding this distinct group of cells, and elucidate the coupling mechanisms which are important within this group and with other functionally distinct groups of neurons.

Chapter 5 describes a simple model that has been build to differentiate between responses to phase shifts in long and short day lengths. In the field of circadian rhythms, it is generally assumed that high amplitude rhythms are more difficult to shift in phase than low amplitude rhythms. This assumption originates from the theory on limit cycle oscillators, which is often used to model either the clock as a whole or individual pacemaker cells. Limit cycle oscillators that have high amplitudes are more difficult to shift in phase than limit cycle oscillators with low amplitudes. Experimental data, shown in chapter 5, showed the contradicting results that short day electrical activity patterns which have a high amplitude, shift more than long day patterns, with a lower amplitude. Using simple simulation studies, where phase response curves (PRCs) were distributed according to long and short day distributions, the experimental findings were confirmed. The results of the simulations indicate that if neurons are more synchronized in phase, the PRCs, or light-sensitive periods, are more compressed and overlap, resulting in a higher number of neurons that shift at the same time in the same direction in response to a light pulse, compared to desynchronized neurons in long days. The highly synchronized state during short days results consequently in a PRC with a higher amplitude, i.e. the shift in phase is larger, for short days compared to long days. As the limit cycle theory may be valid for individual neurons within the network, the network as an ensemble shows different response characteristics as a function of rhythm amplitude. The data presented in chapter 5 provides thereby a clear example that neuronal networks are governed by different rules than single cell oscillators and also shows the underlying explanation for this difference.

Chapter 6 provides a model to investigate the coupling mechanisms of two regions in the SCN after a shift of the light-dark cycle. The model is based on the ventral and the dorsal regions of the SCN, which are both considered endogenous oscillators in our simulations. The two oscillating regions interact with each other using non-uniform coupling mechanisms.

The ventral region of the SCN is influenced by the external light-dark cycle according to a PRC. The coupling between the ventral and dorsal regions of the SCN is described by PRCs as well. This coupling exists of excitatory, but also inhibitory influences. The ventral and dorsal regions are self-organizing according to their coupling strengths under the influence of an external light-dark regime. The model was able to qualitatively simulate results from different experimental phase shifting studies. The results indicate that in the SCN different oscillatory regions may exist each consisting of groups of cooperating neurons with their own phase resetting characteristics. The different oscillatory regions are interacting with each other, and transmit phase information. Chapter 6 emphasizes that phase shifting properties of the SCN emerge primarily at the network level.

In our approach we used simple models to elucidate the working mechanisms of the clock network. These simple models provided evidence that different levels of organization are responsible for different properties of the clock. While the endogenous rhythms are clearly a property of single cells, properties such as entrainment, resetting, or day length encoding arise at the neuronal network level.

A first step has been taken to better understand the neuronal network properties of the SCN. This thesis shows that a simple model can provoke questions that can guide future experimental research. For example, an interesting question is about which mechanisms underly the propagation of the instantaneous effects of light on the SCN to different regions in the SCN. Future research should be directed at determining the phase response curves to light for the different regions of the SCN, and for the interaction between the regions.

While we have distinguished between a dorsal and a ventral SCN, particular subregions may be present that are essential for phase resetting. Future research should target the functional meaning of different subregions in the SCN and consider also a division of the ventral and dorsal regions in different functional subregions.

Furthermore, the present studies did not consider direct single cell interactions. Phase distributions between neurons could explain a number of properties of the clock, but for now it is unknown how the cells are able to

organize themselves in these phase distributions. Also the communication mechanisms between cells in different regions or subregions have not been considered. The next step is to gain more knowledge about the coupling mechanisms between the neurons in the SCN in different functional groups within the SCN.

While the communication between neurons is immediate, after a shift of the light dark cycle the ventral region of the SCN shifts immediately to the new phase, but the dorsal region does not. This may be caused by the way the network is organized. However, other factors may play a role as well. A neuron may have a sensitive period for shifting its phase, which determines its PRC. The neuron also receives signals from other cells that produce a driving force for shifting its phase. The interplay between the sensitive period and the driving force is able to shift the phase of the neuron. This driving force constitutes different inputs from different cells and may differ between cell types. The driving force may differ throughout the circadian cycle and could contain an excitatory and an inhibitory period. The actual coupling signals from cell to cell should be the subject of future studies in order to identify this driving force.

Finally, we only used small and simple models to investigate questions about the network properties of the biological clock. For certain questions regarding different types of neurons cooperating in different regions in a large network of about 10,000 cells, corresponding with the real size of one SCN, simple models may not be sufficient. Larger models may be applicable to investigate these larger networks, as long as caution is taken to make the model unnecessarily complicated. These larger models are challenging for computer science studies and may demand the use of larger computers or larger networks of computers, such as grid-networks.

It is a challenge to combine different scientific disciplines. This thesis shows an example that the coordinated efforts of computer science and life sciences enrich each other and leads to scientific progress. The results that have been acquired could not have been found with separated efforts, showing that the results are more than the sum of parts.

Chapter 8

References

Abe M, Herzog ED, Yamazaki S, Straume M, Tei H, Sakaki Y, Menaker M, Block GD (2002) Circadian rhythms in isolated brain regions. J Neurosci 22:350-356.

Achermann P, Kunz H (1999) Modeling circadian rhythm generation in the suprachiasmatic nucleus with locally coupled self-sustained oscillators: phase shifts and phase response curves. J Biol Rhythms 14:460-468.

Albus H, Vansteensel MJ, Michel S, Block GD, Meijer JH (2005) A GABAergic mechanism is necessary for coupling dissociable ventral and dorsal regional oscillators within the circadian clock. Curr Biol 15:886-893.

Antle MC, Foley DK, Foley NC, Silver R (2003) Gates and oscillators: a network model of the brain clock. J Biol Rhythms 18:339-350.

Antle MC, Foley NC, Foley DK, Silver R (2007) Gates and oscillators II: zeitgebers and the network model of the brain clock. J Biol Rhythms 22:14-25.

Antle MC, Silver R (2005) Orchestrating time: arrangements of the brain circadian clock. Trends Neurosci 28:145-151.

Aschoff J (1960) Exogenous and endogenous components in circadian rhythms. Cold Spring Harb Symp Quant Biol 25:11-28.

Aschoff J (1965a) Circadian rhythms in man. Science 148:1427-1432.

Aschoff J (1965b) The phase-angle difference in circadian periodicity. In: Circadian clocks (Aschoff J, ed), pp 262-278. North Holland Press.

Aschoff J, Pohl H (1978) Phase relations between a circadian rhythm and its zeitgeber within the range of entrainment. Naturwissenschaften 65:80-84.

Aschoff J, Wever R (1962) Spontanperiodik des Menschen bei Ausschluß aller Zietgeber. Die Naturwissenschaften 49:337-342.

Aton SJ, Colwell CS, Harmar AJ, Waschek J, Herzog ED (2005) Vasoactive intestinal polypeptide mediates circadian rhythmicity and synchrony in mammalian clock neurons. Nat Neurosci 8:476-483.

Aton SJ, Herzog ED (2005) Come together, right...now: synchronization of rhythms in a mammalian circadian clock. Neuron 48:531-534.

Beersma DG (2005) Why and how do we model circadian rhythms? J Biol Rhythms 20:304-313.

Beersma DG, van Bunnik BA, Hut RA, Daan S (2008) Emergence of circadian and photoperiodic system level properties from interactions among pacemaker cells. J Biol Rhythms 23:362-373.

Bernard S, Gonze D, Cajavec B, Herzel H, Kramer A (2007) Synchronization-Induced Rhythmicity of Circadian Oscillators in the Suprachiasmatic Nucleus. PLoS Comput Biol 3:e68.

Best JD, Maywood ES, Smith KL, Hastings MH (1999) Rapid resetting of the mammalian circadian clock. J Neurosci 19:828-835.

Brown SA, Fleury-Olela F, Nagoshi E, Hauser C, Juge C, Meier CA, Chicheportiche R, Dayer JM, Albrecht U, Schibler U (2005a) The period length of fibroblast circadian gene expression varies widely among human individuals. PLoS Biol 3:e338.

Brown TM, Colwell CS, Waschek JA, Piggins HD (2007) Disrupted neuronal activity rhythms in the suprachiasmatic nuclei of vasoactive intestinal polypeptide-deficient mice. J Neurophysiol 97:2553-2558.

Brown TM, Hughes AT, Piggins HD (2005b) Gastrin-releasing peptide promotes suprachiasmatic nuclei cellular rhythmicity in the absence of vasoactive intestinal polypeptide-VPAC2 receptor signaling. J Neurosci 25:11155-11164.

Carre IA (2001) Day-length perception and the photoperiodic regulation of flowering in Arabidopsis. J Biol Rhythms 16:415-423.

Choi HJ, Lee CJ, Schroeder A, Kim YS, Jung SH, Kim JS, Kim dY, Son EJ, Han HC, Hong SK, Colwell CS, Kim YI (2008) Excitatory actions of GABA in the suprachiasmatic nucleus. J Neurosci 28:5450-5459.

Colwell CS (2005) Bridging the gap: coupling single-cell oscillators in the suprachiasmatic nucleus. Nat Neurosci 8:10-12.

Colwell CS, Foster RG, Menaker M (1991) NMDA receptor antagonists block the effects of light on circadian behavior in the mouse. Brain Res 554:105-110.

Colwell CS, Michel S, Itri J, Rodriguez W, Tam J, Lelievre V, Hu Z, Liu X, Waschek JA (2003) Disrupted circadian rhythms in VIP- and PHI-deficient mice. Am J Physiol Regul Integr Comp Physiol 285:R939-R949.

Crosthwaite SK, Loros JJ, Dunlap JC (1995) Light-induced resetting of a circadian clock is mediated by a rapid increase in frequency. Cell 81:1003-1012.

Daan S, Albrecht U, van der Horst GT, Illnerova H, Roenneberg T, Wehr TA, Schwartz WJ (2001) Assembling a clock for all seasons: are there M and E oscillators in the genes? J Biol Rhythms 16:105-116.

Daan S, Berde C (1978) Two coupled oscillators: simulations of the circadian pacemaker in mammalian activity rhythms. J Theor Biol 70:297-313.

Daan S, Pittendrigh CS (1976) A functional analysis of circadian pacemakers in nocturnal rodents. II. The variabilliy of phase response curves. J Comp Physiol 106:267-290.

Dawson A, King VM, Bentley GE, Ball GF (2001) Photoperiodic control of seasonality in birds. J Biol Rhythms 16:365-380.

De Jeu M, Pennartz C (2002) Circadian modulation of GABA function in the rat suprachiasmatic nucleus: excitatory effects during the night phase. J Neurophysiol 87:834-844.

de la Iglesia HO, Cambras T, Schwartz WJ, ez-Noguera A (2004) Forced desynchronization of dual circadian oscillators within the rat suprachiasmatic nucleus. Curr Biol 14:796-800.

de la Iglesia HO, Meyer J, Carpino A, Jr., Schwartz WJ (2000) Antiphase oscillation of the left and right suprachiasmatic nuclei. Science 290:799-801.

de la Iglesia HO, Meyer J, Schwartz WJ (2003) Lateralization of circadian pacemaker output: Activation of left- and right-sided luteinizing hormone-releasing hormone neurons involves a neural rather than a humoral pathway. J Neurosci 23:7412-7414.

DeCoursey PJ (1960) Daily light sensitivity rhythm in a rodent. Science 131:33-35.

Devlin PF, Kay SA (2001) Circadian photoperception. Annu Rev Physiol 63:677-694.

Ding JM, Chen D, Weber ET, Faiman LE, Rea MA, Gillette MU (1994) Resetting the biological clock: mediation of nocturnal circadian shifts by glutamate and NO. Science 266:1713-1717.

Drescher K, Cornelius G, Rensing L (1982) Phase response curves obtained by perturbing different variables of a 24 hr model oscillator based on translational control. J Theor Biol 94:345-353.

Eilers PHC (2003) A perfect smoother. Anal Chem 75:3631-3636.

Elliott JA, Pittendrigh CS (1996) Time course of hamster clock resetting following single light pulses. pp 105-157.

Elliott JA, Tamarkin L (1994) Complex circadian regulation of pineal melatonin and wheel-running in Syrian hamsters. J Comp Physiol [A] 174:469-484.

Enright JT (1980a) Temporal precision in circadian systems: a reliable neuronal clock from unreliable components? Science 209:1542-1545.

Enright JT (1980b) The Timing of Sleep and Wakefulness: On the Substructure and Dynamics of the Circadian Pacemakers Underlying the Wake-Sleep Cycle. Berlin: Springer Verlag.

Forger DB, Kronauer RE (2002) Reconciling mathematical models of biological clocks by averaging on approximate manifolds. SIAM J Appl Math 62:1281-1298.

Forger DB, Peskin CS (2003) A detailed predictive model of the mammalian circadian clock. Proc Natl Acad Sci U S A 100:14806-14811.

Forger DB, Peskin CS (2004) Model based conjectures on mammalian clock controversies. J Theor Biol 230:533-539.

Gallego M, Eide EJ, Woolf MF, Virshup DM, Forger DB (2006) An opposite role for tau in circadian rhythms revealed by mathematical modeling. Proc Natl Acad Sci U S A 103:10618-10623.

Gilette MU, DeMarco SJ, Ding JM, Gallman EA, Faiman LE, Liu C, McArthur AJ, Medanic M, Richard D, Tcheng TK, et al. (1993) The organization of the suprachiasmatic circadian pacemaker of the rat and its regulation by neurotransmitters and modulators. J Biol Rhythms Suppl 8:53-58.

Goel NS, Maitra SC, Montroll EW (1971) On the Volterra and other nonlinear models of interacting populations. Rev Modern Phys 43:319-324.

Goldbeter A (1995) A model for circadian oscillations in the Drosophila period protein (PER). Proc Biol Sci 261:319-324.

Goldman BD (2001) Mammalian photoperiodic system: formal properties and neuroendocrine mechanisms of photoperiodic time measurement. J Biol Rhythms 16:283-301.

Gomes Cardoso FR, de Oliveira Cruz FA, Silva D, Martins Cortez C (2009) Computational modeling of synchronization process of the circadian timing system of mammals.

Goodwin BC (1965) Oscillatory behavior in enzymatic control processes. Adv Enzyme Regul 3:425-438.

Granados-Fuentes D, Prolo LM, Abraham U, Herzog ED (2004) The suprachiasmatic nucleus entrains, but does not sustain, circadian rhythmicity in the olfactory bulb. J Neurosci 24:615-619.

Gribkoff VK, Pieschl RL, Dudek FE (2003) GABA receptor-mediated inhibition of neuronal activity in rat SCN in vitro: pharmacology and influence of circadian phase. J Neurophysiol 90:1438-1448.

Gribkoff VK, Pieschl RL, Wisialowski TA, Park WK, Strecker GJ, de Jeu MT, Pennartz CM, Dudek FE (1999) A reexamination of the role of GABA in the mammalian suprachiasmatic nucleus. J Biol Rhythms 14:126-130.

Griffith JS (1968) Mathematics of cellular control processes. I. Negative feedback to one gene. J Theor Biol 20:202-208.

Groos G, Hendriks J (1982) Circadian rhythms in electrical discharge of rat suprachiasmatic neurones recorded in vitro. Neurosci Lett 34:283-288.

Guala F (2002) Models, Simulations and Experiments. In: Model-Based Reasoning: Science, Technology, Values. (Magnani L, Nersessian NJ, eds), pp 59-74. New York: Kluwer Academic/Plenium Publisher.

Hamada T, Antle MC, Silver R (2004) Temporal and spatial expression patterns of canonical clock genes and clock-controlled genes in the suprachiasmatic nucleus. Eur J Neurosci 19:1741-1748.

Harmar AJ, Marston HM, Shen S, Spratt C, West KM, Sheward WJ, Morrison CF, Dorin JR, Piggins HD, Reubi JC, Kelly JS, Maywood ES, Hastings MH (2002) The VPAC(2) receptor is essential for circadian function in the mouse suprachiasmatic nuclei. Cell 109:497-508.

Hastings M (2001) Modeling the molecular calendar. J Biol Rhythms 16:117-123.

Hastings MH, Herzog ED (2004) Clock genes, oscillators, and cellular networks in the suprachiasmatic nuclei. J Biol Rhythms 19:400-413.

Hastings MH, Reddy AB, Garabette M, King VM, Chahad-Ehlers S, O'Brien J, Maywood ES (2003) Expression of clock gene products in the suprachiasmatic nucleus in relation to circadian behaviour. Novartis Found Symp 253:203-217.

Hazlerigg DG, Ebling FJ, Johnston JD (2005) Photoperiod differentially regulates gene expression rhythms in the rostral and caudal SCN. Curr Biol 15:R449-R450.

Herzog ED, Aton SJ, Numano R, Sakaki Y, Tei H (2004) Temporal precision in the mammalian circadian system: a reliable clock from less reliable neurons. J Biol Rhythms 19:35-46.

Herzog ED, Schwartz WJ (2002) A neural clockwork for encoding circadian time. J Appl Physiol 92:401-408.

Herzog ED, Takahashi JS, Block GD (1998) Clock controls circadian period in isolated suprachiasmatic nucleus neurons. Nat Neurosci 1:708-713.

Hofman MA (2004) The brain's calendar: neural mechanisms of seasonal timing. Biol Rev Camb Philos Soc 79:61-77.

Honma S, Shirakawa T, Katsuno Y, Namihira M, Honma K (1998) Circadian periods of single suprachiasmatic neurons in rats. Neurosci Lett 250:157-160.

Illnerova H, Vanecek J (1982) Two-oscillator structure of the pacemaker controlling the circadian rhythm of N-acetyltransferase in the rat pineal gland. J Comp Physiol 145:539-548.

Inagaki N, Honma S, Ono D, Tanahashi Y, Honma K (2007) Separate oscillating cell groups in mouse suprachiasmatic nucleus couple photoperiodically to the onset and end of daily activity. Proc Natl Acad Sci U S A 104:7664-7669.

Indic P, Schwartz WJ, Herzog ED, Foley NC, Antle MC (2007) Modeling the behavior of coupled cellular circadian oscillators in the suprachiasmatic nucleus. J Biol Rhythms 22:211-219.

Jagota A, de la Iglesia HO, Schwartz WJ (2000) Morning and evening circadian oscillations in the suprachiasmatic nucleus in vitro. Nat Neurosci 3:372-376.

Jewett ME, Forger DB, Kronauer RE (1999) Revised limit cycle oscillator model of human circadian pacemaker. J Biol Rhythms 14:493-499.

Johnson CH (1999) Forty years of PRCs--what have we learned? Chronobiol Int 16:711-743.

Johnston JD (2005) Measuring seasonal time within the circadian system: regulation of the suprachiasmatic nuclei by photoperiod. J Neuroendocrinol 17:459-465.

Johnston JD, Ebling FJ, Hazlerigg DG (2005) Photoperiod regulates multiple gene expression in the suprachiasmatic nuclei and pars tuberalis of the Siberian hamster (Phodopus sungorus). Eur J Neurosci 21:2967-2974.

Kalmus H, Wigglesworth LA (1960) Shock excited systems as models for biological rhythms. In: Cold Spring Harbor Symposia on Quantitative Biology Vol XXV pp 211-216.

Kawato M (1981) Transient and steady state phase response curves of limit cycle oscillators. J Math Biology 12:13-30.

Kawato M, Fujita K, Suzuki R, Winfree AT (1982) A three-oscillator model of the human circadian system controlling the core temperature rhythm and the sleep-wake cycle. J Theor Biol 98:369-392.

Kawato M, Suzuki R (1980) Two coupled neural oscillators as a model of the circadian pacemaker. J Theor Biol 86:547-575.

Klein DC, Moore RY (1979) Pineal N-acetyltransferase and hydroxyindole-O-methyltransferase: control by the retinohypothalamic tract and the suprachiasmatic nucleus. Brain Res 174:245-262.

Klein DC, Moore RY, Reppert SM (1991) Suprachiasmatic Nucleus: The Mind's Clock. New York: Oxford University Press, Inc.

Klerman EB, Dijk DJ, Kronauer RE, Czeisler CA (1996) Simulations of light effects on the human circadian pacemaker: implications for assessment of intrinsic period. Am J Physiol 270:R271-R282.

Klotter K (1960a) General properties of oscillating systems. In: Cold Spring Harbor Symposia on Quantitative Biology Vol XXV pp 185-188.

Klotter K (1960b) Theoretical analysis of some biological models. In: Cold Spring Harbor Symposia on Quantitative Biology Vol XXV pp 189-196.

Kronauer RE (1990) A quantitative model for the effects of light on the amplitude and phase of the deep circadian pacemaker, based on human data. In: Sleep '90 (Horne JA, ed), pp 306-309. Bochum, Germany: Pontenagel.

Kronauer RE, Czeisler CA, Pilato SF, Moore-Ede MC, Weitzman ED (1982) Mathematical model of the human circadian system with two interacting oscillators. Am J Physiol 242:R3-17.

Kronauer RE, Forger DB, Jewett ME (1999) Quantifying human circadian pacemaker response to brief, extended, and repeated light stimuli over the phototopic range. J Biol Rhythms 14:500-515.

Kume K, Zylka MJ, Sriram S, Shearman LP, Weaver DR, Jin X, Maywood ES, Hastings MH, Reppert SM (1999) mCRY1 and mCRY2 are essential components of the negative limb of the circadian clock feedback loop. Cell 98:193-205.

Kunz H, Achermann P (2003) Simulation of circadian rhythm generation in the suprachiasmatic nucleus with locally coupled self-sustained oscillators. J Theor Biol 224:63-78.

Leloup JC, Goldbeter A (1998) A model for circadian rhythms in Drosophila incorporating the formation of a complex between the PER and TIM proteins. J Biol Rhythms 13:70-87.

Leloup JC, Goldbeter A (2000) Modeling the molecular regulatory mechanism of circadian rhythms in Drosophila. Bioessays 22:84-93.

Leloup JC, Goldbeter A (2001) A molecular explanation for the long-term suppression of circadian rhythms by a single light pulse. Am J Physiol Regul Integr Comp Physiol 280:R1206-R1212.

Leloup JC, Goldbeter A (2003) Toward a detailed computational model for the mammalian circadian clock. Proc Natl Acad Sci U S A 100:7051-7056.

Leloup JC, Goldbeter A (2004) Modeling the mammalian circadian clock: sensitivity analysis and multiplicity of oscillatory mechanisms. J Theor Biol 230:541-562.

Leloup JC, Gonze D, Goldbeter A (1999) Limit cycle models for circadian rhythms based on transcriptional regulation in Drosophila and Neurospora. J Biol Rhythms 14:433-448.

Lincoln GA, Andersson H, Loudon A (2003) Clock genes in calendar cells as the basis of annual timekeeping in mammals--a unifying hypothesis. J Endocrinol 179:1-13.

Liu C, Reppert SM (2000) GABA synchronizes clock cells within the suprachiasmatic circadian clock. Neuron 25:123-128.

Liu C, Weaver DR, Strogatz SH, Reppert SM (1997) Cellular construction of a circadian clock: period determination in the suprachiasmatic nuclei. Cell 91:855-860.

Long MA, Jutras MJ, Connors BW, Burwell RD (2005) Electrical synapses coordinate activity in the suprachiasmatic nucleus. Nat Neurosci 8:61-66.

Lowrey PL, Takahashi JS (2004) Mammalian circadian biology: elucidating genome-wide levels of temporal organization. Annu Rev Genomics Hum Genet 5:407-441.

Mason R (1991) The effects of continuous light exposure on Syrian hamster suprachiasmatic (SCN) neuronal discharge activity in vitro. Neurosci Lett 123:160-163.

Matlab (2007) Matlab version 7.5.0.342 (R2007b). The MathWorks Inc.

Maywood ES, Reddy AB, Wong GK, O'Neill JS, O'Brien JA, McMahon DG, Harmar AJ, Okamura H, Hastings MH (2006) Synchronization and maintenance of timekeeping in suprachiasmatic circadian clock cells by neuropeptidergic signaling. Curr Biol 16:599-605.

Meijer JH (2001) Photic entrainment in mammals. In: Circadian clocks (Takahashi JS, Turek FW, Moore RY, eds), pp 183-210. Kluwer Academic.

Meijer JH (2008) Een kwestie van tijd. Leiden: Oratie Universiteit Leiden.

Meijer JH, de Vries MJ (1995) Light-induced phase shifts in onset and offset of running-wheel activity in the Syrian hamster. J Biol Rhythms 10:4-16.

Meijer JH, Groos GA, Rusak B (1986) Luminance coding in a circadian pacemaker: the suprachiasmatic nucleus of the rat and the hamster. Brain Res 382:109-118.

Meijer JH, Michel S, Vansteensel MJ (2007) Processing of daily and seasonal light information in the mammalian circadian clock. Gen Comp Endocrinol.

Meijer JH, Rietveld WJ (1989) Neurophysiology of the suprachiasmatic circadian pacemaker in rodents. Physiol Rev 69:671-707.

Meijer JH, Rusak B, Ganshirt G (1992) The relation between light-induced discharge in the suprachiasmatic nucleus and phase shifts of hamster circadian rhythms. Brain Res 598:257-263.

Meijer JH, Schaap J, Watanabe K, Albus H (1997) Multiunit activity recordings in the suprachiasmatic nuclei: in vivo versus in vitro models. Brain Res 753:322-327.

Messager S, Hazlerigg DG, Mercer JG, Morgan PJ (2000) Photoperiod differentially regulates the expression of Per1 and ICER in the pars tuberalis and the suprachiasmatic nucleus of the Siberian hamster. Eur J Neurosci 12:2865-2870.

Messager S, Ross AW, Barrett P, Morgan PJ (1999) Decoding photoperiodic time through Per1 and ICER gene amplitude. Proc Natl Acad Sci U S A 96:9938-9943.

Michel S, Colwell CS (2001) Cellular communication and coupling within the suprachiasmatic nucleus. Chronobiol Int 18:579-600.

Mirollo RE, Strogatz SH (1990) Synchronization of pulse-coupled biological oscillators. SIAM J Appl Math 50:1645-1662.

Moore RY (1996) Neural control of the pineal gland. Behav Brain Res 73:125-130.

Moore RY, Eichler VB (1972) Loss of a circadian adrenal corticosterone rhythm following suprachiasmatic lesions in the rat. Brain Res 42:201-206.

Moore RY, Lenn NJ (1972) A retinohypothalamic projection in the rat. J Comp Neurol 146:1-14.

Moore RY, Silver R (1998) Suprachiasmatic nucleus organization. Chronobiol Int 15:475-487.

Moore RY, Speh JC, Leak RK (2002) Suprachiasmatic nucleus organization. Cell Tissue Res 309:89-98.

Morin LP, Allen CN (2006) The circadian visual system, 2005. Brain Res Rev 51:1-60.

Mrugala M, Zlomanczuk P, Jagota A, Schwartz WJ (2000) Rhythmic multiunit neural activity in slices of hamster suprachiasmatic nucleus reflect prior photoperiod. Am J Physiol Regul Integr Comp Physiol 278:R987-R994.

Muskulus M, Rohling J (2009) Asymmetrically coupled two oscillator model of circadian clock in the suprachiasmatic nucleus. to be published.

Nagano M, Adachi A, Nakahama K, Nakamura T, Tamada M, Meyer-Bernstein E, Sehgal A, Shigeyoshi Y (2003) An abrupt shift in the day/night cycle causes desynchrony in the mammalian circadian center. J Neurosci 23:6141-6151.

Naito E, Watanabe T, Tei H, Yoshimura T, Ebihara S (2008) Reorganization of the suprachiasmatic nucleus coding for day length. J Biol Rhythms 23:140-149.

Nakamura W, Yamazaki S, Takasu NN, Mishima K, Block GD (2005) Differential response of Period 1 expression within the suprachiasmatic nucleus. J Neurosci 25:5481-5487.

Nelder JA, Mead R (1965) A simplex method for function minimization. The Computer Journal 7:308-313.

Nelson DE, Takahashi JS (1991) Sensitivity and integration in a visual pathway for circadian entrainment in the hamster (*Mesocricetus auratus*). J Physiol 439:115-145.

Nuesslein-Hildesheim B, O'Brien JA, Ebling FJ, Maywood ES, Hastings MH (2000) The circadian cycle of mPER clock gene products in the suprachiasmatic nucleus of the siberian hamster encodes both daily and seasonal time. Eur J Neurosci 12:2856-2864.

Ohta H, Yamazaki S, McMahon DG (2005) Constant light desynchronizes mammalian clock neurons. Nat Neurosci 8:267-269.

Orynski F, Pawlowski W (2004) Simulation and experimentational research of the grinder's wheelhead dynamics. J Vibr Contr 10:915-930.

Pavlidis T (1971) Populations of biochemical oscillators as circadian clocks. J Theor Biol 33:319-338.

Pavlidis T (1978a) Qualitative similarities between the behavior of coupled oscillators and circadian rhythms. Bull Math Biol 40:675-692.

Pavlidis T (1978b) What do mathematical models tell us about circadian clocks? Bull Math Biol 40:625-635.

Pikovsky A, Rosenblum M, Kurths J (2001) Synchronization: a universal concept in nonlinear sciences. Cambridge, United Kingdom: Cambridge University Press.

Pittendrigh CS (1960) Circadian rhythms and the circadian organization of living systems. Cold Spring Harb Symp Quant Biol 25:159-184.

Pittendrigh CS (1981a) Circadian organization and the photoperiodic phenomena. In: Biological clocks in reproductive cycles (Follett BK, ed), pp 1-35. John Wright.

Pittendrigh CS (1981b) Circadian systems: entrainment. In: Biological rhythms (Aschoff J, ed), pp 95-124. Plenum Press.

Pittendrigh CS, Bruce VG (1959) Daily rhythms as coupled oscillator systems and their relation to thermoperiodism and photoperiodism. In: Photoperiodism and related phenomena in plant and animals (Withrow RB, ed), pp 475-505. Washington: A.A.A.S.

Pittendrigh CS, Bruce VG, Kaus P (1958) On the significance of transients in daily rhythms. Proc Natl Acad Sci U S A 44:965-973.

Pittendrigh CS, Daan S (1976a) A functional analysis of circadian pacemakers in nocturnal rodents. I. the stability and lability of spontaneous frequency. J Comp Physiol [A] 106:223-252.

Pittendrigh CS, Daan S (1976b) A functional analysis of circadian pacemakers in nocturnal rodents: V. Pacemaker structure: a clock for all seasons. J Comp Physiol [A]333-355.

Pittendrigh CS, Elliott J, Takamura T (1984) The Circadian Component in Photoperiodic induction. In: Photoperiodic Regulation of Insect and Molluscan Hormones (Porter R, Collins JM, eds), pp 26-47. London: Pitman.

Pittendrigh CS, Kyner WT, Takamura T (1991) The amplitude of circadian oscillations: temperature dependence, latitudinal clines, and the photoperiodic time measurement. J Biol Rhythms 6:299-313.

Prosser RA (1998) In vitro circadian rhythms of the mammalian suprachiasmatic nuclei: comparison of multi-unit and single-unit neuronal activity recordings. J Biol Rhythms 13:30-38.

Quintero JE, Kuhlman SJ, McMahon DG (2003) The biological clock nucleus: a multiphasic oscillator network regulated by light. J Neurosci 23:8070-8076.

Ralph MR, Foster RG, Davis FC, Menaker M (1990) Transplanted suprachiasmatic nucleus determines circadian period. Science 247:975-978.

Reddy AB, Field MD, Maywood ES, Hastings MH (2002) Differential resynchronisation of circadian clock gene expression within the suprachiasmatic nuclei of mice subjected to experimental jet lag. J Neurosci 22:7326-7330.

Refinetti R (2002) Compression and expansion of circadian rhythm in mice under long and short photoperiods. Integr Physiol Behav Sci 37:114-127.

Reppert SM, Weaver DR (2001) Molecular analysis of mammalian circadian rhythms. Annu Rev Physiol 63:647-676.

Reppert SM, Weaver DR (2002) Coordination of circadian timing in mammals. Nature 418:935-941.

Roenneberg T, Merrow M (2001) Seasonality and photoperiodism in fungi. J Biol Rhythms 16:403-414.

Roenneberg T, Mittag M (1996) The circadian program of algae. Semin Cell Dev Biol 7:753-763.

Rohling J, Meijer JH, VanderLeest HT, Admiraal J (2006a) Phase differences between SCN neurons and their role in photoperiodic encoding; a simulation of ensemble patterns using recorded single unit electrical activity patterns. J Physiol Paris 100:261-270.

Rohling J, Wolters L, Meijer JH (2006b) Simulation of day-length encoding in the SCN: from single-cell to tissue-level organization. J Biol Rhythms 21:301-313.

Schaap J, Albus H, VanderLeest HT, Eilers PH, Detari L, Meijer JH (2003) Heterogeneity of rhythmic suprachiasmatic nucleus neurons: Implications for circadian waveform and photoperiodic encoding. Proc Natl Acad Sci U S A 100:15994-15999.

Schwartz WJ, de la Iglesia HO, Zlomanczuk P, Illnerova H (2001) Encoding le quattro stagioni within the mammalian brain: photoperiodic orchestration through the suprachiasmatic nucleus. J Biol Rhythms 16:302-311.

Schwartz WJ, Gross RA, Morton MT (1987) The suprachiasmatic nuclei contain a tetrodotoxin-resistant circadian pacemaker. Proc Natl Acad Sci U S A 84:1694-1698.

Sharma L (2007) Lifestyles, flying and associated health problems in flight attendants. J R Soc Health 127:268-275.

Sharma VK, Chandrashekaran MK (2000) Probing the circadian oscillator of a mammal by two-pulse perturbations. Chronobiol Int 17:129-136.

Shibata S, Watanabe A, Hamada T, Ono M, Watanabe S (1994) N-methyl-D-aspartate induces phase shifts in circadian rhythm of neuronal activity of rat SCN in vitro. Am J Physiol Regul Integr Comp Physiol 267:R360-R364.

Shiflet AB, Shiflet GW (2006) Introduction to Computational Science: Modeling and Simulation for the Sciences. Princeton University Press.

Steinlechner S, Jacobmeier B, Scherbarth F, Dernbach H, Kruse F, Albrecht U (2002) Robust circadian rhythmicity of Per1 and Per2 mutant mice in constant light, and dynamics of Per1 and Per2 gene expression under long and short photoperiods. J Biol Rhythms 17:202-209.

Stephan FK, Zucker I (1972) Circadian rhythms in drinking behavior and locomotor activity of rats are eliminated by hypothalamic lesions. Proc Natl Acad Sci U S A 69:1583-1586.

Sterman JD (1991) A skeptic's guide to computer models. In: Managing a nation: the microcomputer software catalog (Barney GO, Kreutzer WB, Garrett MJ, eds), pp 209-229. Boulder, CO: Westview Press.

Strogatz SH (2003) Sync: How order emerges from chaos in the universe, nature, and daily life. New York: Hyperion Books.

Strogatz SH, Stewart I (1993) Coupled oscillators and biological synchronization. Sci Am 269:102-109.

Sumova A, Jac M, Sladek M, Sauman I, Illnerova H (2003) Clock gene daily profiles and their phase relationship in the rat suprachiasmatic nucleus are affected by photoperiod. J Biol Rhythms 18:134-144.

Sumova A, Travnickova Z, Illnerova H (2000) Spontaneous c-Fos rhythm in the rat suprachiasmatic nucleus: location and effect of photoperiod. Am J Physiol Regul Integr Comp Physiol 279:R2262-R2269.

Sumova A, Travnickova Z, Peters R, Schwartz WJ, Illnerova H (1995) The rat suprachiasmatic nucleus is a clock for all seasons. Proc Natl Acad Sci U S A 92:7754-7758.

Takahashi JS, Turek FW, Moore RY (2001) Circadian Clocks. New York: Kluwer Academic/Plenum Publishers.

Takahashi M, Nakata A, Arito H (2002) Disturbed sleep-wake patterns during and after short-term international travel among academics attending conferences. Int Arch Occup Environ Health 75:435-440.

Tauber E, Kyriacou BP (2001) Insect photoperiodism and circadian clocks: models and mechanisms. J Biol Rhythms 16:381-390.

Tournier BB, Menet JS, Dardente H, Poirel VJ, Malan A, Masson-Pevet M, Pevet P, Vuillez P (2003) Photoperiod differentially regulates clock genes' expression in the suprachiasmatic nucleus of Syrian hamster. Neuroscience 118:317-322.

Ukai H, Kobayashi TJ, Nagano M, Masumoto KH, Sujino M, Kondo T, Yagita K, Shigeyoshi Y, Ueda HR (2007) Melanopsin-dependent photo-perturbation reveals desynchronization underlying the singularity of mammalian circadian clocks. Nat Cell Biol 9:1327-1334.

van den Pol AN (1980) The hypothalamic suprachiasmatic nucleus of rat: intrinsic anatomy. J Comp Neurol 191:661-702.

van den Pol AN (1991) The Suprachiasmatic Nucleus: Morphological and Cytochemical Substrates for Cellular Interaction. In: Suprachiasmatic Nucleus: The Mind's Clock (Klein DC, Moore RY, Reppert SM, eds), pp 17-50. New York: Oxford University Press, Inc.

van Oosterhout F, Michel S, Deboer T, Houben T, van de Ven RC, Albus H, Westerhout J, Vansteensel MJ, Ferrari MD, van den Maagdenberg AM, Meijer JH (2008) Enhanced circadian phase resetting in R192Q Cav2.1 calcium channel migraine mice. Ann Neurol 64:315-324.

VanderLeest HT, Houben T, Michel S, Deboer T, Albus H, Vansteensel MJ, Block GD, Meijer JH (2007) Seasonal encoding by the circadian pacemaker of the SCN. Curr Biol 17:468-473.

VanderLeest HT, Rohling JH, Michel S, Meijer JH (2009) Phase shifting capacity of the circadian pacemaker determined by the SCN neuronal network organization. PLoS One 4:e4976.

Vansteensel MJ, Michel S, Meijer JH (2008) Organization of cell and tissue circadian pacemakers: a comparison among species. Brain Res Rev 58:18-47.

Vansteensel MJ, Yamazaki S, Albus H, Deboer T, Block GD, Meijer JH (2003) Dissociation between circadian Per1 and neuronal and behavioral rhythms following a shifted environmental cycle. Curr Biol 13:1538-1542.

Vasalou C, Herzog ED, Henson MA (2009) Small-world network models of intercellular coupling predict enhanced synchronization in the suprachiasmatic nucleus. J Biol Rhythms 24:243-254.

Vuillez P, Jacob N, Teclemariam-Mesbah R, Pevet P (1996) In Syrian and European hamsters, the duration of sensitive phase to light of the suprachiasmatic nuclei depends on the photoperiod. Neurosci Lett 208:37-40.

Wagner S, Castel M, Gainer H, Yarom Y (1997) GABA in the mammalian suprachiasmatic nucleus and its role in diurnal rhythmicity. Nature 387:598-603.

Wagner S, Sagiv N, Yarom Y (2001) GABA-induced current and circadian regulation of chloride in neurones of the rat suprachiasmatic nucleus. J Physiol 537:853-869.

Watanabe K, Deboer T, Meijer JH (2001) Light-Induced resetting of the circadian pacemaker: quantitative analysis of transient versus steady-state phase shifts. J Biol Rhythms 16:564-573.

Waterhouse J, Reilly T, Atkinson G, Edwards B (2007) Jet lag: trends and coping strategies. Lancet 369:1117-1129.

Wayne NL (2001) Regulation of seasonal reproduction in mollusks. J Biol Rhythms 16:391-402.

Wehr TA (2001) Photoperiodism in humans and other primates: evidence and implications. J Biol Rhythms 16:348-364.

Weinert D, Freyberg S, Touitou Y, Djeridane Y, Waterhouse JM (2005) The phasing of circadian rhythms in mice kept under normal or short photoperiods. Physiol Behav 84:791-798.

Welsh DK (2007) VIP activates and couples clock cells. Focus on "Disrupted neuronal activity rhythms in the suprachiasmatic nucleus of vasoactive intestinal polypeptide-deficient mice". J Neurophysiol 97:1885-1886.

Welsh DK, Logothetis DE, Meister M, Reppert SM (1995) Individual neurons dissociated from rat suprachiasmatic nucleus express independently phased circadian firing rhythms. Neuron 14:697-706.

Westfall R (1993) The Life of Isaac Newton. Cambridge, UK: Cambridge University Press.

Wever R (1962) Zum Mechanismus der biologischen 24-Stunden-Periodik (I). Kybernetik 1:139-154.

Wever R (1965) A mathematical model for circadian rhythms. In: Circadian clocks (Aschoff J, ed), pp 49-63. Amsterdam: North Holland.

Wever R (1972) Virtual synchronization towards the limits of the range of entrainment. J Theor Biol 36:119-132.

Wever R (1985) Internal interactions within the human circadian system: the masking effect. Experientia 41:332-342.

Wever R (1989) Light effects on human circadian rhythms: a review of recent Andechs experiments. J Biol Rhythms 4:161-185.

Winfree AT (1967) Biological rhythms and the behavior of populations of coupled oscillators. J Theor Biol 16:15-42.

Winfree AT (2000) The Geometry of Biological Time. New York: Springer.

Yamaguchi S, Isejima H, Matsuo T, Okura R, Yagita K, Kobayashi M, Okamura H (2003) Synchronization of cellular clocks in the suprachiasmatic nucleus. Science 302:1408-1412.

Yamazaki S, Numano R, Abe M, Hida A, Takahashi R, Ueda M, Block GD, Sakaki Y, Menaker M, Tei H (2000) Resetting central and peripheral circadian oscillators in transgenic rats. Science 288:682-685.

Yan L, Silver R (2002) Differential induction and localization of mPer1 and mPer2 during advancing and delaying phase shifts. Eur J Neurosci 16:1531-1540.

Yan L, Silver R (2004) Resetting the brain clock: time course and localization of mPER1 and mPER2 protein expression in suprachiasmatic nuclei during phase shifts. Eur J Neurosci 19:1105-1109.

Yannielli PC, Brewer JM, Harrington ME (2004) Blockade of the NPY Y5 receptor potentiates circadian responses to light: complementary in vivo and in vitro studies. Eur J Neurosci 19:891-897.

Zlomanczuk P, Margraf RR, Lynch GR (1991) In vitro electrical activity in the suprachiasmatic nucleus following splitting and masking of wheel-running behavior. Brain Res 559:94-99.

Nederlandse samenvatting

Netwerkeigenschappen van de circadiane klok van zoogdieren

Het combineren van verschillende wetenschappen is een uitdaging. Wetenschappers uit verschillende disciplines spreken vaak niet dezelfde taal en zijn het zeker niet altijd eens over de methodologie en de bewijsvoering. Als men echter het risico durft te nemen dan kunnen de gecombineerde inspanningen ook leiden tot nieuwe en verrassende resultaten voor de betrokken wetenschappelijke disciplines: de resultaten kunnen meer zijn dan de som der delen.

In dit proefschrift verenigen de computerwetenschappen en de levenswetenschappen hun krachten. Meer specifiek wordt in dit proefschrift besproken hoe computationele modellen kunnen bijdragen aan het onderzoek naar de biologische klok, die aanwezig is in alle levende organismen.

De rotatie van de aarde rond zijn as onderwerpt ieder organisme aan een dagelijkse cyclus van 24 uur. Daarnaast zorgt de rotatie van de aarde om de zon ervoor dat ieder organisme beïnvloed wordt door de seizoenen. Als een organisme kan anticiperen op deze dagelijkse veranderingen en deze seizoensveranderingen levert dit een evolutionair voordeel op. Muizen zijn bijvoorbeeld ’s nachts actief, terwijl hun natuurlijke vijanden vooral tijdens

de dag actief zijn. Om niet ten prooi te vallen aan de roofdieren moeten de muizen dus al voor de zon opgaat terug zijn in hun hol. Met andere woorden, ze moeten kunnen anticiperen op de tijd van zonsopgang. Ook in de seizoenen zien we dit anticiperende gedrag terug in het reproductieproces. De meeste dieren krijgen hun nageslacht in de periode van het jaar dat de kans dat het jong het overleeft het grootst is.

In alle organismen worden de dagelijkse ritmes en de seizoensritmes verzorgd door de zogenaamde biologische klok. De locatie van deze klok verschilt per organisme. In zoogdieren is deze klok gelokaliseerd in de Suprachiasmatische Nuclei (SCN). Deze centrale pacemaker speelt een kritische rol in de regulering van ritmische functies. Het dient als de centrale klok die in staat is zich aan te passen aan de omgevingscycli en die dit ritme oplegt aan andere lichaamsfuncties.

Omdat de licht-donker cyclus zowel de dagelijkse ritmes alsook de seizoensritmes het meest adequaat weergeeft, wordt deze meest betrouwbare omgevingsfactor door de SCN gebruikt. De lengte van de dag, ook wel fotoperiode genoemd, is een uiterst precieze indicatie voor de tijd van het jaar. In de zomer zijn de dagen immers langer dan in de winter. De klok reageert op lichtinvloeden en past zich aan de licht-donker cyclus aan.

In een experimentele omgeving kan men mensen of dieren in constante condities houden, zoals in constant donker of constant licht. In deze omstandigheden kan het ritme van de klok zelf, het zogenaamde endogene ritme, worden gemeten. Dit ritme heeft een periode van ongeveer 24 uur. Dit endogene ritme wordt gegenereerd in de individuele neuronen zelf op basis van een moleculaire terugkoppeling. Het basisprincipe van deze terugkoppeling is verrassend genoeg vergelijkbaar in verschillende organismen. De moleculaire mechanismen in de mensen lijken sterk op die in muizen, maar ook op die in fruitvliegjes en algen.

Het tijdstip van het organisme in zijn eigen, endogene cyclus wordt de fase genoemd van het organisme. Het organisme moet zijn eigen ritme aanpassen, of synchroniseren, aan het ritme van de externe licht-donker cyclus die precies 24 uur is. Organismen met een endogene cyclus die iets minder is dan 24 uur, moeten hun fase iedere dag iets naar achteren verschuiven. Organismen met een endogeen ritme van iets meer dan 24 uur,

zoals de mens, moeten hun fase iets naar voren verschuiven. De mate van verschuiving voor een organisme over de gehele endogene cyclus kan worden bepaald in een functie, de zogenaamde fase-respons-curve (PRC). Deze PRC geeft aan hoeveel de fase van een organisme voor- of achteruitschuift op een bepaald moment in de endogene cyclus, ofwel in een bepaalde fase van het organisme.

Om een eenduidig signaal door te geven van de individuele klokcellen aan de andere lichaamsfuncties die afhankelijk zijn van deze centrale klok moeten de individuele ritmes van de verschillende cellen worden gesynchroniseerd. Dit gebeurt door middel van intercellulaire communicatiemechanismen tussen de neuronen. Door deze communicatiemechanismen, ook wel koppelingsmechanismen genoemd, zijn de neuronen van de klok met elkaar verbonden en vormen ze een netwerk. Bepaalde eigenschappen van de klok ontstaan als gevolg van deze koppeling tussen de neuronen en vinden niet plaats in cellen zelf.

In dit proefschrift zijn computationele modellen ontworpen om onderzoek te doen naar de biologische klok in zoogdieren, en meer specifiek onderzoek naar de organisatie van de suprachiasmatische nuclei (SCN) en de communicatiemechanismen tussen cellen en subpopulaties van cellen in de SCN.

Hoofdstuk 2 van dit proefschrift geeft een overzicht van de verschillende koppelingsmechanismen die aanwezig zijn in de SCN. Er wordt beschreven dat de SCN onderverdeeld kan worden in verschillende gebieden, zoals een zogenaamd dorsaal en ventraal gebied. De koppelingsmechanismen tussen de SCN neuronen verschillen onder meer van elkaar doordat het ene mechanisme bijvoorbeeld beter geschikt is voor de communicatie tussen neuronen binnen een van de gebieden, bijvoorbeeld binnen het ventrale of dorsale gebied, terwijl andere koppelingsmechanismen de communicatie verzorgen tussen neuronen van het ene naar het andere gebied en omgekeerd. Het precieze karakter van deze koppelingsmechanismen is tegenwoordig een belangrijke focus van veel onderzoekslijnen in het onderzoeksveld naar circadiane ritmiek, omdat het steeds duidelijker wordt dat de koppeling van klok neuronen sterk bijdraagt aan de functie van de SCN pacemaker om dagelijkse ritmes en seizoensritmes te reguleren.

Er zijn al verschillende modelleer studies voor het circadiane systeem uitgevoerd, in het bijzonder voor de SCN. Een overzicht van de belangrijkste onderzoeksrichtingen van deze modelleerstudies over de biologische klok zijn gepresenteerd in hoofdstuk 2. In de eerste modellen werd de klok gemodelleerd als één enkele entiteit. Deze modellen bleken echter niet in staat te zijn om alle dynamische eigenschappen van de klok te beschrijven. Tegenwoordig zijn de modellen te verdelen in twee groepen. Sommige modellen richten hun aandacht op de endogene pacemaker cel en het genereren van circadiane ritmes zelf. Deze modellen zijn gebaseerd op moleculaire intracellulaire mechanismen die ervoor zorgen dat een individueel neuron van de SCN ritmisch is. Andere modellen richten hun onderzoek op de netwerk eigenschappen van de SCN. Deze modellen concentreren zich op de heterogene aard van de SCN en gaan vaak uit van simpele oscillerende eenheden. Dit proefschrift laat zien dat simpele modellen op het niveau van het neurale netwerk interessante wetenschappelijke resultaten kunnen opleveren, en dat modellen niet onnodig ingewikkeld hoeven te worden om deze inzichten te produceren.

Een voorbeeld van een bruikbaar simulatiemodel is beschreven in hoofdstuk 3, waarin werd onderzocht hoe de veranderingen in daglengte door de SCN kunnen worden gecodeerd. Enerzijds werd onderzocht hoe verandering van de activiteitspatronen van individuele neuronen kan leiden tot het coderen van de verschillen in daglengte over de seizoenen door de SCN. Dit werd vergeleken met hoe het netwerk van neuronen dit tot stand kan brengen. Door de fase van de verschillende neuronen anders te verdelen in korte en lange dagen bleek dat een zogenaamde kleinere faseverdeling, waarbij de neuronen verdeeld zijn over een beperkte tijdsduur van een paar uur, een korter patroon oplevert. Dit kortere patroon komt overeen met een gemeten patroon behorend bij een korte dag. Door een grote faseverdeling te nemen, waarbij de neuronen werden verdeeld over meerdere uren, bleek dat de duur van een lange dag kon worden gecodeerd. Het aanpassen van de faserelatie tussen neuronen bleek veel effectiever voor het coderen van de seizoenen dan het veranderen van de activiteit van individuele neuronen. Dit betekent dat de codering van de seizoenen door de SCN voornamelijk een

eigenschap is van het netwerk van de SCN en hooguit in beperkte mate een eigenschap van de individuele cel.

In hoofdstuk 4 is een studie beschreven waarin een onderzoek is gedaan naar de regionale organisatie van de SCN. Na een verschuiving van 6 uur van de licht-donker cyclus van de omgeving, wat overeenkomt met een vlucht van Amsterdam naar New York, werd een dissociatie tussen het ventrale en het dorsale gebied van de SCN waargenomen. Het ventrale deel van de SCN verschoof meteen in fase naar de nieuwe licht-donker cyclus, terwijl het dorsale deel pas na zes dagen was aangepast. Uit analyses van de gemeten data bleek dat slechts een klein aantal neuronen uit de totale populatie onmiddellijk verschuift na een achteruitschuiving van het licht-donker regime. De faseverschuivingen lijken dus op gang te worden gebracht door een initiële snelle verschuiving van een relatief kleine groep van neuronen in de SCN. Het is de verwachting dat deze groep gelokaliseerd kan worden in de ventrale SCN, omdat de ventrale SCN een snelle verschuiving laat zien. Omdat de groep neuronen die snel verschuift slechts een deel lijkt te zijn van de gehele ventrale SCN moet er in vervolgonderzoek rekenschap worden gegeven van het feit dat de ventrale SCN ook zelf heterogeen van aard is. De simulatie studies die zijn uitgevoerd laten het bestaan zien van een kleine deelgroep van neuronen die uiteindelijk de faseverschuiving in de gehele SCN tot stand brengt. Experimenteel onderzoek kan zich richten op het vinden van deze bijzondere groep cellen, en de koppelingsmechanismen verhelderen die belangrijk zijn binnen deze groep en tussen deze groep en andere functioneel verschillende groepen neuronen.

In de verschillende seizoenen blijken de faseverschuivingen, die door licht veroorzaakt worden, te verschillen in grootte. In de zomer, als de dagen lang zijn, blijkt de faseverschuivingen klein te zijn, terwijl in de winter de verschuivingen groot zijn. In hoofdstuk 5 wordt aangetoond dat het verschil in de faserelatie tussen neuronen in lange en korte dag de oorzaak kan zijn voor dit verschil in faseverschuiving. De resultaten van de simulaties in hoofdstuk 5 geven aan dat als neuronen meer gesynchroniseerd zijn in fase, er een hoger aantal neuronen op hetzelfde tijdstip in dezelfde richting verschuiven in respons op een lichtpuls de lichtsensitieve periodes

overlappen. In een lange dag zijn de neuronen minder gesynchroniseerd in fase, wat resulteert in een kleinere faseverschuiving. Dit betekent dat ritmen met een hoge amplitude (als gevolg van synchronisatie tussen neuronen) meer verschuiven dan ritmen met een lage amplitude. Voor individuele neuronen geldt het omgekeerde: oscillatoren met een hoge amplitude zijn moeilijker te verschuiven in fase dan oscillatoren met een lage amplitude. De data die gepresenteerd worden in hoofdstuk 5 leveren daarmee een voorbeeld van het feit dat voor neurale netwerken andere regels gelden dan voor individuele oscillatoren en geven tegelijk de onderliggende verklaring voor dit verschil.

In hoofdstuk 6 wordt een model gepresenteerd waarmee de koppelingsmechanismen tussen twee gebieden in de SCN wordt onderzocht na een verschuiving van de licht-donker cyclus. Het model is gebaseerd op de ventrale en dorsale gebieden van de SCN, die beiden worden beschouwd als endogene oscillatoren in deze simulaties. Het model was in staat om resultaten van verschillende experimentele studies naar faseverschuivingen kwalitatief te simuleren. De resultaten geven aan dat in de SCN verschillende oscillerende gebieden kunnen bestaan die ieder bestaan uit groepen samenwerkende neuronen met hun eigen faseverschuivende karakteristieken. De verschillende oscillerende gebieden communiceren met elkaar en delen op deze manier informatie over hun fase. In hoofdstuk 6 wordt benadrukt dat faseverschuivingen voornamelijk een eigenschap zijn van het netwerk van klokneuronen.

In dit proefschrift zijn er simpele modellen gebruikt om de werking van het netwerk van de klok te verhelderen. Deze simpele modellen leveren bewijs dat verschillende niveaus van organisatie verantwoordelijk zijn voor verschillende eigenschappen van de klok. Terwijl de endogene ritmes een eigenschap zijn van de neuronen zelf, ontstaan eigenschappen zoals de aanpassing aan de licht-donker cyclus, het verwerken van een faseverschuiving van de licht-donker cyclus, of het coderen voor daglengte op het niveau van het neuronale netwerk.

Het is een uitdaging om verschillende wetenschappelijke disciplines met elkaar te combineren. De hechte samenwerking tussen de levenswetenschappen en de computerwetenschappen in dit onderzoek

zorgden ervoor dat het proces waarin het onderzoek werd gedaan heel dynamisch werd. Hierbij werden de data van de empirische levenswetenschappen samengebracht met de computersimulaties. Afhankelijk van de resultaten van de simulaties werden de experimenten aangepast om te kunnen zoeken naar specifieke fenomenen die uit de simulatieresultaten naar voren kwamen, terwijl de experimenten op hun beurt weer resultaten opleverden waarmee de modellen konden worden verbeterd. Dit proefschrift laat daarmee zien dat de gecoördineerde inspanningen van computerwetenschappen en levenswetenschappen een verrijking zijn voor beide disciplines en leiden tot wetenschappelijke voortgang.

Glossary

ACSF	artificial cerebrospinal fluid
AIC	Akaike information criterion
AVP	arginine vasopressin
Bmal1	Bmal1 gene
BMAL1	BMAL1 protein
CalB	Calbindin – calcium binding proteins
Clock	Clock gene
CLOCK	Clock protein
Cry1	Cryptochrome1 gene
Cry2	Cryptochrome2 gene
CRY1	Cryptochrome1 protein
CRY2	Cryptochrome2 protein
CT	circadian time
Cx36	connexin 36 – gap junction protein
E-M model	evening-morning model as defined by Pittendrigh and Daan (1976)
GABA	γ-amino butyric acid
GRP	gastrin-releasing peptide
LD	light-dark
LL	constant light
DD	constant darkness
mBmal1	messenger RNA of Bmal1
mCry1	messenger RNA of Cry1

mPer1	messenger RNA of Per1
mPer2	messenger RNA of Per2
mRNA	messenger RNA (Ribonucleic acid)
MUA	multi unit activity
NKCC1	Na^+-K^+-$2Cl^-$ Cotransporter isoform1
NMDA	N-methyl-D-aspartic acid
ODE	ordinary differential equation
PACAP	pituitary adenylyl cyclase-activating peptide
Per1	Period1 gene
Per2	Period2 gene
Per3	Period3 gene
PER1	Period1 protein
PER2	Period2 protein
PER3	Period3 protein
PHI	peptide histidine isoeucine
PRC	phase response curve
Rev-Erbα	Rev-Erbα gene
REV-ERBα	Rev-Erbα protein
RHT	retino-hypothalamic tract
RNA	ribonucleic acid
SCN	suprachiasmatic nuclei (location of the biological clock in mammals)
SUA	single unit activtiy
Tim	Timeless gene of *Drosophila* clock
TIM	Timeless protein of *Drosophila* clock
VIP	vasoactive intestinal polypeptide
vip-/-	VIP deficient mouse
vipr-/-	VPAC2 receptor deficient mouse
VPAC2	receptor for VIP and PACAP
ZT	Zeitgeber time

List of publications

	Chapter
• Rohling, J., Wolters, L., and Meijer, J.H., Simulation of day-length encoding in the SCN: from single-cell to tissue-level organization. J. Biol. Rhythms 21, 2006, 301-313.	3
• Rohling, J., Meijer, J.H., VanderLeest, H.T., Admiraal, J., Phase differences between SCN neurons and their role in photoperiodic encoding; a simulation of ensemble patterns using recorded single unit electrical activity patterns. Journal of Physiology - Paris 100, 2006, 261–270.	3
• Jos Rohling, Lex Wolters, and Johanna H. Meijer, Simulation of Day-Length Encoding in the SCN, in proceedings of the 13th Annual Conference of the Advanced School for Computing and Imaging (ASCI), June 2007, Heijen, The Netherlands, pp 414-421.	3
• VanderLeest, H.T., Rohling, J.H.T., Michel, S., and Meijer, J.H. (2009). Phase shifting capacity of the circadian pacemaker determined by the SCN neuronal network organization. PLoS One. 4, e4976.	5
• Rohling, J.H.T., vanderLeest, H.T., Michel, S., Vansteensel, M.J., Meijer, J.H., Phase resetting caused by rapid shifts of small population of ventral SCN neurons. In preparation.	4
• Rohling, J.H.T. and Muskulus, M. A two oscillator model for jet lag. In preparation.	6
• Muskulus, M. and Rohling, J.H.T. Asymmetrically coupled two oscillator model of circadian clock in the suprachiasmatic nucleus. In preparation.	6

Acknowledgements

Lots of people were very important to me in the time that I worked on this thesis. My fellow clock researchers, the people at the institutes where I did the job, the contacts in the biological clock field, among which the CTR, they were encouraging and inspiring me during this time. My friends kept supporting me even though I could not see them as often as I sometimes wanted. I hope that I can enjoy your friendships for years to come. There are too many of you to mention here, but I am grateful to all of you.

For some people I would like to make an exception. These people were of vital importance to me during these thesis-years. First of all I want to mention Joke and Lex. Thank you for the time that you gave me, the lessons that I learned from you, and above all, for being pleasant and warm persons.

Bij alles wat ik deed heb ik altijd het gevoel gehad dat ik gesteund werd door mijn ouders. Dat is een bijzonder fijn gevoel. Mijn moeder wil ik graag heel in het bijzonder danken. Ze is voor mij een voorbeeld door de manier waarop ze haar leven weer oppakte nadat mijn vader was overleden. Bedankt mam!

Last, but not least, I want to thank Marja, my wife. You were able to give me the freedom to finish this thesis. Thank you! Be it coincidence or not, in the same week that I send my thesis to the reading committee, we learned that Marja is pregnant and we will be having our first child! Life will change a lot, but I hope I can still enjoy the company of all the people that I love for a long time to come.

Curriculum vitae (in Dutch)

Jos Rohling werd geboren op 24 januari 1970 te Schoonebeek. In 1989 behaalde hij zijn VWO diploma aan het Katholiek Drents College in Emmen. In 1993 studeerde hij met goed gevolg af aan de Hogeschool Drenthe in de afstudeerrichting 'Technische Informatica'. Hij vervolgde zijn studie aan de Universiteit van Amsterdam waar hij in 1994 met goed gevolg de propedeuse artificiële intelligentie afmaakte en in 1996 afstudeerde in de wijsbegeerte, met als specialisatie 'Filosofie en Cognitiewetenschap'. De titel van zijn scriptie was: "Mogelijkheidsvoorwaarden voor Leren" en het had als onderwerp in hoeverre computers in staat zijn te leren op eenzelfde wijze als een mens. In datzelfde jaar werd hij toegelaten tot het prestigieuze programma 'The Japan Prizewinners Programme', waar hij de mogelijkheid kreeg om 5 maanden een stage te doen in een Japans onderzoekslaboratorium waar men onderzoek deed naar intelligentie en het brein. Jos hielp mee met het ontwerpen van een 'breinchip': een computerchip die een deel van het brein simuleerde. In 1997 begon hij te werken bij Translogic BV, een klein softwarebedrijf dat slimme software schreef waarmee computerchips kunnen worden geprogrammeerd. Hier maakte hij eerst deel uit van het ontwikkelteam. Later gaf hij trainingen bij klanten en deed hij de technische marketing voor het product. Hij merkte dat het onderzoek hem trok en in 2000 vervolgde hij zijn carrière bij het Nationaal Lucht en Ruimtevaartlaboratorium (NLR). Hier deed hij onderzoek naar luchtverkeersleiding, waarvoor hij software ontwikkelde en projecten leidde. Toch was dit toegepaste onderzoek niet helemaal wat hij

zocht. Zijn passie ligt in het wetenschappelijk onderzoek en in 2004 begon hij aan een promotietraject, dat uiteindelijk tot dit proefschrift heeft geleid. In deze baan kwam alles samen, het programmeren, het breinonderzoek waar hij in Japan bij betrokken was, en de interesse voor wetenschappelijk onderzoek. Het is dan ook niet vreemd dat hij doorgaat in dit onderzoek, nu hem die kans is geboden. Op dit moment heeft hij een positie als onderzoeker bij het LUMC.